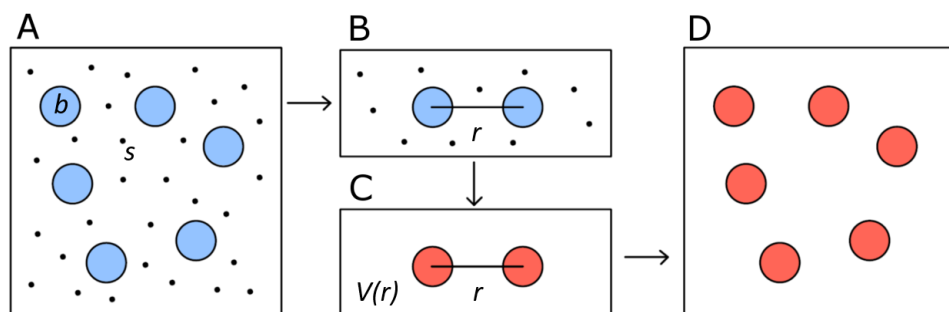

Computational Physics: Material Science

M.Sc. Physics and M.Sc. Applied Physics



Prof. Joachim Dzubiella
Applied Theoretical Physics - Computational Physics
Institute of Physics - University of Freiburg
Summer 2021 - Version 0.2

Version 0.3: April 2023

Updates: Some little corrections and restructuring to adapt for the lecture in summer semester 2023.

Version 0.2: September 2021

Updates: following the lecture in the summer semester 2021, the script was carefully scrutinized again, corrected in some places, re-structured, and some sections and chapters significantly extended. In particular a new section was added on 'Speeding up MD Simulations'.

Version 0.1: April 2021

Note: This document is the first version of a LateX implementation of the handwritten script of the Master lecture on 'Computational Physics: Materials Science' held in the summer semester 2019 at the Institute of Physics in Freiburg by Prof. Joachim Dzubiella. It contains open questions and likely some errors (e.g., typographical errors present already in the original material). It also does not provide all contents, and it does not reflect the order of topics given in the real lecture (as now in summer semester 2021). It just serves as an orientation, and it will be dynamically completed, corrected and adapted during the course as well as in future courses. The script is mostly based on the books mentioned in the Bibliography. JD appreciates the great work by Rolf Schimmer and Sebastien Groh in LaTeXing, illustrating, and proof-reading the current script.

Contents

| | | |
|----------|--|-----------|
| 1 | Introduction | 8 |
| I | Theory | 9 |
| 2 | Phase diagrams and states | 10 |
| 3 | Interactions and potentials | 13 |
| 3.1 | Interatomic pair potentials | 15 |
| 3.2 | Many-body potentials: MEAM (Modified Embedded Atom Method) | 18 |
| 4 | Recap of thermodynamics and statistical mechanics | 22 |
| 4.1 | Basic thermodynamic quantities | 22 |
| 4.2 | Macro- vs. microstates | 24 |
| 4.3 | Ergodicity and averages | 26 |
| 5 | Structure-property relationships | 28 |
| 5.1 | From fluctuations to material properties | 28 |
| 5.1.1 | Heat capacity and compressibility | 28 |
| 5.1.2 | Time correlation function | 29 |
| 5.1.3 | Einstein diffusion law (random walk) | 30 |
| 5.2 | From the structure to material properties in the <u>canonical</u> ensemble | 31 |
| 5.2.1 | The one-body density profile $\rho(\vec{r})$ | 31 |
| 5.2.2 | The radial distribution function, $g(r)$ | 32 |
| 5.2.3 | From $g(r)$ to macroscopic observables | 35 |
| 5.2.4 | Relation of $g(r)$ to scattering | 37 |
| 6 | Coarse-graining of multi-component systems: effective interactions | 39 |
| 6.1 | Potential of mean force: effective interaction | 40 |
| 6.1.1 | Two-body approximation | 41 |
| 6.1.2 | Internal degree of freedom | 42 |
| 6.2 | Typical coarse-graining procedure | 42 |
| 6.3 | Effective macromolecular interactions: examples | 44 |
| 6.3.1 | Depletion Potential | 44 |
| 6.3.2 | DLVO interaction (Hamaker and Debye-Hückel) | 47 |
| 7 | Polyatomic molecules and polymers | 51 |
| 7.1 | Introduction | 51 |
| 7.1.1 | Molecules | 51 |
| 7.1.2 | Polymers | 51 |
| 7.1.3 | Structures and architectures | 52 |
| 7.1.4 | Example of specific polymers | 53 |

| | | |
|-----------|--|------------|
| 7.1.5 | Definitions | 54 |
| 7.2 | Chain models | 56 |
| 7.2.1 | Freely jointed chain (FJC) model | 56 |
| 7.2.2 | Freely rotating chain (FRC) model | 57 |
| 7.2.3 | Hindered rotation model | 59 |
| 7.2.4 | The Gaussian (or Rouse) chain | 59 |
| 7.2.5 | Form factor | 60 |
| 7.2.6 | Real chains | 60 |
| II | Simulation methods | 62 |
| 8 | Molecular dynamics (MD) computer simulations | 63 |
| 8.1 | Newton and forces | 63 |
| 8.2 | Numerical integration | 64 |
| 8.3 | Choice of time step & computing time | 65 |
| 8.4 | Mean and standard derivation | 66 |
| 8.5 | Connection to thermodynamics and velocity rescaling | 66 |
| 8.6 | Initial conditions and steps to set up a MD simulation | 67 |
| 9 | Particle-resolved simulations of finite systems | 69 |
| 9.1 | Computational boxes and periodic boundary conditions | 69 |
| 9.2 | Implementation of short-ranged pair potentials: cutoffs and truncation | 71 |
| 9.3 | Solutions to speed-up particle-based codes | 72 |
| 9.3.1 | Verlet/neighbor list | 72 |
| 9.3.2 | Link-cell | 73 |
| 9.3.3 | Parallel solutions | 74 |
| 9.4 | Errors | 75 |
| 9.4.1 | Systematic errors | 75 |
| 9.4.2 | Statistical errors | 76 |
| 9.5 | Units | 77 |
| 10 | Long range interactions: Electrostatics in molecular physics | 78 |
| 10.0.1 | Molecular Dynamics simulations of ions and charged particles | 80 |
| 10.0.2 | Truncation methods | 81 |
| 10.0.3 | Ewald method | 82 |
| 11 | MD simulation in different ensembles | 84 |
| 11.1 | Canonical (<i>NVT</i>) ensemble | 84 |
| 11.2 | The isobaric/isothermal (NPT) ensemble | 91 |
| 12 | Force field for molecules and polymers | 96 |
| 12.1 | Molecular force fields | 96 |
| 12.2 | Mixing rules | 98 |
| 12.3 | Constrained dynamics | 98 |
| 13 | Langevin and Brownian Dynamics | 100 |
| 13.1 | Langevin equation | 101 |
| 13.2 | Brownian Dynamics computer simulations | 103 |

| | |
|---|------------|
| 14 Sampling methods and reaction coordinates | 105 |
| 14.1 Free energy calculations and entropy | 105 |
| 14.1.1 Thermodynamic Integration | 105 |
| 14.1.2 Particle insertion method | 107 |
| 14.1.3 Free energy perturbation approach | 108 |
| 14.1.4 Reaction coordinate | 109 |
| 14.1.5 Importance sampling & Umbrella sampling | 110 |
| 14.2 From free energies to phase diagrams | 111 |
| 15 Appendix | 115 |
| 15.1 Complexity diagram | 116 |
| 15.2 Overview of interatomic potentials | 117 |
| 15.3 Numerical integration and energy conservation | 120 |
| 15.4 Simulations of finite systems: simulation boxes, periodic boundary conditions and periodic images | 122 |
| 15.5 Fluctuations and errors | 126 |
| 15.6 Thermostats | 128 |
| 15.7 Structure of liquids; examples for $g(r)$ | 129 |
| 15.8 Molecules and polymers | 134 |
| 15.9 Force fields | 137 |
| 15.10 Coarse graining; Hamaker, DLVO and Depletion potentials | 141 |

List of Figures

| | | |
|------|---|----|
| 2.1 | Pressure-temperature phase diagram | 10 |
| 2.2 | Temperature-density phase diagram | 11 |
| 2.3 | Pair distributions functions $g(r)$ of different phases. | 12 |
| 3.1 | Scheme of pair, $V^{(2)}$, and the three body potential, $V^{(3)}$ | 14 |
| 3.2 | The complexity of a system can vary in shapes, polydispersity, and components (x -axis) and the form of external potentials, possibly driving the system out of equilibrium. Real systems are typically found on the top right corner of such a diagram. | 14 |
| 3.3 | Typical atomic pair potential | 15 |
| 3.4 | Phase (liquid/solid) as a function of the packing fraction. | 17 |
| 4.1 | Bulk modulus | 23 |
| 5.1 | Random walk and diffusion | 30 |
| 5.2 | Forces of pair potentials | 31 |
| 5.3 | Density distribution from averaging | 32 |
| 5.4 | Shell histogram | 33 |
| 5.5 | (a) Pair distribution function, $g(r)$, and (b) corresponding coordination number. | 34 |
| 5.6 | Applied external pressure | 36 |
| 5.7 | scattering at macromolecular liquids | 37 |
| 6.1 | Examples for two-component mixtures | 39 |
| 6.2 | Binary system | 40 |
| 6.3 | Coarse graining a one component system, with internal degree of freedom | 42 |
| 6.4 | Typical coarse-graining procedure | 43 |
| 6.5 | V_{eff} through simulation | 43 |
| 6.6 | Binary system with colloids and polymers | 45 |
| 6.7 | Binary system with colloids and polymers | 45 |
| 6.8 | Overlap volume of two colloids | 45 |
| 6.9 | Total effective pair interaction | 46 |
| 6.10 | Van der Waals interaction | 47 |
| 6.11 | Interaction between i and k across medium j | 48 |
| 6.12 | Hamaker interaction | 48 |
| 6.13 | Charged colloids and salt in a water solution | 49 |
| 6.14 | Sketch of the DLVO potential | 50 |
| 7.1 | Structures and architectures of polymers | 52 |
| 7.2 | Dendrimer | 53 |
| 7.3 | Polypeptide backbone | 53 |
| 7.4 | Definition of bond parameters | 54 |
| 7.5 | Torsion angle vs. energy | 54 |

| | | |
|------|---|-----|
| 7.6 | Contour length | 55 |
| 7.7 | Center-of-mass of polymer | 56 |
| 7.8 | Freely jointed chain | 56 |
| 7.9 | Freely rotating chain | 57 |
| 7.10 | Energy landscape and torsion angle | 59 |
| 7.11 | The Gaussian chain | 59 |
| 9.1 | (A) Simulation cell with boundary walls | 69 |
| 9.2 | Simulation cell with applied external potential | 70 |
| 9.3 | Shifted cut-off force | 71 |
| 9.4 | Verlet list method | 72 |
| 9.5 | Link-cell method | 73 |
| 9.6 | Strategies for parallelization of a particle-based code | 75 |
| 9.7 | Block averages | 76 |
| 10.1 | Examples for charged structures 1 | 78 |
| 10.2 | Examples for charged structures 2 | 78 |
| 10.3 | Charged sphere | 80 |
| 10.4 | Truncation methods | 81 |
| 10.5 | Gaussian screening of the charge density | 82 |
| 11.1 | Isothermal-Isobaric ensemble, canonical ensemble and Grand Canonical ensemble | 84 |
| 11.2 | Coupling to an external system with heat exchange | 89 |
| 11.3 | Applied external pressure | 91 |
| 11.4 | Pseudo mass and velocity | 93 |
| 12.1 | Simple bonded potential | 97 |
| 12.2 | United-atom model | 98 |
| 12.3 | SPC/E water model | 99 |
| 13.1 | Brownian motion | 100 |
| 13.2 | Velocity ACF and MSD in LE | 102 |
| 13.3 | Friction in fluid | 103 |
| 14.1 | Bad sampling potential | 106 |
| 14.2 | Solvation of a LJ-sphere in water | 106 |
| 14.3 | Particle insertion method | 107 |
| 14.4 | Insertion of multiple particles | 108 |
| 14.5 | Sampling unlikely states | 110 |
| 14.6 | Umbrella sampling | 111 |
| 14.7 | Free energy vs. density | 111 |
| 14.8 | Phase diagrams with binodal and spinodal curves | 114 |

List of Tables

| | | |
|-----|---|----|
| 3.1 | MEAM parameters | 20 |
| 4.1 | Thermodynamic potentials | 23 |
| 7.1 | Kuhn lengths | 58 |
| 9.1 | Verlet list algorithm | 73 |
| 9.2 | Link cell algorithm | 73 |
| 9.3 | Error propagation rules | 76 |
| 9.4 | Units used in particle-resolved simulation techniques | 77 |

Chapter 1

Introduction

This lecture is about how to use computational approaches, such as molecular dynamics computer simulations, to model simple and complex materials. In this lecture we focus on length scales beyond the quantum and electronic scales, that is, we start from semi-classical representations of atoms and Hamiltonians to address classical many-body systems on nanometer (nanosecond) scales. Further 'coarse-graining' leads to Hamiltonians which can model even larger scales, such as micrometer and -seconds scales in dissipative, Langevin-type of simulations. Examples of relevant material systems are simple solids (e.g., metals or organic and colloidal crystals), fluids (liquid argon, water, electrolytes, organic solvents) or systems of macromolecules (polymers, biomacromolecules such as DNA or proteins) and colloids (cells, micelles, hydrogel particles), and many more, all constituted by atoms and molecules. A complex material has many components and dynamic interactions between those, such that the material has certain properties which guarantee that the material can even perform useful functions (like a contact lens or a biological cell). Computational approaches, such as molecular dynamics (MD) simulations are a powerful and now standard (while steadily improved) tool in academia and industry to understand better the origins of a complex material function.

When we talk about materials from a macroscopic point of view, we can easily categorize them in states, e.g., fluid or solid. Obviously, their properties, for example, (visco)elasticity, are very different. The reason is the very different structural and dynamic behavior of their constituting atoms and molecules. The latter we can study with models in statistical physics and computer simulations. From insights of these models we can identify how microscopic structure changes macroscopic properties, i.e., we can try to establish 'Quantitative structure-property relations (QSPR)'. If these are known, we can try to design structure to optimize or generate a certain macroscopic property, a specific response to an external field, or a desired, useful function. Statistical thermodynamics ("Theory") gives us the models and analytical tools to define these QSPRs, which we deal with in Part I of the script. The numerical, molecular simulation models ("Simulation Methods"), most prominently MD simulations, provide the microscopic structure and dynamics in form of trajectory data and time averages. The technicalities of the simulations, in particular algorithms, force fields, and (thermodynamic) boundary conditions are described in Part II of this script.

Part I

Theory

Chapter 2

Phase diagrams and states

Let us first look at the phases of a so called "simple" system. A simple system has only one-component (one type) of particles, no external fields, and is interacting only with an isotropic pair potential, i.e., an interaction energy just depending on the scalar distance between a pair of particles. A simple system has only three states, or 'phases': vapor (or gas), liquid, and solid. Phase diagrams can be visualized either in a pressure (P)-temperature (T) representation as seen in Figure 2.1 or a temperature-density (ρ) representation as seen in Figure 2.2. For further reading, see standard thermodynamics books, for example [1], or the books by Hansen and McDonald or Barrat and Hansen [2, 3].

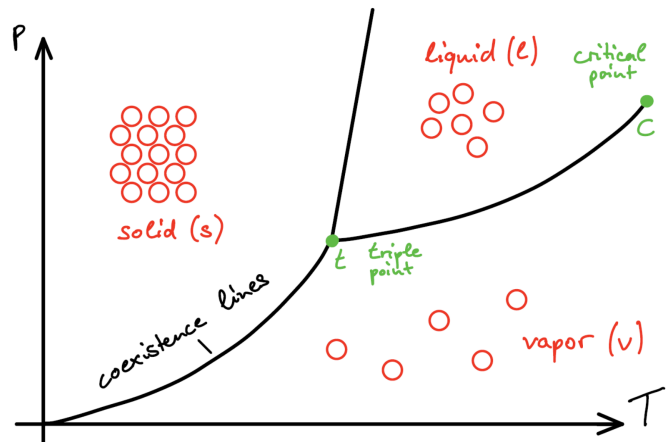


Figure 2.1: Displayed is the pressure P - temperature T phase diagram of a simple system with coexistence lines (black solid lines) between the states, solids, liquid, and vapor, and a triple point t as well as a critical point c . At the triple point, all three phases coexist. At the critical point, the distinction between liquid and vapor vanishes, then, beyond the critical point, often just called only 'gas'.

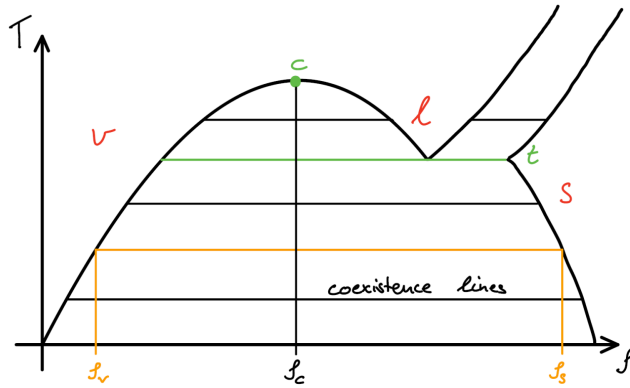


Figure 2.2: Displayed is the temperature T - density ρ diagram of a simple system with co-existence lines between the states and a triple line t as well as a critical point c at a critical pressure ρ_c . In such a diagram the coexisting densities (ρ_v and ρ_s in this example) can be easily read off. The coexistence lines are also called 'binodal lines' and can be constructed from a Maxwell-construction, see section 14.2, as taught in every basic Thermodynamics lecture. By the way, the 'spinodal lines' (not shown here) embrace the instability region in which the system compressibility diverges [2, 3].

The particle number density of a system is defined as

$$\rho = \frac{N}{V} \quad (2.1)$$

where N indicates the number of particles and V the fixed volume of the system. For an ideal gas, where particles do not interact in terms of attraction or excluded volume, and just statistical collisions of singular points are considered, we can easily write down the exact so-called (thermic) 'equation of state' (EOS),

$$P = P(N, V, T) = k_B T \rho, \quad (2.2)$$

providing a relation between state variables P , N , and T , and k_B is Boltzmann's constant. For the ideal gas also the 'caloric' equation of state for the energy $E(N, V, T)$ is exactly known and reads, $E = 3Nk_B T/2$. It does not depend on volume in the particular case of the ideal gas and consists only of kinetic energy K . (The $3k_B T/2$ energy per particle is explained in statistical mechanics from the equipartitioning theorem [1]).

A 'real gas' has corrections to the equation of state due to physical particle-particle interactions beyond point collision (only momentum exchange). This typically leads to a van der Waals (vdW) form of the EOS

$$(P + a\rho^2)(V - Nb) = k_B T, \quad (2.3)$$

where a is a pressure correction due to attraction, and b a volume correction due to excluded volume. Such an equation of state can already explain and derive liquid-vapor coexistence lines and critical points (see 14.2), as in the phase diagrams above. Attractions are needed to cluster particles into a liquid. Typically the attraction is of energetic origin and its action becomes stronger for lower temperatures. See also section 14.2 how to construct a phase diagram from inspecting the free energy behavior.

More generally one can expand the pressure in a virial expansion in orders of ρ :

$$\beta P/\rho = 1 + B_2 \rho^2 + \dots, \quad (2.4)$$

where $\beta = 1/k_B T$ and B_2 is the second virial coefficient. It can be derived from statistical mechanics that $B_2 = -(1/2) \int d\vec{r} [\exp(-\beta V(r)) - 1]$ just depends on the pair interaction potential

between particles, $V(r)$, where r is the particle-to-particle distance. This provides a tool to derive vdW EOS and construct phase diagrams from pair potentials, which are also an essential input in simulation models. Then, simulations can be compared and verified in some limits. The number density ρ does not describe the structural arrangements of particles. A measure for the structural arrangements is the so called "pair distribution function" $g(r)$ which gives the probability density of finding a second particle at a pair distance r , if the first one is fixed at $r = 0$. In Figure 2.3 the radial distribution function for the vapor, liquid and solid phase are shown. A proper statistical mechanics definition will come later in section 5 of the script.

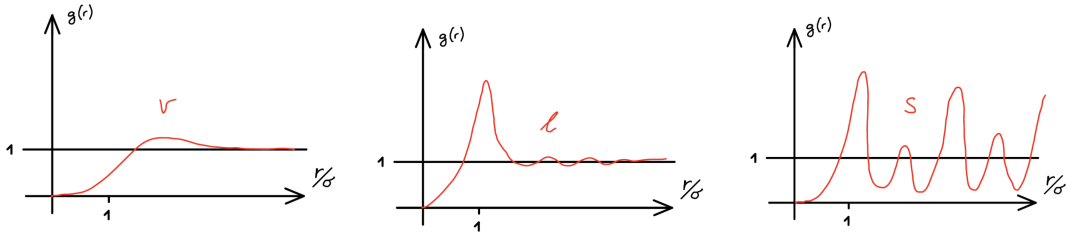


Figure 2.3: Shown is the pair distribution function of vapor v , liquid l and solid s phase. σ indicates the diameter of the particles. When particles pack densely, high probability peaks occur at distances of multiples of their diameter. Details depend on the pair potential and exact packing structure. In the ideal gas and very dilute phases, the $g(r)$ is close to unity as none or not much correlations exist. More concrete examples can be found in the Appendix or literature [2, 3].

The phases and the structure of systems, apart from thermodynamic variables such as T , P and ρ , are determined by atomic interactions. Specific examples of atomic interactions will follow in the next section.

Chapter 3

Interactions and potentials

To describe a system of N particles we consider their positions and momenta and how they change in time. These are trajectories in phase space $\{\vec{r}^N(t), \vec{p}^N(t)\}$. Generally, the trajectories derive from a Hamiltonian H of typical form

$$H = H_{\text{kin}} + H_{\text{ext}} + H_{\text{int}}. \quad (3.1)$$

The kinetic energy H_{kin} is defined as

$$H_{\text{kin}} \equiv \hat{K} = \sum_{i=1}^N \frac{\vec{p}_i^2}{2m_i} \quad (3.2)$$

with \vec{p}_i and m_i being the momentum and mass of the particle i , respectively, and the symbol $\hat{}$ indicates an instantaneous value (not an average). H_{ext} describes the action of an external potential V_{ext} (e.g., an electrostatic field)

$$H_{\text{ext}} = \sum_{i=1}^N V_{\text{ext}}(\vec{r}_i) \quad (3.3)$$

acting on particle i at position \vec{r}_i .

In general the force field can be defined by the negative gradient of the potential energy from particle-particle interactions:

$$\vec{F}_i = -\nabla_i H_{\text{int}}. \quad (3.4)$$

The instantaneous potential energy from particle-particle interactions can be approximated as

$$H_{\text{int}} \simeq \frac{1}{2} \sum_{i \neq j}^N V_{ij}^{(2)}(\vec{r}_i, \vec{r}_j) + \frac{1}{6} \sum_{i \neq j \neq k}^N V_{ijk}^{(3)}(\vec{r}_i, \vec{r}_j, \vec{r}_k) + \text{higher order contributions} \quad (3.5)$$

with $V^{(2)}$ being the pair potential and $V^{(3)}$ the three body contribution (see Fig. 3.1). The latter expresses the change in the interaction of two particles, if a third one approaches. It can often be neglected but its magnitude is system-dependent and should be scrutinized. It is for example non-negligible in highly polarizable systems. The pair potential approximation is applied almost in every study. Usually one simply denotes the pair potential with $V(r)$.

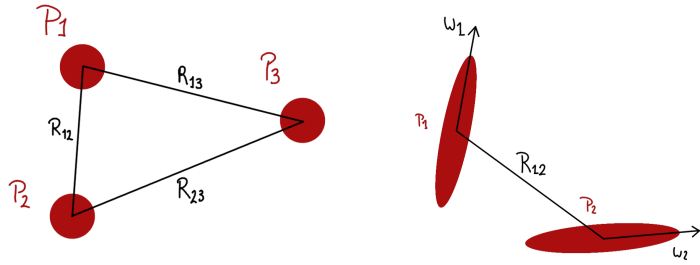


Figure 3.1: Pair potential, $V^{(2)}$, between particle i and j , and three body potential, $V^{(3)}$, represented by an angular potential.

Definition of a "simple" system:

- **consists of only pair potentials** (no triplet or higher order)
- **only distant dependent potentials** (no anisotropic (angle-dependent) potentials)
 $V(\vec{r}_1, \vec{r}_2) \equiv V(|\vec{r}_1 - \vec{r}_2|) \equiv V(r)$
- **no bonded potentials** (such as molecules, polymers etc.)

Definition of a "complex" system: everything else!

We will mostly discuss simple systems, in particular, when we talk about 'theory', but of course in simulations we want to address more complex systems, including, e.g., metals with many-body interactions or bonded molecules, such as complex solvents or polymers. A nice diagram of complexity of an interacting many-particle system is shown in Fig. 3.2.

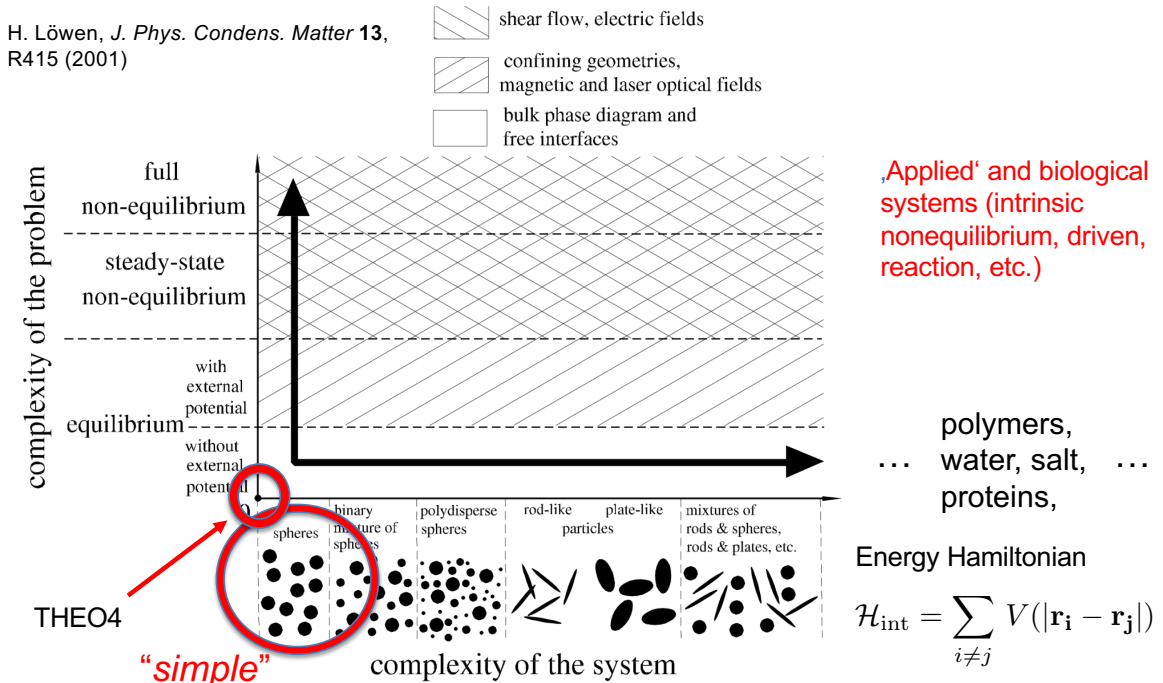


Figure 3.2: The complexity of a system can vary in shapes, polydispersity, and components (x -axis) and the form of external potentials, possibly driving the system out of equilibrium. Real systems are typically found on the top right corner of such a diagram.

Let us now look at some examples for pair potentials.

3.1 Interatomic pair potentials

With 'inter'-atomic potentials we mean interactions between atoms or particles which are not part of the same molecule. A very nice summary of interactions can be found in the book by Israelachvilli [4].

Except for the case of ideal gas where particles are not interacting with each other, i.e. $V(r) = 0$, all atoms have a **short-ranged** repulsion due to the Pauli exclusion principle (Born-Mayer 1932):

$$V_{\text{sr}}(r) = Ae^{-\alpha r} \quad (3.6)$$

Also all atoms have a dispersion (**van der Waals**) attraction due to the inherent fluctuating electronic polarization:

$$V_{\text{vdW}}(r) = -\frac{c_6}{r^6} \quad c_6 \equiv \text{material constant} \quad (3.7)$$

To model a complete atomic pair potential, both contributions have to be taken into account. The combination of both effects can be seen in Figure 3.3.

Combining both contributions we get the "**Buckingham**" pair potential for atoms (1938):

$$\begin{aligned} V_B(r) &= Ae^{-\alpha r} - \frac{c_6}{r^6} \\ &= \frac{\epsilon}{\alpha r_{\min} - 6} \left(6e^{-2\alpha(r-r_{\min})} - \alpha r_{\min} \left(\frac{r_{\min}}{r} \right)^6 \right) \end{aligned} \quad (3.8)$$

or, a slightly modified but more popular version, the **Lennard-Jones** pair potential (~1930):

$$\begin{aligned} V_{\text{LJ}}(r) &= 4\epsilon \left(\left(\frac{\sigma}{r} \right)^{12} - \left(\frac{\sigma}{r} \right)^6 \right) \\ &= \epsilon \left(\left(\frac{r_{\min}}{r} \right)^{12} - 2 \left(\frac{r_{\min}}{r} \right)^6 \right) \end{aligned} \quad (3.9)$$

with the identities $r_{\min} = \sigma^{2/6}$ and $V_{\text{LJ}}(\sigma) = 0$ and $V_{\text{LJ}}(r_{\min}) = -\epsilon$. The approximation of the short-ranged part as r^{-12} is simply taken for convenience as this way it just becomes also a power-law, like the van-der-Waals-potential $\propto r^{-6}$.

In shorter terms with $A = 4\epsilon\sigma^{12}$ and $C = 4\epsilon\sigma^6$ we can write

$$V_{\text{LJ}}(r) = \frac{A}{r^{12}} - \frac{C}{r^6} \quad (3.10)$$

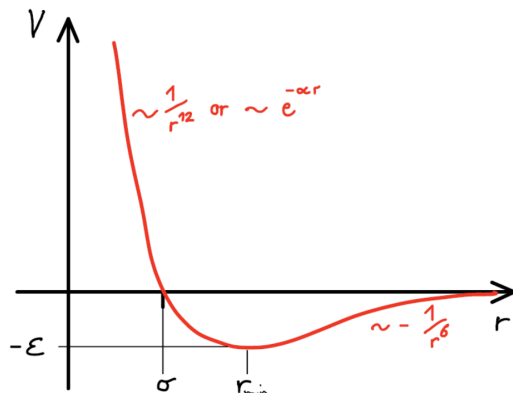


Figure 3.3: Schematic Lennard-Jones atomic pair potential with minimum at r_{\min} .

The Lennard-Jones force is thus given by the negative gradient of $V_{\text{LJ}}(r)$:

$$F_{\text{LJ}}(r) = -\nabla_r V_{\text{LJ}}(r) = 4\epsilon \left(12 \frac{\sigma^{12}}{r^{13}} - 6 \frac{\sigma^6}{r^7} \right) \quad (3.11)$$

The generalization of the 12-6 Lennard-Jones potential is the **n-m Mie potential**:

$$V_{\text{n-m}}(r) = \frac{\epsilon}{m-n} \left(\frac{m^m}{n^n} \right)^{\frac{1}{m-n}} \left(\left(\frac{\sigma}{r} \right)^m - \left(\frac{\sigma}{r} \right)^n \right) \quad (3.12)$$

with the identities $r_{\min} = \epsilon \left(\frac{m}{n} \right)^{\frac{1}{m-n}}$ and $V_{\text{n-m}}(\sigma) = 0$. The prefactor is defined such that ϵ still describes the minimum energy of the potential. Due to the arbitrary exponents it is a very versatile potential form to fit, e.g., coarse-grained macromolecular interactions.

The **Morse-potential** is an intramolecular potential which can be described as the following:

$$V_{\text{Morse}}(r) = \epsilon \left(e^{-2\alpha(r-r_{\min})} - 2e^{-\alpha(r-r_{\min})} \right) \quad (3.13)$$

It is a good model for metals as the potential is more "bonding"-like.

The **Weeks, Chandler, Anderson** (WCA) pair-potential, is an intermolecular potential to describe interactions for all particles on all scales, i.e. colloid ($\approx 10 - 100$ nm macromolecules dispersed in a solvent, blood, cells bacteria, ...). The WCA potential is well suited to describe short ranged, steric "excluded volume" repulsion. It is like a step repulsion which goes to zero at $r = \sigma 2^{1/6}$. The functional form of the WCA is given by:

$$V_{\text{WCA}}(r) = \begin{cases} V_{\text{LJ}}(r) + \epsilon & \text{if } r \leq \sigma 2^{1/6} \\ 0 & \text{otherwise} \end{cases} \quad (3.14)$$

If we consider charged, **Ionic materials**, we have to take into account Coulomb interactions:

$$\frac{V_C}{k_B T}(r) = \frac{\lambda_B}{r} Z_1 Z_2 \quad (3.15)$$

where Z_i indicates the ion valency and $\lambda_B = \frac{e^2}{4\pi\epsilon_0\epsilon k_B T}$ the Bjerrum length. The Bjerrum length indicates the separation at which the electrostatic interaction between two elementary charges is comparable in magnitude to the thermal energy scale, $k_B T$.

For charge-induced polarization the potential is given as:

$$V_{\text{pol}}(r) = -\frac{Z^2 \alpha}{2(4\pi\epsilon_0)^2} \frac{1}{r^4} \quad (3.16)$$

where α is polarization and Z is the ion valency.

The **Born-Mayer potential** is a way to describe ions by combining the short-ranged potential with the Coulomb potential:

$$V_{ij}(r) = A e^{-2r_{ij}} + \frac{B}{r_{ij}} Z_i Z_j \quad (3.17)$$

This works well for ionic crystals as for example $i = +, -$ in a NaCl-crystal (sodium chloride).

Ions in water

Alternatively one could use the Lennard-Jones with the Coulomb potential for ions in water:

$$\frac{V_{ij}}{k_B T} = \frac{4\epsilon}{k_B T} \left(\left(\frac{\sigma}{r} \right)^{12} - \left(\frac{\sigma}{r} \right)^6 \right) + \frac{\lambda_B}{r_{ij}} Z_i Z_j \quad (3.18)$$

which is a very popular version in literature, in particular for molecular simulations in biophysics.

More complicated interactions for molecules ("force fields") can be built by including *bonded* potentials, as discussed later in this script (polymers in Part I and force fields in Part II). The quantum and statistical mechanics of simple molecules (for instance, bond vibration energy and entropy, distributions, etc.) can be found in advanced stat. mech. books, as the McQuarrie (perhaps included later in this script, also on possible demand of students.)

paragraphHard sphere potential

Finally, we note also on a simple model pair potential between two particles: the **hard-sphere/disk** (HS) potential is a convenient potential to model particles in the statistical mechanical theory of fluids and solids for all scales. It's particularly a good model for simple colloids, that is, mesoscale spherical macromolecules, see also chapter 6 on coarse-graining. Within this potential, particles are defined simply as impenetrable spheres/disks that cannot overlap in space. The functional form of such a model is given by:

$$V_{HS}(r) = \begin{cases} \infty & \text{if } 0 \leq r \leq \sigma \\ 0 & \text{otherwise} \end{cases} \quad (3.19)$$

Note there is no energy in the system in equilibrium (no overlapping states)! Hence, the whole system behavior is only driven by entropy. It is such a good reference model for 'excluded-volume' interactions. The packing fraction defines the fraction of space filled by particles brought together. Assuming hard-sphere with diameter σ , the packing fraction is defined as:

$$\phi = \frac{\pi}{6} \sigma^3 \frac{N}{V} = v_{HS} \rho \text{ with } 0 < \phi < 1 \quad (3.20)$$

where $v_{HS} = \frac{4}{3}\pi r^3$ and ρ being the HS volume and the density, respectively. As sketched in fig. 3.4, a first order transition between liquid/gas and solid occurs for $0.45 < \phi < 0.58$, while $\phi = 0.74$ corresponds to a closed-packed structure such the one obtained for a fcc crystal structure. The reason for the phase transition is that the free volume per sphere can be increased (leading to a maximization in entropy) by assuming an ordered crystal state. Hence, in a hard system order is driven by entropy!

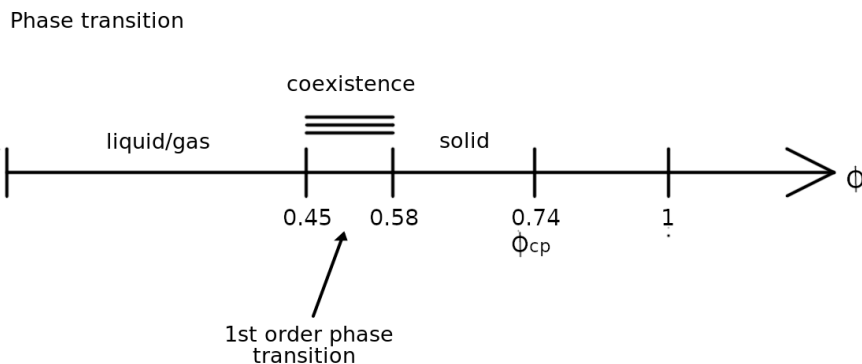


Figure 3.4: Phase (liquid/solid) as a function of the packing fraction.

3.2 Many-body potentials: MEAM (Modified Embedded Atom Method)

The MEAM is a good model for the description of metals. To describe these highly polarizable and weakly 'bonded' systems well, however, many-body potentials are required. Here, the total energy of an atomic system, E , is calculated by summing over the individual 'embedding energies' F_i (\neq force!) of each atom i in the atomic aggregate, defines as in the following:

$$E = \underbrace{\sum_i F_i \left(\sum_{i \neq j} \rho^{(i)}(r_{ij}) \right)}_{\text{energy it costs to introduce atom in environment}} + \underbrace{\frac{1}{2} \sum_{ij} \Phi_{ij}(r_{ij})}_{\text{pair potential}} \quad (3.21)$$

with j being any neighbouring atom, r_{ij} the distance between i and j , Φ_{ij} the pair potential, and $\rho^{(i)}$ the electron density.

First we will have to define the parameters Φ_{ij} , $F_i(\rho)$ and $\rho(r_{ij})$.

Embedding Function:

$$F(\rho) = AE_c \frac{\rho}{\rho_e} \ln \frac{\rho}{\rho_e} \quad (3.22)$$

ρ denotes the background electron density, whereas ρ_e is the electron density evaluated at the equilibrium in the reference structure. E_c is the cohesive energy in the reference structure and A represents an adjustable parameter.

Pair Potential:

$$E(r) = -E_c \left(-\alpha \left(\frac{r}{r_e} - 1 \right) \right) e^{-\alpha(\frac{r}{r_e} - 1)} \quad (3.23)$$

with $\alpha^2 = \frac{9\Omega B}{E_c}$ where r_e denotes the nearest neighbour distance, Ω the atomic volume and B the bulk modulus.

In equilibrium the pair potential reduces to:

$$E \Big|_{\text{eq.}} = -E_c \quad \frac{dE}{dr} \Big|_{\text{eq.}} = 0 \quad \frac{d^2E}{dr^2} \Big|_{\text{eq.}} = \frac{9\Omega B}{r_e^2} \quad (3.24)$$

Electron Density

ρ^2 is defined as the sum of terms with s, p, d, f symmetry from neighbouring $t^{(1)} \propto$ MEAM parameter atoms.

$$\rho^2 = \sum_{h=0}^3 t^{(h)} \left(\rho^{(h)} \right)^2 \quad (3.25)$$

with $h = 0 - 3$ correspond to s, p, d, f symmetry and $\rho^{(h)}$ being the partial electron density.

We normalize everything with respect to the s symmetry:

$$t^{(0)} = \Lambda \Big|_{t^{(1)}, t^{(2)}, t^{(3)}} \quad (3.26)$$

For $\rho^{(h)} \ll \rho^{(0)}$, $h = 1 - 3$ the Taylor expansion is

$$\rho = \rho^{(0)} \left(1 + \frac{1}{2} \sum_{h=1}^3 t^{(h)} \frac{\rho^{(h)}{}^2}{\rho^{(0)}} + \dots \right) \quad (3.27)$$

For $t^{(h)} < 0$ these equations have the potential of yielding a negative density or square of density for particular atomic configuration. An alternative for ρ is to take the asymptotic value:

$$\rho = \rho^{(0)} \exp \left\{ \frac{1}{2} \sum_{h=1}^3 t^{(h)} \frac{\rho^{(h)}}{\rho^{(0)}}^2 \right\} \quad (3.28)$$

In the model s, p, d, f ($\rho^{(0)}, \rho^{(1)}, \rho^{(2)}, \rho^{(3)}$) can be a measure of volume, polarization, shear, lack of inversion of symmetry.

The contribution of the density is given by:

$$\rho^{(0)} = \sum_u f^{(0)}(r^u) \quad (3.29)$$

$$\left(\rho^{(1)} \right)^2 = \sum_i \sum_{uv} f^{(1)}(r^u) f^{(1)}(r^v) \frac{r_i^u r_i^v}{r^u r^v} \quad (3.30)$$

where u, v represent the neighbouring atoms, $f^{(h)}(r)$ are radial functions that represent a decrease in the contribution with distance and i, j, k describe the 3 coordinates.

$$\left(\rho^{(2)} \right)^2 = \sum_{ij} \sum_{uv} f^{(2)}(r^u) f^{(2)}(r^v) \frac{r_i^u r_j^u r_i^v r_j^v}{(r^u r^v)^2} - \frac{1}{3} \sum_{uv} f^{(2)}(r^u) f^{(2)}(r^v) \quad (3.31)$$

r_i^u is the component i of the vector r^u connecting two neighbouring atoms.

The above equations can be rewritten via

$$\sum_i \frac{r_i^u r_i^v}{r^u r^v} = \cos \theta^{uv} \quad (3.32)$$

where θ^{uv} is the angle at atom site between the neighbours u and v .

The radial functions $f^{(h)}(r)$ can be approximated to

$$f^{(h)}(r) = \exp \left\{ -\beta^{(h)} \left(\frac{r}{r_e} - 1 \right) \right\} \quad (3.33)$$

as in chemistry the electron density roughly decreases exponentially with increasing distance r .

For $t^{(1)} = t^{(2)} = t^{(3)} = 0$ and $\rho = \rho^{(0)} = f^{(0)}(r) = \exp \left\{ -\beta^{(0)} \left(\frac{r}{r_e} - 1 \right) \right\}$ this approach equals the **EAM**.

The **MEAM** parameters and their relation to material properties are given in Table 3.1.

| parameter | material parameter | relation |
|---------------|------------------------------|--|
| E_c | sublimation energy | |
| r_e | atomic volume | $r_e^3 = \sqrt{2}\Omega$ |
| α | bulk modulus | $\sqrt{9\Omega B/E_c}$ |
| A | BCC \rightarrow FCC energy | numerical |
| $\beta^{(0)}$ | magnitude of instable fault | numerical |
| $\beta^{(1)}$ | internal relaxation | fixed |
| $\beta^{(2)}$ | shear elastic constant | numerical |
| $\beta^{(3)}$ | surface relaxation | numerical |
| $t^{(1)}$ | vacancy formation energy | $(t^{(1)} + \frac{2}{3}t^{(2)} + t^{(3)}) = \text{const.}$ |
| $t^{(2)}$ | shear elastic constant | numerical |
| $t^{(3)}$ | c/a or FCC \rightarrow HCP | numerical |
| C_{\max} | iterative process | numerical |
| C_{\max} | iterative process | numerical |

Table 3.1: **MEAM** parameters and their relation to material parameters as well as the calculation approach.

The pair potential between two atoms separated by R is given by:

$$\Phi(R) = \frac{2}{Z}(E^u(R) - F(\rho_0(R))) \quad (3.34)$$

where Z equals the number of first atoms, $\rho_0(R)$ represents the background of the electron in the reference structure and $E(R)$ denotes the energy of atom in the reference structure as a function of the distance from DFT or from universal equation of state by Rose et al. (1984) [19].

Rather than being only radial, the MEAM framework introduces an angular dependency to smooth out the interatomic interaction.

Angular screening

There is a need to limit the range of interaction. Both atomic electron density, $\rho^{(h)}$, and pair potential between i and k , $\Phi(R_{ik})$, are multiplied by a screening function S_{ik} that ranges from 0 to 1 as seen in Figure ... resulting in

$$\bar{\Phi}_{ij} = \Phi_{ij}(R_{ij})S_{ij} \quad (3.35)$$

as well as

$$\rho^{(0)} = \sum_u f^{(0)}(r^u) \rightarrow \rho_i^{(0)} = \sum_{i \neq j} f^{(0)}(r_{ij})S_{ij} \quad (3.36)$$

where u is the sum over all pair of neighbouring atoms and i and j are first neighbours.

The screening function is thus given by a product of function S_{ijk} dependent on atoms j that are located between i and k :

$$S_{ik} = \prod_{j \neq i, k} S_{ijk} \quad (3.37)$$

To evaluate S_{ijk} , we consider the ellipse that passes through i , j and k with the minor axis of the ellipse determined by the distance between i and k as seen in Figure ... The equation of the ellipse is given by:

$$x^2 + \frac{1}{c}y^2 = \left(\frac{1}{2}r_{ik}\right)^2 \quad \text{with} \quad c = \frac{2(x_{ij} + x_{jk}) - (x_{ij} - x_{jk}^2 - 1)}{1 - (x_{ij} - x_{jk})^2} \quad (3.38)$$

where $x_{ij} = \left(\frac{r_{ij}}{r_{jk}}\right)^2$ and $x_{jk} = \left(\frac{r_{jk}}{r_{ik}}\right)^2$.

1. if atom j is equidistant from i and k , then $x_{ij} = x_{jk}$. This configuration represents an equilateral triangle of the three nearest neighbours in the FCC structure. This results in $c = 3$.
2. if i and k are second neighbours in a BCC structure with j as a first neighbour to i and k , then this results in $c = 2$.

1 and 2 are the limiting case for perfect or no screening.

Chapter 4

Recap of thermodynamics and statistical mechanics

Statistical mechanics and Thermodynamics are well introduced and summarized, for example, in [1, 2].

4.1 Basic thermodynamic quantities

For convenience, here follows a brief summary of your thermodynamics lectures. Thermodynamics is essential to characterize materials, because it shows us how state variables depend on each other and how we can derive material properties from state functions or thermodynamic potentials. In simulations one can often 'measure' some of the variables and thermodynamics helps us to derive other important properties. Many variables that describes states ("state variables") exist, such as volume V or pressure P , which can be extensive or intensive, respectively. Thermodynamics provides (often using differential forms) useful relations between these state variables. In particular, derivatives of thermodynamic potentials with respect to their natural variables deliver other important state variables. Thermodynamic potentials are linked with Legendre Transforms. If you have forgotten about this, it would be useful to recall the basics by looking into a standard thermodynamics book (e.g., Greiner *et al.* [1]).

| | | |
|--------|---------------------------|---|
| N | number of particles | extensive ~ scale linearly with system size |
| V | volume | |
| K | kinetic energy | |
| U | potential energy | |
| E | internal energy ($U+K$) | |
| S | entropy | |
| H | enthalpy ($E+PV$) | |
| ρ | density | intensive independent of system size |
| P | pressure | |
| T | temperature | |
| μ | chemical potential | |

| Thermodynamic potentials | natural variables | standard differential forms |
|--------------------------|--------------------------------|-----------------------------|
| Internal energy | E | NVS |
| Helmholtz free energy | $F = E - TS$ | NVT |
| Gibbs free energy | $G = H - TS$ | NPT |
| Grand potential | $\Omega = E - TS - \mu N = PV$ | μVT |

Table 4.1: Thermodynamic potentials and their natural variables related by the standard differential forms obtained by Legendre transformation. The index i here goes over particle types in a multi-component system. The particle number per type i is N_i .

Useful relations using the example of the Helmholtz free energy:

$$S = -\left(\frac{\partial F}{\partial T}\right)_{V,\{N_i\}} \quad P = -\left(\frac{\partial F}{\partial V}\right)_{T,\{N_i\}} \quad \mu_i = \left(\frac{\partial F}{\partial N_i}\right)_{T,V,\{N_i\}} \quad (4.1)$$

Maxwell relations follow from the second (mixed) derivatives, e.g.:

$$\left(\frac{\partial S}{\partial N_i}\right)_{T,V,\{N_i\}} = -\left(\frac{\partial \mu_i}{\partial T}\right)_{V,\{N_i\}} \quad (4.2)$$

The Gibbs-Duhem relation

$$SdT - VdP + \sum_i N_i d\mu_i = 0 \quad (4.3)$$

is an useful relationship between intensive parameters, e.g., for fixed T and only a one-component system, $i = 1$, $\frac{\partial \mu}{\partial P} = \rho$

These relations are particularly useful in computer simulations. For example, some variables, such as free energy or entropy, are not easy to access directly. But we can access better, e.g., the pressure as a function of volume and then integrate it to get a free energy. Or, if one knows how the free energy changes in the simulation with temperature, one can access the entropy by the derivative $S = -(\partial F / \partial T)_{N,V}$.

All material descriptors (even structure in density functional theory (DFT) framework) can in principle also be derived from the free energy or related state variables. For example, the isothermal compressibility χ_T

$$\chi_T = -\frac{1}{V} \left(\frac{\partial V}{\partial P}\right)_T \quad (4.4)$$

is the inverse of the bulk modulus $K = \chi_T^{-1}$ and related to the linear elasticity $\frac{\Delta V}{V} = \chi_T P$. Generalization to anisotropic stress (tensors) and nonlinear elasticity are contents of the field of 'Continuum Mechanics' and important in finite-element method (FEM) simulations in engineering.

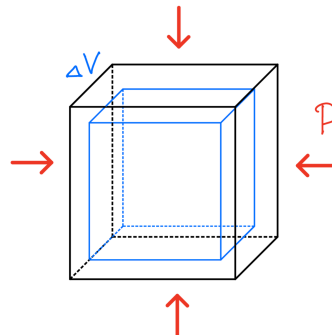


Figure 4.1: Deformation of a volume by ΔV under constant pressure P can be described by the bulk modulus $K = \chi_T^{-1}$.

Another important example is the heat capacity:

$$c_V = \left(\frac{\partial E}{\partial T} \right)_V \quad \text{isochoric heat capacity} \quad (4.5)$$

$$c_P = \left(\frac{\partial E}{\partial T} \right)_P \quad \text{isobaric heat capacity} \quad (4.6)$$

from which the relation

$$c_P - c_V = VT \frac{\alpha^2}{\chi_T} \quad (4.7)$$

with α being the thermal expansion coefficient, $\alpha = \left(\frac{\partial V}{\partial T} \right)_P$ can be acquired [1].

4.2 Macro- vs. microstates

What we just discussed are the "macrostates" as thermodynamical states of a system, e.g., they describe the average properties of a system with some natural variables, for example N , V and T ("thermodynamical constraints") for the Helmholtz free energy F in a closed system.

In contrast, the "microstate" describes an instantaneous realization, e.g., a state with the kinetic energy $\sum_i^N p_i^2/2m$ for identical particles of mass m and momentum p_i and the interaction potential energy $H_{\text{int}} = \frac{1}{2} \sum_i^N \sum_j^N V(|\vec{r}_i - \vec{r}_j|)$ at a time t and given positions \vec{r}_i of the particles. Recall, we try to denote microstate operators with $\hat{\cdot}$, that is, describing the value of a microstate and not an average. Note that in macroscopic thermodynamics, for reasons of notation brevity explicit average symbols which we introduce in the following, $\langle \dots \rangle$, are usually dropped. For example, $E = \langle \hat{E} \rangle$.

The connection between both macro- and micro-states is given by *statistical mechanics*. A microstate is defined as a point $\{\vec{r}^N(t), \vec{p}^N(t)\}$ in the $6N$ -dimensional *phase space* with:

$$\vec{r}^N = \{\vec{r}_1, \dots, \vec{r}_N\} \quad \text{and} \quad \vec{p}^N = \{\vec{p}_1, \dots, \vec{p}_N\} \quad (4.8)$$

Given an instantaneous realization of the quantity $X(\{\vec{r}^N\}; \{\vec{p}^N\})$ we can define the time average \overline{X} of the phase space trajectories as:

$$\overline{X} = \frac{1}{\tau} \int_0^\tau X(t) dt \quad (4.9)$$

whereas τ should be long enough to sample a representative region of the phase space. This is what you learned in statistical mechanics in terms of 'Ergodicity'. If a system is ergodic (which is a good assumption for most systems as demonstrated by Liouville's theorem in statistical mechanics [1]), we do not have to follow the dynamic trajectory because we know the system 'samples' phase space in some representative fashion. For example, all states of the same fixed energy are equally frequently visited in isolated systems (in stat. mech. the 'microcanonical ensemble') which is the most fundamental theorem of statistical mechanics. In closed systems ('canonical ensembles'), phase space is sampled according to the Boltzmann weight.

Hence, for equilibrium properties we do not care about the path in time, just the probability in being a microstate and corresponding representative sampling. We define a "statistical ensemble" as a large number of possible realization of the system and its states the system can realize with a probability $w(\{\vec{r}^N\}; \{\vec{p}^N\})$. The important ensemble average $\langle X \rangle$ is then given by:

$$\langle X \rangle = \text{tr} \left(X(\{\vec{r}^N\}; \{\vec{p}^N\}) w(\{\vec{r}^N\}; \{\vec{p}^N\}) \right)$$

with trace $\text{tr} = \frac{1}{h^{3N} N!} \int d\vec{r}_1 \dots \int d\vec{r}_N \int d\vec{p}_1 \dots \int d\vec{p}_N$

(4.10)

whereas w is normalized by $\text{tr}(w) = 1$. Recall, the normalization prefactor $1/(h^{3N} N!)$ originates from two things: the phase space has a quantum nature and is discrete with a coarseness

given by Planck's constant h . For N particles in three dimensions, thus the unit h^{3N} . In addition, in classical statistical mechanics (Boltzmann) we have to correct for the quantum indistinguishability of particles and consider the Gibb's factor $1/N!$ to not overcount microstates in phase space.

Depending on the thermodynamical natural variables we have different statistical ensembles. Here are three important examples:

- **Microcanonical ensemble** (isolated system with $E = \text{const.}$ and natural variables NVS)

$$\boxed{\begin{aligned} w &= \frac{1}{z} \delta(E - H) & z &= \text{tr}(\delta(E - H)) \\ S &= k_B \ln z & & (\text{Boltzmann entropy}) \end{aligned}} \quad (4.11)$$

- **Canonical ensemble** (closed system, NVT)

$$\boxed{\begin{aligned} w &= \frac{1}{Z} e^{-\beta H} & Z &= \text{tr}(e^{-\beta H}) \\ && & \text{Boltzmann weight and canonical partition sum} \\ F(N, V, T) &= -k_B \ln Z & & (\text{free energy}) \end{aligned}} \quad (4.12)$$

- **Grand canonical ensemble** (open system, μVT , particle exchange with a reservoir governed by the chemical potential μ)

$$\boxed{\begin{aligned} w &= \frac{1}{\Xi} e^{-\beta(H-\mu N)} & \Xi &= \text{tr}(e^{-\beta(H-\mu N)}) \\ \Omega(\mu, V, T) &= -k_B \ln \Xi & & (\text{grand potential}) \end{aligned}} \quad (4.13)$$

In general, the system is always described by a Hamiltonian $H = H(\{\vec{r}^N\}; \{\vec{p}^N\})$, which describes the energy of a microstate. Quite generally, we can write

$$H = \sum_i^N \frac{p_i^2}{2m} + H_{\text{int}}\{\vec{r}^N\} + H_{\text{ext}}\{\vec{r}^N\}, \quad (4.14)$$

where the first term is the microstate kinetic energy $\hat{K} = \sum_i p_i^2 / (2m)$ (assuming all particles are identical with mass m), an interaction energy H_{int} , depending only on positions, and an external potential H_{ext} , also depending only on the positions. The interaction potential is often assumed to be a sum of pair potentials, that is, $H_{\text{int}} = (1/2) \sum_i \sum_j V(r_{ij})$, where $r_{ij} = |\vec{r}_i - \vec{r}_j|$ is the pair distance. Both, interactions and external potential, contribute to the total (instantaneous) potential energy \hat{U} .

In an isolated system, represented by the microcanonical ensemble, the system energy is fixed to H and conserved. The sum of the potentials H_{int} and V_{ext} we can identify as operator \hat{U} , the potential energy of a microstate, while $\hat{E} = H$ includes also the kinetic energy. In the canonical ensemble, the state probability is weighted according to the Boltzmann weight $\propto \exp(-\beta H)$ at fixed (bath) temperature T [1].

As an example, we sketch the results for the ideal gas in the canonical ensemble in the absence of an external field. Here, all interactions vanish in the Hamiltonian and only the kinetic term remains. The partition sum (from eqs. (4.10), (4.12), and (4.14)) factorizes for the N particles and can be easily integrated out to

$$Z_{\text{id}} = \frac{1}{N!} \frac{V^N}{\Lambda^{3N}} \quad (4.15)$$

The momenta in particular were integrated out, as

$$\int d\vec{p}^N e^{-\beta \hat{K}} = \int d\vec{p}^N w_p = (2\pi m k_B T)^{\frac{3N}{2}} = \left(\frac{h}{\Lambda}\right)^{3N} \quad (4.16)$$

defining the thermal (de Broglie) wavelength Λ

$$\Lambda = \sqrt{\frac{h^2}{2\pi m k_B T}}. \quad (4.17)$$

In between we identify the Maxwell-Boltzmann velocity distribution in equilibrium for the absolute velocity $v = p/m$:

$$p(v) = 4\pi \left(\frac{m}{2\pi k_B T}\right)^{3/2} v^2 e^{-\frac{v^2}{2k_B T}}, \quad (4.18)$$

that is, $p(v)dv$ telling us the probability of finding a particle with absolute velocity v in the interval dv . Similar distributions can be written for momenta, cartesian components of velocity, or the kinetic energy [1].

The free energy of the ideal gas follows as $F = -k_B T \ln Z_{\text{id}}$. This can be approximated for large $N \gg 1$ using the Stirling approximation $\ln N! \simeq N \ln N - N$ leading to

$$F_{\text{id}} = N k_B T [\ln(\rho \Lambda^3) - 1]. \quad (4.19)$$

Using known thermodynamic relations, such as $S = -\partial F / \partial T$ and $E = F + TS$, the ideal gas entropy and energy follows easily [1]. For the ideal gas, $E = K = \langle \hat{K} \rangle$, that is, we have only kinetic energy that contributes to the total energy.

4.3 Ergodicity and averages

Ergodic hypothesis:

The time average \bar{X} equals the ensemble average $\langle X \rangle$ for long times τ :

$$\boxed{\bar{X} \underset{\tau \rightarrow \infty}{=} \frac{1}{\tau} \int_0^\tau X(t) dt \equiv \langle X \rangle} \quad (4.20)$$

Ergodicity is challenging to achieve in most complex systems! In particular, in computationally expensive simulations, e.g., with many millions of atoms, often the system does not move out of (meta)stable minima in the energy landscape. Then only a sub-space of phase space is sampled. Typically this is defined via $\bar{X} = \langle X \rangle_{\text{local}}$, sampled from a "local equilibrium" (= local region in phase space). Hence, one has to be careful with the interpretation of averages. One should also critically think about systematic and statistical errors, see later in the simulation part.

In molecular dynamics simulations the application of the average is typically done in the canonical ensemble, where NVT is fixed. Typically, mean values and standard deviations are calculated, but more generally whole probability distributions are interesting to look at. Simple and typical examples for average mean values are the potential and kinetic energy in the canonical ensemble, via

$$\begin{aligned} U = \langle \hat{U} \rangle &= \frac{1}{Z_U} \int d\vec{r}^N \hat{U} e^{-\beta \hat{U}} \quad \text{with} \quad Z_U = \int d\vec{r}^N e^{-\beta \hat{U}} \\ K = \langle \hat{K} \rangle &= \frac{1}{Z_K} \int d\vec{r}^N \hat{K} e^{-\beta \hat{K}} \quad \text{with} \quad Z_K = \int d\vec{r}^N e^{-\beta \hat{K}} \end{aligned} \quad (4.21)$$

where in equilibrium statistical equipartitioning dictates that $\langle \hat{K} \rangle = \frac{3}{2} N k_B T$. In simulations it is important to watch these averages of $\hat{E} = \hat{U} + \hat{K}$ and \hat{K} because they tell us about behavior (conservation and drift) of total energy and temperature, respectively. We will reconsider the latter when we talk, for example, about thermostating a simulation. Other quantities are of course of interest as well in simulations. Since all trajectories (particle positions and velocities at time t) are in principle available, most observables can be directly averaged. In the next sections we will talk about averages of fluctuations but also about averages of structures, which have important physical meanings as well.

Note again, the entropy S and the free energy $F = U - TS$ are not directly accessible by averages, but from probability distributions ($F = -k_B T \ln P$) or T -dependencies ($S = -\frac{\partial F}{\partial T}$).

Chapter 5

Structure-property relationships

Liquid state theory is the overarching statistical mechanics framework to describe correlated, interacting systems, such as liquids. It is well discussed in [2].

5.1 From fluctuations to material properties

Materials properties can also be derived from the fluctuations of physical observables. Let us first recall what is a statistical variance and standard deviation (SD) of a variable x :

| | |
|--------------------|--|
| Ensemble mean | $\langle x \rangle$ |
| Variance | $\langle (\langle x \rangle - x)^2 \rangle = \langle x^2 \rangle - \langle x \rangle^2 = \sigma_x^2$ |
| Standard deviation | $\sigma_x = \sqrt{\sigma_x^2}$ |

(5.1)

When we talk about 'fluctuations' we mean exactly this, a variance or SD of an observable.

5.1.1 Heat capacity and compressibility

How are fluctuations related to macroscopic properties? Consider, for example, the definition of the average total energy $E = \langle \hat{E} \rangle$ in the canonical ensemble:

$$E = \text{tr} \left(\frac{1}{Z(T)} \hat{E} e^{-\beta \hat{E}} \right) \quad (5.2)$$

Thermodynamics tell us that the heat capacity is then obtained by the derivative of E with respect to T , at fixed volume:

$$\begin{aligned} \frac{\partial E}{\partial T} \Big|_V &= \text{tr} \left(\frac{1}{Z(T)} \frac{\hat{E}^2}{k_B T^2} e^{-\beta \hat{E}} \right) + \text{tr} \left(\hat{E} e^{-\beta \hat{E}} \left(\frac{1}{Z(T)^2} \frac{\partial Z(T)}{\partial T} \right) \right) \\ &= \frac{\langle \hat{E}^2 \rangle}{k_B T^2} + \text{tr} \left(\frac{\hat{E}}{k_B T^2} e^{-\beta \hat{E}} \left(\frac{\partial \ln Z}{\partial \beta} \right) \right) \\ &= \frac{1}{k_B T^2} \left(\langle \hat{E}^2 \rangle - \langle \hat{E} \rangle^2 \right) \\ &= \frac{\sigma_E^2}{k_B T^2} = c_V \end{aligned} \quad (5.3)$$

The heat capacity is thus given by the energy fluctuations in the canonical ensemble! It also scales with the size of the system $\sim N$, as $\sigma_E \sim \sqrt{N}$.

Relative Gaussian fluctuations $\frac{\sigma_E}{E} \sim \frac{\sqrt{N}}{N} = \frac{1}{\sqrt{N}}$ are thus very small for large systems. That is why we can talk about 'sharp' macroscopic state variables in thermodynamics.

Similarly one can show in the *NPT*-ensemble, that the compressibility χ_T is given by the volume fluctuations:

$$V k_B T \chi_T = \sigma_V^2 \quad (5.4)$$

whereas in an μVT -ensemble, it is given by the number fluctuations:

$$\frac{N^2}{V} k_B T \chi_T = \sigma_N^2 \quad (5.5)$$

Note again, standard deviation describes physical fluctuations of the system, not the error! Many other examples exist. Calculating mean AND fluctuations in theory and simulations is thus a very important way to connect to macroscopic observables.

5.1.2 Time correlation function

Fluctuations have a life time, i.e., it takes some time before a perturbation in the system relaxes away. These times are interesting for physical reasons (they tell us how fast a perturbation is 'forgotten') but also to estimate errors in our system, which can be particularly large if the simulation time is comparable to the system's fluctuation or 'memory' time scales.

To reveal in which way and how fast microscopic fluctuations decay, we define a time correlation function between two observables A and B :

$$\begin{aligned} C_{AB}(t, t') &= \langle A(t), B(t') \rangle \\ C_{AB}(\tau) &= \langle A(\tau), B(0) \rangle \\ &= \lim_{T \rightarrow \infty} \frac{1}{T} \int_0^T A(t + \tau) B(t) dt \end{aligned} \quad (5.6)$$

In practice, we average over all initial times in order to increase statistics. In other words, every time of the simulation can be taken as $t = 0$ from which the ACF can be defined as origin. This of course only makes sense for stationary systems, where observables depend only on $t - t'$ and not on absolute time t .

More general the correlation is given in reference to the mean:

$$C_{AB}(t) = \langle A(t) - \langle A \rangle \rangle \langle B(0) - \langle B \rangle \rangle \quad (5.7)$$

For convenience, it is often normalized to their means, i.e., $\tilde{C}_{AB}(\tau) = C_{AB}(\tau) / (\langle A \rangle \langle B \rangle)$

The auto correlation function (ACF) is defined as $C_{AA}(\tau)$.

Generally, time correlation functions are important to calculate macroscopic transport properties [1, 2]. One of the most important example for a correlation function is the velocity auto correlation function (VACF):

$$C_{vv}(t) = \langle \vec{v}(t) \vec{v}(0) \rangle \quad (5.8)$$

with $\langle \vec{v} \rangle = 0$ and $\langle \vec{v}^2 \rangle = \frac{3k_B T}{m}$ in equilibrium.

The normalized auto correlation function is then given by:

$$\tilde{C}_{vv}(t) = \frac{\langle \vec{v}(t) \vec{v}(0) \rangle}{\langle \vec{v}^2 \rangle} = \frac{3k_B T}{m} \langle \vec{v}(t) \vec{v}(0) \rangle. \quad (5.9)$$

Time correlation functions are important for various reasons. Apart from telling us about how fast and in what manner fluctuations and correlations decay in time, they are also helpful to estimate statistical errors of time series, cf. section ???. Integration over correlation functions also yield useful macroscopic dynamic features such as diffusion and friction, and also provide definition of linear response functions (in presence of perturbative fields). We will discuss in examples section ?? when we also know more about the dynamics of complex systems.

5.1.3 Einstein diffusion law (random walk)

The Einstein diffusion law is defined in three dimensions (3D) as

$$D = \lim_{t \rightarrow \infty} \frac{1}{6t} \langle \vec{r}^2 \rangle \quad (5.10)$$

with $\langle \vec{r}^2 \rangle$ being the mean square displacement (MSD) of the particles as seen in Figure 5.1. More generally, we can define the MSD for a particle i as $\langle (\vec{r}_i(t) - \vec{r}_i(0))^2 \rangle$ with initial position $r_i(0)$ and also average this over all particles, and over all initial times, to increase the statistics in evaluating the simulations. Note that the random walk is independent in every cartesian direction and we can also evaluate diffusion in every space directions, e.g., $D_x = \lim_{t \rightarrow \infty} \frac{1}{2t} \langle x^2 \rangle$, with a prefactor 2 in every cartesian direction.

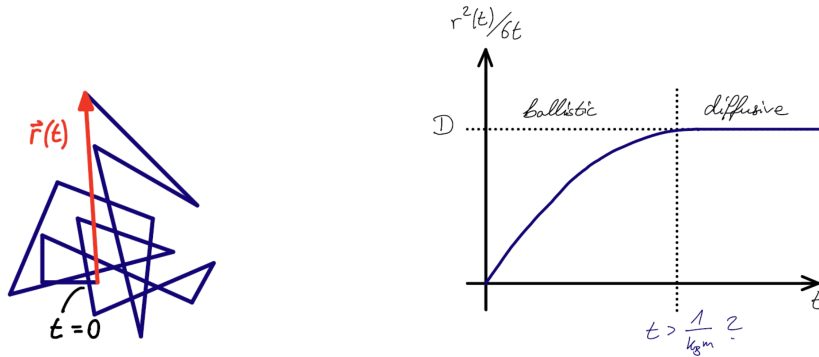


Figure 5.1: The MSD of the particles is given by averaging $\langle (\vec{r}(t) - \vec{r}(0))^2 \rangle$ over all \vec{r} . Depending on time t , a simple system, such as a free underdamped Brownian (or free 'Langevin') particle [3], can either behave ballistic (short-time) or diffusive (long-time). It typically converges to the long-time self-diffusion constant D for long times. For complex and dense systems, however, there can be many different dynamic regimes.

One can show that the MSD can be expressed by the VACF through

$$\langle \vec{r}^2 \rangle = 2t \int_0^t \langle \vec{v}(t') \vec{v}(0) \rangle dt' \quad (5.11)$$

which leads to the so called "Green-Kubo" relation [2]:

$$D = \lim_{t \rightarrow \infty} \frac{k_B T}{m} \int_0^t \tilde{C}_{vv}(t') dt' = \lim_{t \rightarrow \infty} \frac{1}{3} \int_0^t \langle \vec{v}(t') \vec{v}(0) \rangle dt' \quad (5.12)$$

with D being the long-time self diffusion constant. (D can not be defined this way for ideal, non-interacting systems as they behave fully ballistic. This definition is also problematic for solids and glasses, where diffusion is not possible on observation time scales, only local positional fluctuations.)

One can also show that the ACF of the force acting on a particle i leads to the friction constant

$$\xi_i = \frac{1}{3k_B T m} \int_0^\infty \langle \vec{F}_i(t') \vec{F}_i(0) \rangle dt' \quad (5.13)$$

with the forces $\vec{F}_i = -\sum_j \nabla V(|\vec{r}_i - \vec{r}_j|)$ as seen in Figure 5.2. Through the fluctuations-dissipation theorem (FDT) [3], the friction constant is related to the noise in Brownian motion.

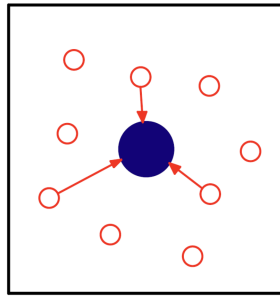


Figure 5.2: The force ACF is calculated using the forces derived from the pair potential $\vec{F}_i = -\sum_j \nabla V(|\vec{r}_i - \vec{r}_j|)$

In particular, in the simplest form of the FDT for memoryless (Markovian) stochastic processes, the diffusion D and the friction constant ξ are related by the Einstein relation (Einstein 1905!)

$$D = \frac{k_B T}{\xi m} \quad (5.14)$$

that is, system fluctuations (represented by the diffusion constant) are directly proportional to temperature, and also directly related (inversely proportional) to the dissipation in the system quantified by friction. The latter is a response to external perturbations and not *a priori* connected to fluctuations. However, the FDT and other historically important developments (Einstein, and, for example, Onsager's regression hypothesis [3]) have suggested and finally proven this fundamental connection.

Note:

- Similar Green-Kubo relations exist for bulk viscosity, shear viscosity and thermal conductivity (see Appendix)
- The short-time behaviour is linked to static averages and fluctuations, e.g.

$$\langle \vec{v}(t) \vec{v}(0) \rangle \simeq \frac{3k_B T}{m} \left(1 - \frac{\langle |\vec{F}_i|^2 \rangle}{6mk_B T} t^2 + \dots \right), \quad (5.15)$$

defining the so-called Einstein frequency in solids [2].

- Again, fluctuations connect to macro-observables, such as transport by diffusion or friction!

5.2 From the structure to material properties in the canonical ensemble

5.2.1 The one-body density profile $\rho(\vec{r})$

Let us first define and discuss how we can describe the microscopic structure of a many-body system. Then we can try to relate it to a macroscopic material property. First, we consider the "one particle density operator":

$$\hat{\rho}_0 = \sum_{i=1}^N \delta(\vec{r}_i - \vec{r}) \quad (5.16)$$

with \vec{r}_i denoting the position of particle i and δ being the Dirac-function, defined as:

$$\begin{aligned}\int \delta(x) dx &= 1 \\ \int \delta(x - x') f(x') dx' &= f(x).\end{aligned}\quad (5.17)$$

The ensemble average of the so-called "one particle density operator" leads to the equilibrium *one-body* density distribution:

$$\rho_0(\vec{r}) = \left\langle \sum_{i=1}^N \delta(\vec{r}_i - \vec{r}) \right\rangle \equiv \rho^{(1)}(\vec{r}) \equiv \rho(\vec{r}) \quad (5.18)$$

Note that without any external potential $V_{\text{ext}} = 0$, the density distribution is isotropic $\rho(\vec{r} + \vec{a}) = \rho(\vec{r})$ and constant $\rho = \frac{N}{V}$. With an applied external potential though, the density becomes inhomogeneous, cf. Fig. 5.3A. In a simulation setup, often one considers inhomogeneities in one dimensions, such as a fluid confined between two walls. Then the profiles can be obtained statistically by averaging the number of particles in small bins (with meaningfully chosen size), cf. Fig. 5.3B. By dividing by bin size and lateral box area A , one gets the correct units of number density (number per volume).

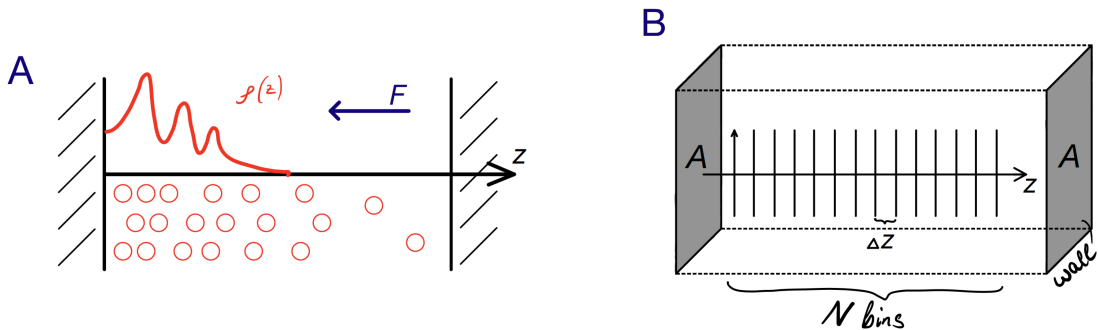


Figure 5.3: A: The density distribution $\rho(z)$ of a fluid in an uniform external force F . Due to packing effects one has a non-trivial layering and inhomogeneities. (This can be compared to an ideal gas in the same field, where the profile is given by the 'barometric height law' $\rho_{\text{id}}(z) = \rho_0 e^{-\beta F z}$.) B: The binning representation with bin size Δz . The density distribution is obtained in a simulation by averaging the number of particles per bin $\langle n \rangle(z) \rightarrow \rho(z) = \frac{\langle n \rangle}{A \Delta z}$, and normalizing by bin volume with bin size Δz and lateral box (wall) area A .

5.2.2 The radial distribution function, $g(r)$

The density operator can be generalized for the two-particle density:

$$\rho^{(2)}(\vec{r}, \vec{r}') = \left\langle \sum_{i \neq j}^N \delta(\vec{r}_i - \vec{r}) \delta(\vec{r}'_j - \vec{r}') \right\rangle \quad (5.19)$$

This method works for $\rho^{(n)}$ analogously. For $\rho^{(2)}$, the pair distribution function (PDF) can be derived via a normalization:

$$g(\vec{r}, \vec{r}') = \frac{\rho^{(2)}(\vec{r}, \vec{r}')}{\rho_0(\vec{r}) \rho_0(\vec{r}')} \quad (5.20)$$

If no external potential is applied, $V_{\text{ext}} = 0$, then the PDF $g(\vec{r}, \vec{r}')$ is isotropic and it follows:

$$\begin{aligned} g(\vec{r}, \vec{r}') &\equiv g(|\vec{r} - \vec{r}'|) \equiv g(r) \\ &= \frac{1}{\rho N} \left\langle \sum_{i \neq j}^N \delta(\vec{r} - (\vec{r}_i - \vec{r}_j)) \right\rangle \quad \text{with} \quad \rho = \text{const.} \end{aligned} \quad (5.21)$$

where $g(\vec{r}, \vec{r}')$ only depends on the distance r_{ij} , or simply r . This defines the "radial distribution function" (RDF), $g(r)$. The latter is the most important function that describes the structure of a classical many-body system. We can interpret it as the probability to find a second particle at distance r if the first one is fixed at the origin. In another view, it describes the one-body density profile $\rho(r)$ of particles around a particle of same type, i.e., if the latter would hypothetically act as a fixed external potential to the others. It can also easily generalized to multi-component systems, then $g_{ij}(r)$ is defined between particles of type i and j [2]. Typical examples for liquids and solids are shown in the Appendix.

In simulations, it is calculated by creating a histogram around particles in shells of size Δr (see Figure 5.4):

$$g(r) = \frac{\langle n \rangle}{\Delta V} \frac{1}{\rho} \quad (5.22)$$

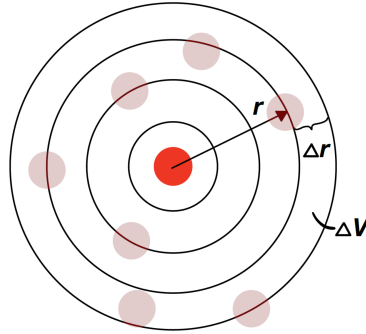


Figure 5.4: Division in shells of size δr that cover a volume of $\Delta V = 4\pi r^2 \Delta r$ each used to calculate the RDF in simulation.

Important features:

- $g(r) = 1$ for an ideal gas, as there exist no correlations.
- $g(r \rightarrow \infty) = 1$ in liquids, as correlations do not occur far away.
- $g(r) = e^{-\beta V(r)}$ is the low density limit $\rho \rightarrow 0$ for the pair potential $V(r)$.
- $\rho_0(r) = \rho g(r)$ is the one-particle density distribution for one particle of the same type. We introduce the (running) "coordination number" $n_c(r)$:

$$n_c(r) = \int_0^r \rho_0(r') d^3 r' = \rho 4\pi \int_0^r dr' g(r') r'^2 \quad (5.23)$$

When integrated to $r = r_1$ being the position of the first minimum of $g(r)$, we get the number of particles in the "first solvation shell" (see Figure 5.5):

$$n_1 \equiv n(r_1) = \rho 4\pi \int_0^{r_1} dr' g(r') r'^2 \quad (5.24)$$

- $g(r_{\max})$ defines the first peak of the RDF and can be related with an association (binding) affinity $\Delta G = -k_B T \ln(g(r_{\max}))$.

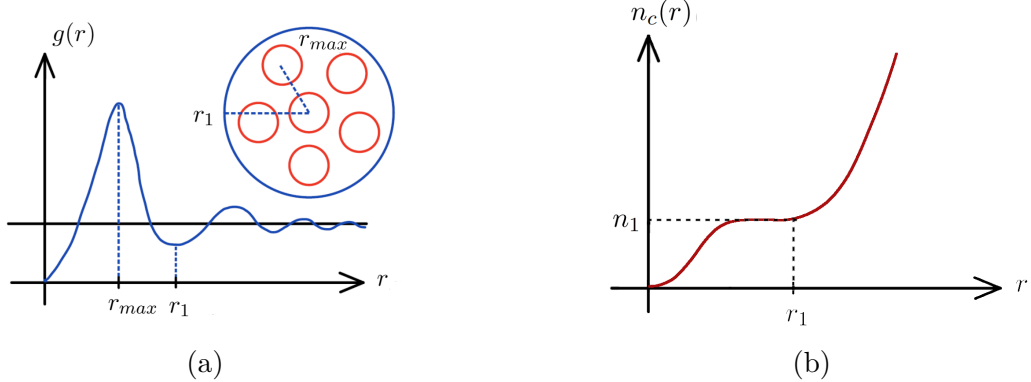


Figure 5.5: (a) Pair distribution function, $g(r)$, and (b) corresponding coordination number.

In the grand-canonical ensemble, the equilibrium *one-body* density distribution is obtained by performing explicitly the ensemble average of the "one particle density operator" given by Eq. 5.16. On obtains:

$$\rho_0(\vec{r}) = \frac{1}{\Xi} \sum_{N=1}^{\infty} \frac{1}{\lambda^{3N}} \frac{z^N}{N!} \int dr_1^3 \dots \int dr_N^3 \exp \left\{ -\beta \sum_{i=1}^N V_{ext}(\vec{r}_i) + H_{int} \right\} \sum_i^N \delta(\vec{r} - \vec{r}_i) \quad (5.25)$$

Considering an ideal gas, $H_{int} = 0$, in the external field $V_{ext}(\vec{r})$, Eq. 5.25 reduces to:

$$\begin{aligned} \rho_0(\vec{r}) &= \underbrace{\frac{1}{\Xi} \sum_{N=1}^{\infty} \frac{z^N}{\lambda^{3N}(N-1)!} \frac{N}{N} \int dr_2^3 \dots \int dr_N^3 \exp \left\{ -\beta \sum_{i=2}^N V_{ext}(\vec{r}_i) \right\} \exp \{-\beta V_{ext}(\vec{r}_1)\}}_{\left[\int dr^3 \exp \{-\beta V_{ext}(r)\} \right]^{N-1}} \\ &= \frac{\langle N \rangle}{V} \exp \{-\beta V_{ext}(\vec{r})\} \\ &\rightarrow \int dr^3 \rho_0(\vec{r}) = \langle N \rangle \end{aligned} \quad (5.26)$$

Similarly, the radial distribution function can be derived by explicitly calculating the ensemble average of the two-particles density operator in the grand-canonical ensemble. Assuming a homogeneous ideal gas, one obtains:

$$\begin{aligned} g(r) &= \frac{\rho^{(2)}}{\rho^2} \\ &= \frac{1}{\rho^2} \sum_{N=2}^{\infty} \frac{Z^N}{\lambda^{3N}} \frac{1}{\Xi} \frac{1}{(N-2)!} \int dr_3^3 \dots \int dr_N^3 \\ &= \frac{z^2}{\rho^2} \text{ with } \rho = \frac{\langle N \rangle}{V} = z \\ &= 1 \end{aligned} \quad (5.27)$$

The radial distribution function $g(r)$ is a key quantity! It can be experimentally measured, e.g., by a diffraction (indirect, reciprocal k -space) or confocal microscopy (direct, real-space). A key function to compare to k -space measurements is the static structure factor, which will be introduced below. Additionally, the $g(r)$ provides structure-property relationships as also demonstrated in the following.

5.2.3 From $g(r)$ to macroscopic observables

Potential energy: One can easily show that the mean potential energy of the system can be obtained through the knowledge of the $g(r)$ and the pair interaction potential $V(r)$. Consider the average potential energy of a 'bulk' system, that is, in the absence of any external field:

$$\begin{aligned}\langle \hat{U} \rangle &= \left\langle \frac{1}{2} \sum_{i \neq j} V(|\vec{r}_i - \vec{r}_j|) \right\rangle \\ &= \left\langle \frac{1}{2} \sum_{i \neq j} \int d^3 r \delta(\vec{r} - (\vec{r}_i - \vec{r}_j)) V(r) \right\rangle \\ &= \frac{\rho N}{2} \int d^3 r g(r) V(r) \\ \rightarrow \frac{\langle \hat{U} \rangle}{N} &= 2\pi\rho \int_0^\infty dr r^2 g(r) V(r)\end{aligned}\quad (5.28)$$

This equation provides the mean potential energy per particle which is macroscopic observable. Hence, we have here a simple realization of a 'quantitative structure-property relationship' (QSPR), relating micro-structure to a macro-property, by a simple integration.

A similar expression can be derived for the pressure in the absence of external fields (or osmotic pressure):

$$P = \rho k_B T - \frac{2}{3} \pi \rho^2 \int_0^\infty dr r^3 g(r) V'(r) \quad (5.29)$$

This equals to the virial equation of the pressure expressed by $g(r)$, where

$$V'(r) = \frac{dV}{dr} \quad (5.30)$$

is the pair force. In the low density limit, the virial equation is

$$P = \rho k_B T - 2\pi\rho^2 \int_0^\infty dr (e^{-\beta V(r)} - 1) = \rho k_B T + B_2 \rho^2 \quad (5.31)$$

with B_2 being the second virial coefficient. Equation 5.31 represents the virial expansion of the thermal equation of state (EOS) up to second order in ρ . The function $\exp(-\beta V(r)) - 1$ is also called the Mayer-f function [2].

Pressure: In classical mechanics, the mean kinetic energy $\langle K \rangle$ via the Clausius virial theorem can be described as

$$\langle \hat{K} \rangle = -\frac{1}{2} \sum_i \langle \vec{F}_i^{\text{tot}} \cdot \vec{r}_i \rangle = -\frac{1}{2} \sum_i \langle \vec{F}_i^{\text{int}} \cdot \vec{r}_i \rangle - \frac{1}{2} \sum_i \langle \vec{F}_i^{\text{ext}} \cdot \vec{r}_i \rangle = -\frac{1}{2} \theta_{\text{int}} - \frac{1}{2} \theta_{\text{ext}} \quad (5.32)$$

with θ_{int} and θ_{ext} defining the internal and external interactions. The external interactions are imposed on the system through a pressure P_0 as can be seen in Figure 11.3. This results in

$$\begin{aligned}d\vec{F}_i^{\text{ext}} &= -P_0 \vec{n} dA \\ \sum_i \vec{F}_i^{\text{ext}} \cdot \vec{r}_i &= -P_0 \int \vec{n} \cdot \vec{r} dA\end{aligned}\quad (5.33)$$

where \vec{n} is the normal vector in respect to the surface.

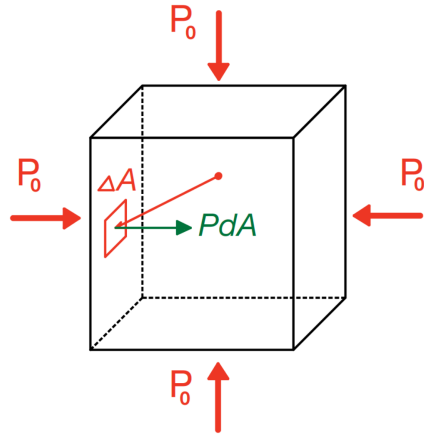


Figure 5.6: Applied external interactions on the volume V by the pressure P_0 .

If we apply the Gauss theorem to the above statement

$$\int \vec{n} \cdot \vec{r} dA = \int \nabla \cdot \vec{r} dV = 3V, \quad (5.34)$$

the external interactions are given by

$$\langle \theta_{\text{ext}} \rangle = -3P_0V \quad (5.35)$$

This derivation is very general and independent of the box shape!

The kinetic energy can also be defined via the equipartitioning theorem as

$$\langle K \rangle = N \frac{1}{2} m \langle v^2 \rangle = \frac{3}{2} N k_B T \quad (5.36)$$

and since the pressure is everywhere the same: $P = \langle P \rangle$, we can derive the virial equation using Equation 11.41:

$$P = \frac{N}{V} k_B T - \frac{1}{3V} \sum_{i=1}^N \vec{r}_i \nabla_i U \quad (5.37)$$

Finally, one can show that:

$$P = \underbrace{\rho k_B T}_{\text{ideal gas}} - \frac{2}{3} \pi \rho^2 \int_0^\infty dr r^3 g(r) \underbrace{V'(r)}_{-dV/dr} \quad (5.38)$$

This equation provides osmotic pressure which is macroscopic observable. Hence, we have here again a QSPR, relating micro-structure to a macro-property, by an integration of the radial distribution function.

A final example is the relation between $g(r)$ and the system's thermal compressibility

$$\chi_T = -\frac{1}{V} \left(\frac{\partial V}{\partial P} \right)_T. \quad (5.39)$$

One can proof that the compressibility χ_T can be expressed in the grand canonical ensemble through the RDF as:

$$\begin{aligned} \rho k_B T \chi_T &= \frac{\langle N^2 \rangle - \langle N \rangle^2}{\langle N \rangle} = 1 + \rho \int d^3r (g(r) - 1) \\ &= 1 + \rho \underbrace{\int d^3r h(r)}_{N_{\text{exc}}} \end{aligned} \quad (5.40)$$

with $h(r) = g(r) - 1$. The N_{exc} can be called the *excess adsorption* around a particle with respect to the ideal gas.

5.2.4 Relation of $g(r)$ to scattering

The scattering structure factor is an experimentally important structure function. It is a result of neutron or X-ray scattering at materials [2, 3]. It is formally defined as:

$$S(\vec{k}) = \left\langle \frac{1}{N} \delta_{\vec{k}} \delta_{-\vec{k}} \right\rangle \quad (5.41)$$

via the average of the density fluctuations with the wave vector \vec{k} which is defined by the Fourier transformation of the density:

$$\delta_{\vec{k}} = \int d^3r \hat{\rho}_0 e^{-i\vec{k}\vec{r}} = \int d^3r \sum_j \delta(\vec{r} - \vec{r}_j) e^{-i\vec{k}\vec{r}} \quad (5.42)$$

It can be shown that the structure factor $S(\vec{k})$ also be rewritten in forms of the RDF [2]:

$$S(\vec{k}) = 1 + \rho \int d^3r \underbrace{(g(r) - 1)}_{h(r)} e^{-i\vec{k}\vec{r}} + \underbrace{(2\pi)^3 \rho \delta(\vec{k})}_{\text{unscattered}} \quad (5.43)$$

We see that the experimentally accessible structure factors is, in principle, only the Fourier Transform of the RDF! Hence, all oscillations and prominent wavelengths appear as peaks in the structure factor. The information is not different from that in the RDF but presented in reciprocal space from a different perspective. In particular, long wavelength effects such as clustering can be better seen in the structure factor.

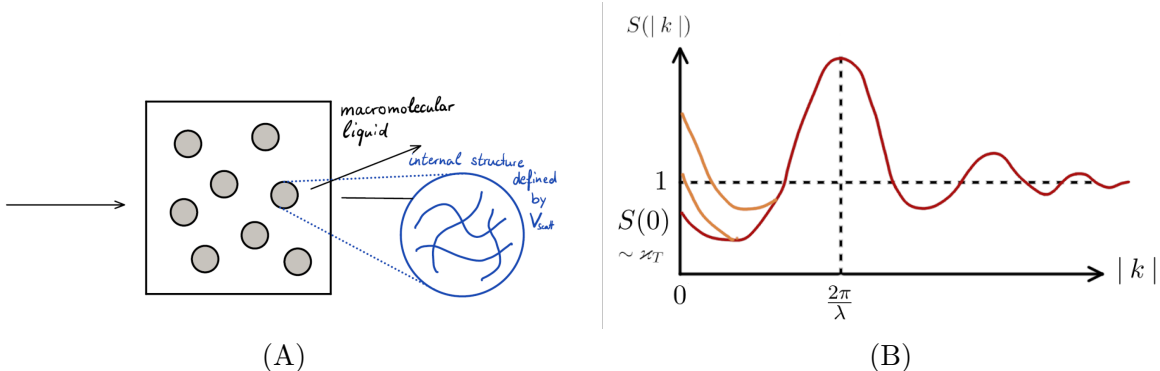


Figure 5.7: (A) Scattering experiments can give insight to the structure of the macromolecular liquid. Depending on the lengthscale probed, we can access the internal structure of the particles (defined by V_{scatt}) which defines the form factor, or we can access the liquid structure in terms of the RDF for larger scales. (B) Representative structure factor, $S(\vec{k})$, in a homogeneous liquid.

However, in experiments only the intensity of the scattered wave can be measured which also includes information on the internal structure of a (macro)molecule. In general, we have for the intensity

$$I(\vec{k}) = N |F(\vec{k})|^2 S(\vec{k}) \quad (5.44)$$

with $F(\vec{k})$ being the 'form factor'

$$F(\vec{k}) = -\frac{m}{2\pi\hbar^2} \int d^3r V_{\text{scatt}}(\vec{r}) e^{-i\vec{k}\vec{r}} \quad (5.45)$$

defined by the internal structure of the particles expressed by an internal scattering potential V_{scatt} . The form factor can be measured at larger wavevectors in diluted systems, where $S(k) \simeq 1$. An important feature is also that

$$S(\vec{k} \rightarrow 0) = 1 + \rho \int d^3r (g(r) - 1) e^{-\vec{k}\vec{r}} = \rho k_B T \chi_T, \quad (5.46)$$

In words, the small wavevector behavior of the structure factor gives us direct information about the compressibility of the system. Close to a phase transition and/or critical behavior, $S(\vec{k} \rightarrow 0)$ is diverging due to long wavelength fluctuations in the system [2, 3].

Numerically, a Fourier Transform can be solved by given routines as in Python or Numerical recipes. Note that for a radially symmetric function, the FT simplifies into a quasi-1D transform. One can show that the 3D trafo of $f(r)$

$$\tilde{f}(\vec{k}) = \int d^3r f(r) e^{-\vec{k}\vec{r}} \quad (5.47)$$

can be simplified into a 1D-sinus Trafo of $f(r)r$ of the form:

$$\tilde{f}(k) = \frac{4\pi}{k} \int dr [f(r)r] \sin(kr) \quad (5.48)$$

Chapter 6

Coarse-graining of multi-component systems: effective interactions

For modeling larger systems and larger length- and timescales we need to integrate out smaller degrees of freedom (DOFs) to arrive at effective mesoscale Hamiltonians. This can reduce the computational cost by orders of magnitude because instead of many microscopic DOFs, one simulates only a few effective ones of interest. For example, consider salt ions in water and we want to access the osmotic pressure of the salt. Instead of an all-atom simulations of 100 salt pairs in 10,000 water molecules with a microscopic Hamiltonian, one can define effective water-mediated corrections to the ion-ion pair potential to take water effects approximately into account. This can be done by inverting ion-ion RDFs (see Appendix) to define effective pair potentials [5]. Such a coarse-graining strategy applies to all kind of multi-component systems, where small and large-scale DOFs are present and the small (and quickly relaxing) DOFs are not of explicit interest. Some examples are shown in Fig. 6.1. In the following we discuss how formally a 'coarse-graining' can be done by integrating out DOFs and defining a 'potential of mean force' or 'effective interaction' or 'effective pair potentials' [2, 3].

Examples for **two-component mixtures** are presented in Figure 6.1.

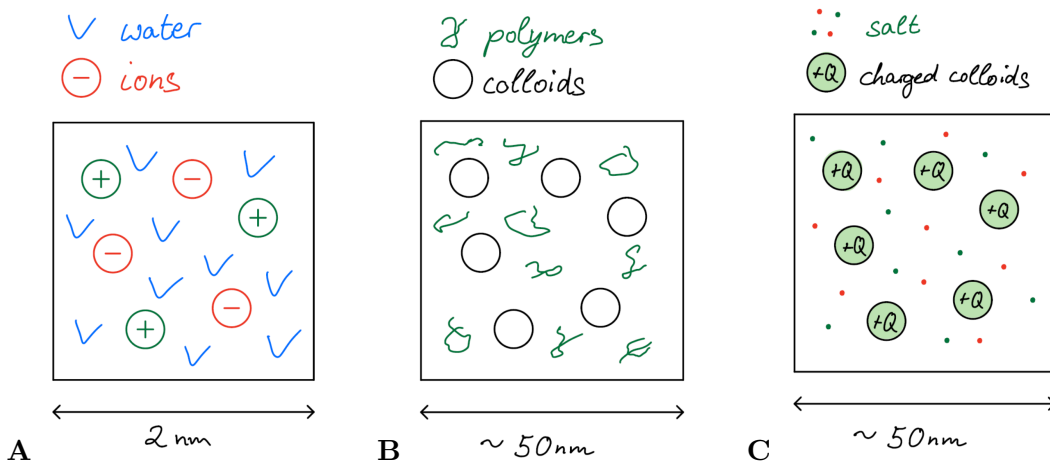


Figure 6.1: Examples for two-component mixtures: **A** ions in water, **B** colloids and polymers, **C** charged colloids and salt.

6.1 Potential of mean force: effective interaction

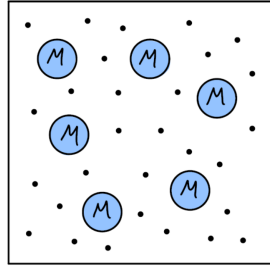


Figure 6.2: A binary system with N_M macroparticles at distances \vec{R}_i and N_m microparticles at distances \vec{r}_i .

Consider the Hamiltonian of a two-component system as in Figure 6.2, formally given as:

$$\mathcal{H} = K_M + V_{MM} + K_m + V_{mm} + V_{Mm} \quad (6.1)$$

with K_i being the kinetic terms and V_{ij} being the interactive terms, e.g., based on a sum of pair potentials

$$V_{Mm} = \sum_i^{N_M} \sum_j^{N_m} V(|\vec{R}_i - \vec{r}_j|) \quad (6.2)$$

The goal now is to integrate out the DOFs of the small, microparticles (m) to define effective interactions between the macroparticles (M). The total partition sum is defined as:

$$Z = \langle e^{-\beta \mathcal{H}} \rangle = \langle \langle e^{-\beta \mathcal{H}} \rangle_m \rangle_M = \langle e^{-\beta \mathcal{H}_{\text{eff}}} \rangle_M \quad (6.3)$$

where $\langle \dots \rangle$ is based on the trace over all coordinates

$$\int d\vec{P}_1 \dots d\vec{P}_{N_M} \int d\vec{p}_1 \dots d\vec{p}_{N_m} \times \int d\vec{R}_1 \dots d\vec{R}_{N_M} \int d\vec{r}_1 \dots d\vec{r}_{N_m} \quad (6.4)$$

and $\langle \dots \rangle_m$ is just the integral over the m coordinates. Eq. (6.3) is the defining equation for the effective Hamiltonian: the exact partition sum (or free energy) follows from integrations over all configuration of the macroparticles using their effective Hamiltonian. With the expression

$$\langle e^{-\beta \mathcal{H}} \rangle_m = e^{-\beta(K_M + V_{MM})} \langle e^{-\beta(K_m + V_{mm} + V_{Mm})} \rangle_m, \quad (6.5)$$

the effective Hamiltonian is then written as

$$\mathcal{H}_{\text{eff}} = K_M + V_{MM} - \underbrace{k_B T \ln (\langle e^{-\beta(K_m + V_{mm} + V_{Mm})} \rangle_m)}_{\text{free energy of } m\text{-particles in external field of } M\text{-particles}} \quad (6.6)$$

$$\mathcal{H}_{\text{eff}} = K_M + \underbrace{V_{MM} + \mathcal{F}(T, [\rho_m(\vec{r})], \{\vec{R}_i\})}_{V_{\text{eff}}^{\text{tot}}(\{\vec{R}_i\}) = V_{MM}(\{\vec{R}_i\}) + V_{\text{eff}}(\{\vec{R}_i\})} \quad (6.7)$$

The effective interaction $V_{\text{eff}}^{\text{tot}}$ is then the sum of the intrinsic (vacuum) $M - M$ interactions and the microparticle (solvent)-induced free energy V_{eff} . This is an exact result that is generally valid.

The effective force, \vec{F}_i is derived by:

$$\begin{aligned}\vec{F}_i &= -\nabla_{\vec{R}_i} V_{\text{eff}}^{\text{tot}}(\{\vec{R}_j\}) = \underbrace{-\nabla_{\vec{R}_i} V_{MM}}_{\text{pair forces}} \quad \underbrace{-\nabla_{\vec{R}_i} V_{\text{eff}}}_{\text{induced many-body forces}} \\ &= -\nabla_{\vec{R}_i} V_{MM} - k_B T \frac{\langle \beta \nabla_{\vec{R}_i} V_{Mm} e^{-\beta(K_M + V_{mm} + V_{Mm})} \rangle_m}{\langle e^{-\beta(K_M + V_{mm} + V_{Mm})} \rangle_m} \\ &= -\nabla_{\vec{R}_i} V_{MM} - \langle \nabla_{\vec{R}_i} V_{Mm} \rangle_m\end{aligned}\quad (6.8)$$

The effective force of a macroparticle i is thus identical to the sum of the 'vacuum' pair force and the mean force induced by the microparticles. That's why the integrated force, leading to a potential $V_{\text{eff}}^{\text{tot}}$, is called the "potential of mean force" (PMF). Again, this is a formally exact potential (including many-body effects) but in practice almost impossible to calculate because V_{eff} depends on the specific configuration ($\{\vec{R}_j\}$).

Important: If we perform such a calculation for only $N_M = 2$, we obtain an effective pair potential (see ??):

$$V_{\text{eff}}^{\text{tot}}(\{\vec{R}_i\}) \rightarrow V(r) \quad (6.9)$$

This is also how it is done in practice. The mean force or effective potential, see next section, is only calculated for two macroparticles in the sea of microparticles. However, then many-body interactions are neglected. (That is, if a third particle influences the pair potential between the first two). In practice that is a popular approximation (which validity should be scrutinized but is often not considered). Per construction it should be always good at low densities of the (effective) macroparticles in the coarse-grained system.

6.1.1 Two-body approximation

If we perform such a calculation in the two-body approximation ($N_M = 2$), the functional form of the free energy (see eq. 6.7) reduces to:

$$\mathcal{F}(T, [\rho_m(\vec{r})]; \{\vec{R}_i\}) \simeq \underbrace{F_0\left(\frac{N_M}{V}\right)}_{\text{const}} + \frac{1}{2} \sum_{i \neq j}^{N_M} \phi(\vec{r}_i, \vec{r}_j) \quad (6.10)$$

and we obtain the effective two-body pair potential (note that it is usually denoted at $V(r)$):

$$\phi(\vec{r}_i, \vec{r}_j) = \phi(|\vec{r}_i - \vec{r}_j|) = \phi(r) \quad (6.11)$$

Then, the liquid structure follows from equilibrium statistics according to H_{eff} .

$$\rho^{(1)}(\vec{r}) = \left\langle \sum_{i=1}^{N_M} \delta(\vec{r} - \vec{r}_i) \right\rangle_{H_{\text{eff}}} \equiv \rho(\vec{r}) \quad (6.12)$$

$$\rho^{(2)}(\vec{r}, \vec{r}') = \left\langle \sum_{i \neq j}^{N_M} \delta(\vec{r} - \vec{r}_i) \delta(\vec{r}' - \vec{r}_j) \right\rangle_{H_{\text{eff}}} \equiv g(r) \text{ RDF} \quad (6.13)$$

This is also how it is done in practice. The mean force or effective potential, see next section, is only calculated for two macroparticles in the sea of microparticles. However, then many-body interactions are neglected. (That is, if a third particle influences the pair potential between the first two). In practice that is a popular approximation (which validity should be scrutinized but is often not considered). Per construction it should be always good at low densities of the (effective) macroparticles in the coarse-grained system.

6.1.2 Internal degree of freedom

We can now consider that the M macroparticles have m internal degree of freedom as represented in Fig. 6.3, for example monomers in a polymer network (hydrogel).

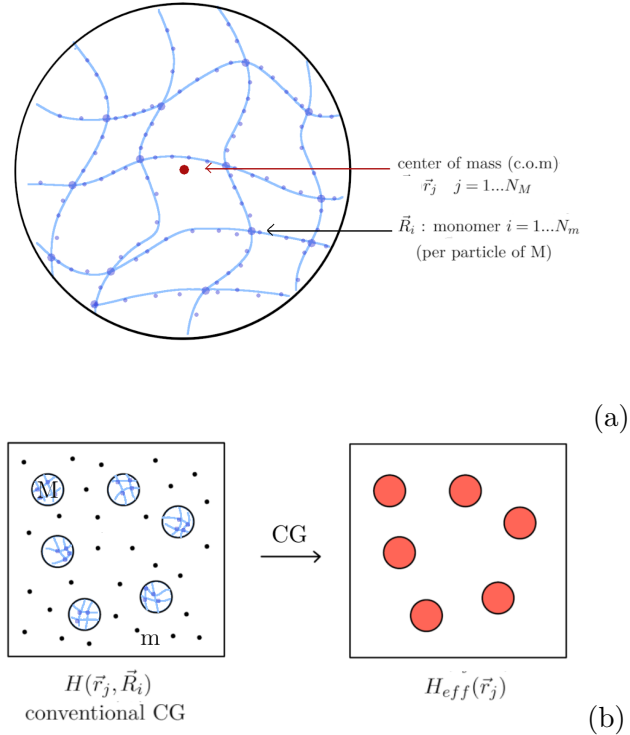


Figure 6.3: Coarse graining a one component system, with internal degree of freedom

Since these particles are so soft and deformable, it would be desirable to still resolve some properties in the C.G model, e.g. the size or shape. In that case, one would need to enrich the effective Hamiltonian with some collective variables that would describe the change of properties such as:

$$H_{\text{eff}}(\vec{r}_i) \rightarrow \tilde{H}_{\text{eff}}(\vec{r}_i; \vec{\sigma}_i) \quad (6.14)$$

- $\vec{\sigma}_i$ =: new CG (collective variable) that can assume different equilibrium values according to some distribution.
- $\vec{\sigma}_i$ or σ_i can be the particle size, but in principle general (shape, charge density, orientation, function, ...)

Details of such a coarse-graining of internal degrees of freedom can be found in Lin *et al.*, *Phys. Rev. E* **102**, 042602 (2020).

6.2 Typical coarse-graining procedure

As a practical example, we look at a binary system with a species of big particles b (the previous macroparticle) and a species of small particles (solvent) s (the previous microparticle), as seen in Figure 6.4, with densities ρ_b , ρ_s and interactions of V_{bb} , V_{ss} and V_{bs} .

Practical question: what **structure** and phase diagram do the **big particles** have?

In the low density limit of the big particles, the interactions reduce to an effective pair potential (see Figure 6.4). By coarse-graining the pair potential, a one-component system of "effective" big particles is derived.

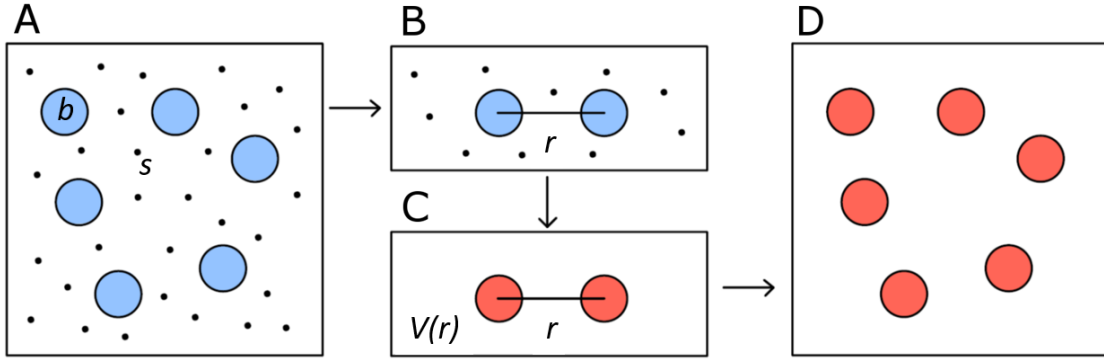


Figure 6.4: Typical coarse-graining procedure: **A** binary system with species of big and small particles which needs to be investigated; **B** consider only the low density limit with $N_b = 2$; **C** Coarse-graining ('integrating out') results into an effective pair potential, leading to **D** a one-component system of "effective" big particles. The final system has much reduced complexity but due to the pair potential approximation is not exactly representing the original system.

How do we calculate V_{eff} in practice?

1. Simulation

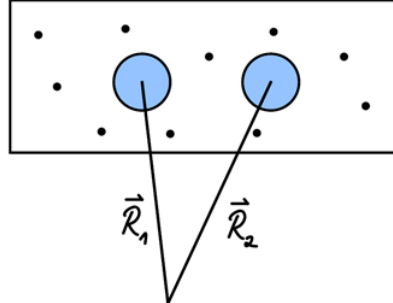


Figure 6.5: Calculating V_{eff} through simulation. Two big particles are at fixed positions \vec{R}_1 and \vec{R}_2 in a fixed distance. The mean force from the small ones can be averaged and will provide typically a net force in direction of the connection axis. Integrating the force along the big particle distance wil provide the PMF, which in this case is equal to the effective (coarse-grained) pair interaction.

In simulations, there are two standard ways for obtaining the effective pair interaction. The first route is based on the calculation of the mean force. The two particles are fixed in their distance, cf. Fig. 6.5. The mean force of all small particles is calculated, formally through

$$\begin{aligned} \vec{F}_{\text{eff}}(\vec{R}_1, \vec{R}_2) &= \left\langle \sum_i \vec{F}_{bs}(\vec{R}_1, \vec{R}_2, \vec{r}_i) \right\rangle \\ &= -2\pi \int_0^\infty \int_{-1}^1 r^2 F_{bs}(r) \rho_s(\vec{r}, \vec{R}_1, \vec{R}_2) \times \omega d\omega dr \end{aligned} \quad (6.15)$$

where $\rho_s(\vec{r}, \vec{R}_1, \vec{R}_2)$ is the triplet-density, ie., the one-body density profile of the small particles if the two big ones are placed at \vec{R}_1 and \vec{R}_2 . In practice, the density profile

has not to be averaged, the mean force can simply be averaged 'on-the-fly' during the simulation. Due to the symmetry of the problem, the scalar force in direction of the distance vector is sufficient. In orthogonal directions the mean force must average out to zero (in practice, this is a small number which gives an indication of the statistical error). Due to actio = reactio, the mean force must be anti-symmetric on both particles. Finally, integrating this mean force over many distances (typically 10-20 well interpolated values) gives the PMF. In this case of only two particles, this is identical to the effective pair potential.

Other sampling methods are possible, too. For example, umbrella sampling (US) [9] is very popular, see also section 14.1.5 in this script. The US method does not calculate forces but reconstructs the effective pair potential (free energy along the distance coordinate) through probability distributions.

There are also other approaches [2, 3] which we just briefly mention:

2. Classical density functional theory (DFT)

This approach uses the liquid state theory. With the approximation $\rho_b \rightarrow \infty$, the triplet correlation $\rho_s(\vec{r}, \vec{R}_1, \vec{R}_2)$ is derived and the mean force calculated.

3. Superposition approximation

One can approximate the triplet correlation $\rho_s(\vec{r}, \vec{R}_1, \vec{R}_2)$ by a product of one-body profiles of only one particle:

$$\rho_s(\vec{r}, \vec{R}_1, \vec{R}_2) \simeq \rho_s^0 g(|\vec{r} - \vec{R}_1|)g(|\vec{r} - \vec{R}_2|) \quad (6.16)$$

This is only an exact treatment for the assumption of the species of small particles being an ideal gas.

6.3 Effective macromolecular interactions: examples

In principle, all pair potentials are in some sense effective interactions. Examples for effective pair interactions are: Lennard-Jones (electrons integrated out), Dispersion (Hamaker: atomic van der Waals integrated out), DLVO theory and potential (mobile charges and ions integrated out), hard core colloids (all chemical DOFs integrated out so that just a 'shape' remains), soft repulsion between polymers (polymer monomers integrated out), hydrophobic interactions (water integrated out), etc.

6.3.1 Depletion Potential

An important example in mixtures or macromolecules in solvents is the so-called "**Depletion potential**" due to solvation forces.

The simplest example of a depletion potential is provided by the **Asakura-Oosawa** (AO) model for **colloid-polymer mixtures**, cf. Fig. 6.6 It can be calculated analytically, so the formal procedure of integrating out DOFs can be performed and followed explicitly!

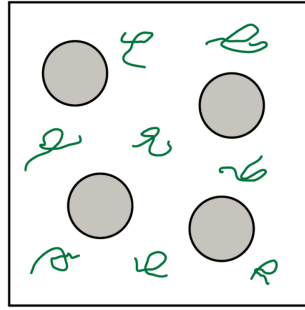


Figure 6.6: A binary system with N_M macroparticles (colloids) and N_p polymers with a density of $\rho_p = \frac{N_p}{V}$ and V being the total volume of the system.

For this, we consider two macroparticles $N_M = 2$ surrounded by polymers as in Fig. 6.7.

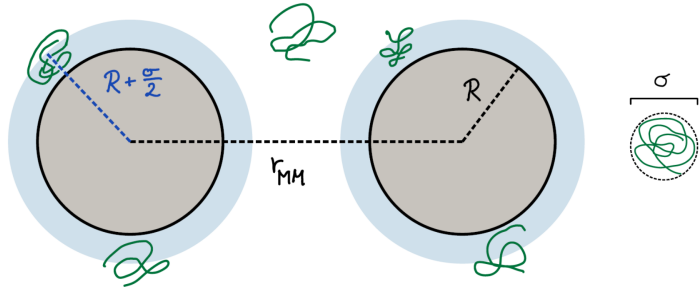


Figure 6.7: $N_M = 2$ macroparticles (colloids) of radius R in a distance r_{MM} . N_p polymers of interaction size σ are surrounding the colloids. The polymers are excluded from spheres of a radius $R + \sigma/2$.

The interactions in the AO model system are:

$$V_{MM} = \begin{cases} \infty & \text{for } r_{MM} < 2R \\ 0 & \text{else} \end{cases} \quad V_{pp} = 0 \quad \text{ideal} \quad V_{Mp} = \begin{cases} \infty & \text{for } r_{Mp} < R + \frac{\sigma}{2} \\ 0 & \text{else} \end{cases} \quad (6.17)$$

Note that all interactions are repulsive and entropic! The polymer-polymer interaction is ideal, which is a good approximation because these chain coils can easily interpenetrate each other. However, if a polymer approaches the big sphere (colloid) there will be an entropic (elastic) penalty and one can assume a hard repulsive excluded-volume interaction between polymers and colloids. Importantly, this creates an excluded volume shell around the colloids for the polymers, see again Fig. 6.7.

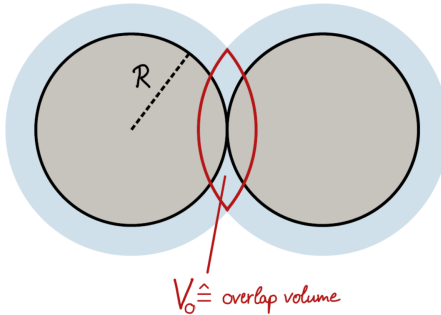


Figure 6.8: If we consider the possible overlap volume of the macromolecules, the accessible volume of the polymer increases.

Now, when the colloids comes closer, the inaccessible volumina start overlapping, cf. Fig. 6.8. We have an overlap volume V_0 . Hence, the overall accessible volume for the polymers increases. More volume means more configurations in space and this means more entropy for the system: the colloids will effectively attract to minimize the system free energy! The accessible polymer volume is given exactly as (see Figure 6.8)

$$V_{\text{acc}} = V - 2V_M + V_0(r_{MM}) = V - \frac{\pi}{6}D^3 \left(1 - \frac{3r_{MM}}{2D} + \frac{r_{MM}^3}{2D^3} \right) \quad (6.18)$$

with V_M the volume of the two colloids, and $D = 2R + \sigma$ their surface-to-surface distance, and $2R \leq r_{MM} < D$.

The free energy of the polymers is purely entropic and given as:

$$\begin{aligned} F = -TS &= k_B T \ln \left(\frac{V_{\text{acc}}^{N_p}}{\Omega^{3N_p} N_p!} \right) = -k_B T \ln Z \\ &= k_B T \left(\ln \left(\frac{V^{N_p}}{\Omega^{3N_p} N_p!} \right) + N_p \ln \left(\frac{V_{\text{acc}}(r_{MM})}{V} \right) \right) \\ &= F_{\text{ideal}}^0 + k_B T N_p \ln \left(\frac{V_{\text{acc}}(r_{MM})}{V} \right) \end{aligned} \quad (6.19)$$

where Z is the partition sum. For $V \gg \frac{\pi}{6}D^3$, we can linearize via $\ln(1 - \epsilon) \simeq -\epsilon$:

$$F = F_{\text{ideal}}^0 - \frac{N_p}{V} k_B T \frac{\pi D^3}{6} \left(1 - \frac{3r_{MM}}{2D} + \frac{r_{MM}^3}{2D^3} \right) \quad (6.20)$$

We define the pair potential as $V_{\text{depl}}(r) \rightarrow 0$ for $r_{MM} \rightarrow \infty$.

$$V_{\text{depl}}(r) = -\rho_p k_B T \frac{\pi D^3}{6} \left(1 - \frac{3r_{MM}}{2D} + \frac{r_{MM}^3}{2D^3} \right) \quad (6.21)$$

with $2R < r < D$.

The effective pair interaction is then given as $V_{\text{tot}} = V_{MM} + V_{\text{depl}}$ as seen in Figure 6.9.

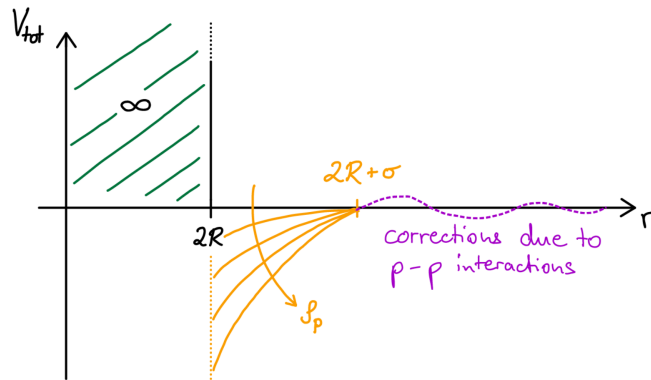


Figure 6.9: Total effective pair interaction as $V_{\text{tot}} = V_{MM} + V_{\text{depl}}$.

Features: the depletion potential

- has an attraction which is proportional to polymer density and attraction range proportional to polymer size which leads to **tunable interactions**

- is always attractive within the AO-model.
- is purely entropic (proportional to $k_B T$).
- is also derivable from a superposition approximation by integrating unbalanced forces.
- is an important interaction that drives particle aggregation or even phase separation

6.3.2 DLVO interaction (Hamaker and Debye-Hückel)

(Derjaguin, Landau, Verweg, Overbeck around 1940 [3]) DLVO developed an important concept based on effective interactions to describe the stability of charged colloids in solution. With 'stability' it is meant that the colloids stay well dispersed in the solvent. If they become 'unstable', it means they cluster and flocculate, precipitating out of solution (a little like in heating sour milk). This is often unwanted. DLVO showed that this stabilization can be controlled by the salt concentration in solution. For low salt concentration, the repulsive electrostatic interaction can then overcome the ubiquitous van der Waals attraction (which alone would lead to clustering and instability).

The DLVO assumption is that the effective interaction between two charged macromolecules (colloids) is given as a sum of effective van der Waals (vdW) and electrostatic potentials:

$$V_{\text{DLVO}}(r) = V_{\text{vdW}}(r) + V_{\text{elec}}(r) \quad (6.22)$$

Van der Waals (Hamaker) interaction

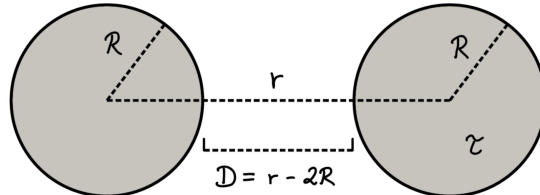


Figure 6.10: Homogeneous atoms with density τ in the sphere volumina $V_1 = V_2 = V$.

The atom-atom van der Waals attraction is $\sim -\frac{C_6}{r^6}$ ($= -\frac{4\epsilon\sigma^6}{r^6}$) as in the Lennard-Jones potential $V_{LJ}(r)$. If we assume that the constituting atoms are all homogeneously distributed over the two colloids with radius R , we can simply add (integrate) all their interactions. This defines the integration for the effective interaction

$$V_{\text{vdW}}(r) = - \int_V d^3r'' \int_V d^3r' \frac{C_6 \tau^2}{|r'' - r'|^6} \quad (6.23)$$

for fixed center-to-center distance r between the spheres of same volume V . **Hamaker** (1936) introduced a general formula for two differently sized spheres of radii R_1 and R_2 :

$$V_{\text{vdW}}(r) = -\pi^2 \tau^2 C_6 \frac{1}{6} \cdot \left(\frac{2R_1 R_2}{r^2 - (R_1 + R_2)^2} + \frac{2R_1 R_2}{r^2 - (R_1 - R_2)^2} + \ln \frac{r^2 - (R_1 + R_2)^2}{r^2 - (R_1 - R_2)^2} \right) \quad (6.24)$$

This equation goes $\sim \frac{1}{r^6}$ for $r \rightarrow \infty$ (derivable through Taylor expansion), which makes sense because far away the spheres look like atom-like points again and we obtain the usual form of dispersion interactions. In the near-field for $D \ll R = R_1 = R_2$, the equation of Hamaker simplifies to:

$$V_{\text{vdW}}(r) \simeq -A \frac{R}{12D} \quad (6.25)$$

where $A = \pi^2 \tau^2 C_6$ is the Hamaker constant, and D the surface-to-surface distance of the two colloids.

The Hamaker integration is possible for all kind of geometries, see the Appendix. Typically we use indexes A_{ijk} to refer to interactions between i and k across a medium j as seen in Figure 6.11. The Hamaker A_{ijk} are thus specific material constants and can be tabulated (see Appendix).

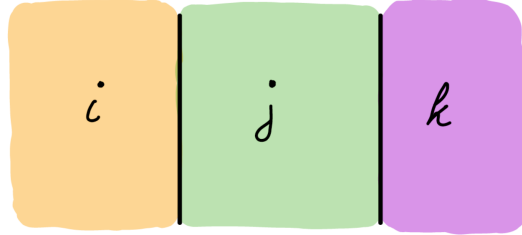


Figure 6.11: Interaction between i and k across medium j .

As a special geometry we also consider a wall (half-space) interacting with an atom. This is important for simulations to define effective interactions between the simulated particles and a confining wall. The Hamaker interaction between an atom and a planar surface as seen in Figure 6.12 is:

$$V_{\text{vdW}}(z_0) = \int_{z_0}^{-\infty} dz \int dh \frac{2\pi h \tau}{(z^2 + h^2)^{\frac{3}{2}}} \quad (6.26)$$

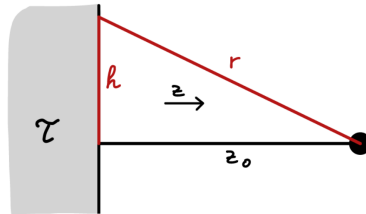


Figure 6.12: Hamaker interaction between a planar surface of homogeneous density τ and an atom.

The result of this Hamaker integration is of '9-3' form:

$$V_{93}(z_0) = 8\pi\tau\epsilon\sigma^3 \left(\left(\frac{\sigma}{z_0}\right)^9 \frac{1}{90} - \left(\frac{\sigma}{z_0}\right)^3 \frac{1}{12} \right) \quad (6.27)$$

This potential is very suitable to model coarse-grained atom-surface interactions, e.g., for liquids confined between smooth planar surfaces.

Electrostatic interactions

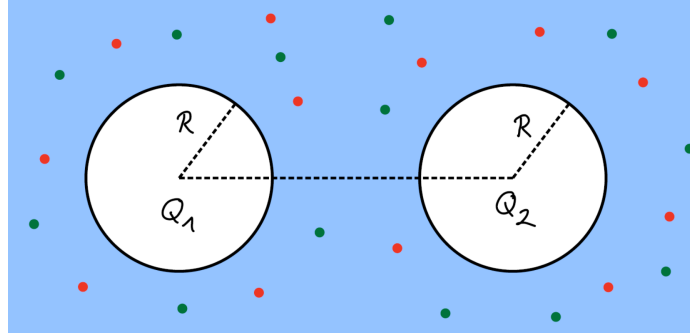


Figure 6.13: Charged colloids and salt in a water solution.

Now we consider two charged colloids with charge $Q_i = Z_i e$, $i = 1, 2$ (with e the elementary or electron charge) as in Figure 6.13. Typically, these colloids are immersed in water and salt (mobile ions) with salt concentration C_s which screen the electrostatic interactions between the colloids. The system can be coarse-grained by integrating out the water and salt contributions. Often for the water, the coarse-graining is not done explicitly, only a continuum background with an appropriate dielectric constant ϵ_r is assumed. This is a good approximation if the colloids are large, much larger than water molecules. Then, one can define the important Bjerrum length $\lambda_B = \frac{e^2}{4\pi\epsilon_0\epsilon_r k_B T}$. The Bjerrum length indicates the separation at which the electrostatic interaction between two elementary charges is comparable in magnitude to the thermal energy scale. It is for example about 0.7 nm for water at normal conditions. Electrostatic theories, like Debye-Hückel or Poisson-Boltzmann (discussed briefly in the simulation part), then lead to the effective interaction between the colloids written as

$$\beta V_{\text{elec}}(r) = \frac{Z_1 Z_2 \lambda_B}{(1 + \kappa_D r)^2} \frac{e^{-\kappa_D(r-2R)}}{r} \quad (6.28)$$

with $\kappa_D = \lambda_D^{-1} = \sqrt{8\pi\lambda_B C_s}$ being the inverse screening length which scales $\propto C_s^{1/2}$ with the salt concentration C_s . The latter has units per nm³ or mol/liter in chemistry. Eq. 6.28 shows that the Coulomb interaction between the colloids is exponentially screened by the ions. The strength and range of the electrostatic interaction can thus be tuned by the salt concentration. The complete **DLVO** term is typically given as:

$$V_{\text{DLVO}}(r) = -\frac{AR}{12(r-2R)} + \tilde{Z}^2 \frac{\lambda_B}{r} e^{-\kappa_D r}, \quad (6.29)$$

where a proper derivation [3] shows that the valencies are effective ones, given by $\tilde{Z} = \frac{Ze^{\kappa_D 2R}}{(1 + \kappa_D R)^2}$. The reason is that for highly charged colloids, some ions condense on the surfaces of the colloids and renormalize the colloidal charge, so that the colloids are seen far away with effective, reduced charges. As we see in Fig. 6.14 the salt now tunes the attraction versus repulsion of the interaction and can thus stabilize/destabilize the dispersion.

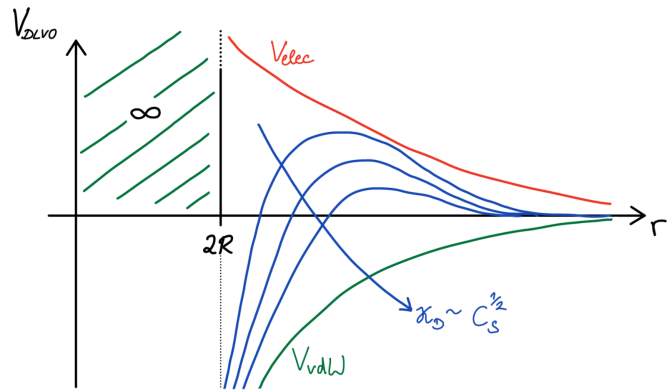


Figure 6.14: The complete DLVO potential plotted over the distance r . The salt concentration C_s tunes the magnitude and strength of the electrostatic interaction. The total interaction can thus range from very repulsive (low salt) to very attractive (high salt).

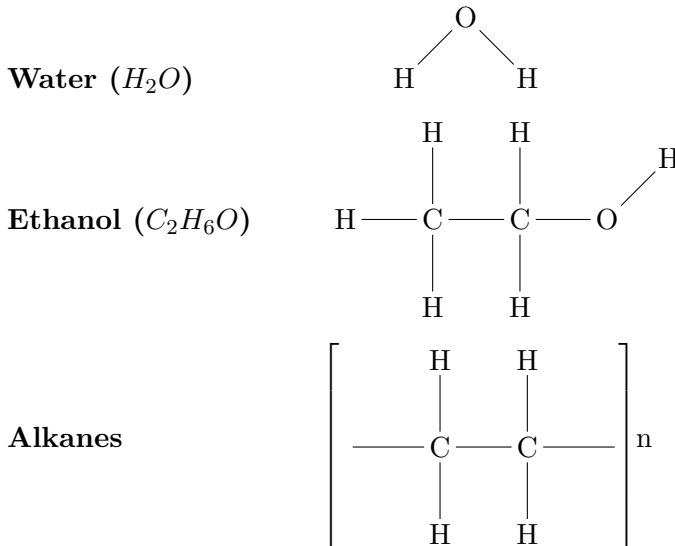
Chapter 7

Polyatomic molecules and polymers

7.1 Introduction

7.1.1 Molecules

Until now we mostly talked about atoms. But obviously complex materials consists of polyatoms (molecules) and polymers. Examples for molecules often occurring in complex systems are:

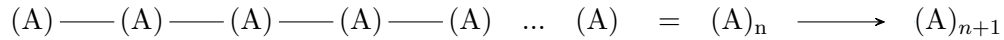


A good description of the statistical mechanics of small molecules (e.g., partition sums of vibrations and rotations) can be found in the book by McQuarrie [6]. (We could discuss this deeper in this lecture on demand by students). Resulting force fields for simple molecules we will discuss later in Part II. Water, for example, can be built by three charged atoms (LJ spheres plus a Coloumb partial charge) which are connected by rigid bonds of fixed length. Since bond vibrations are very fast and small scale the rigidity is a good assumption for water in a larger scale simulation containing thousands of water molecules.

7.1.2 Polymers

A good overview of polymer physics can be found in the book by Rubinstein and Colby [7]. Everything found in this script can be found there in more detail, and of course many more things.

The term "polymers" is derived from the greek words "poly" and "mers" meaning 'many parts'. The elementary unit of a polymer is a so-called "monomer", a small molecule that is capable of polymerizing into a large molecule, e.g.,



where (A) denotes the monomer and n the degree of polymerization which ranges typically between $10^2 \leq n \leq 10^4$. A polymer with $n \leq 20$ is called "oligomer".

If only one form A of monomer occurs it is referred to as a "homopolymer" A_n . Apart from that, many other forms exist, such as "copolymers" having two units of monomers A and B :

Alternating copolymer $A — B — A — B — A — B — A \dots$

Random copolymer $A — A — B — A — B — B — A — B — A — A \dots$

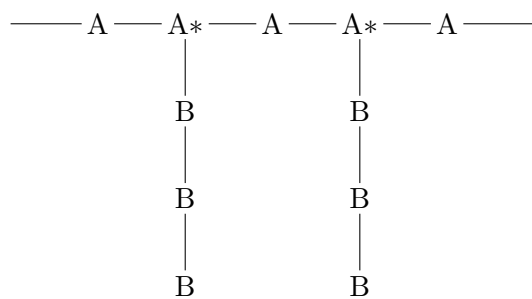
Di-block copolymer $(A)_n — (B)_m$

Tri-block copolymer $(A)_n — (B)_m — (A)_l$

Notes:

Polymers with three different units are referred to as "terpolymers". Proteins have 20 different monomers whereas DNA has four different monomers (GTAC).

Also other architectures such as "grafted polymers" are possible:



7.1.3 Structures and architectures

In general, many different structures and architectures are possible as seen in Figure 7.1 and Figure 7.2.

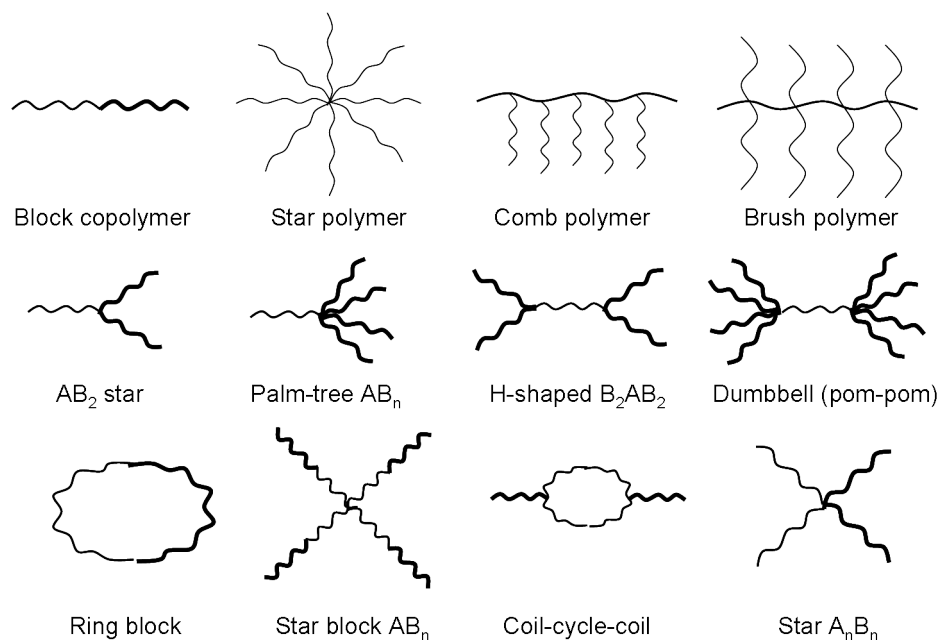


Figure 7.1: Different possible structures and architectures of polymers. ¹

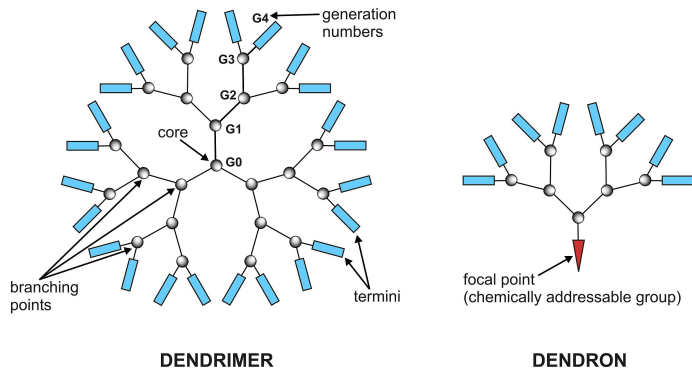
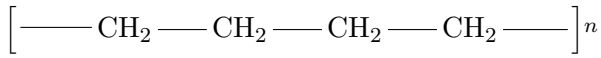


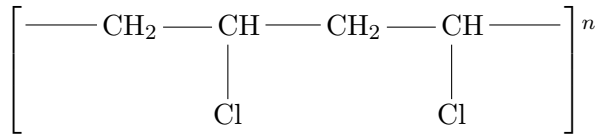
Figure 7.2: Structure of a dendrimer, derived from the Greek word "dendron" meaning tree.²

7.1.4 Example of specific polymers

Polyethylene



Polyvinyl chloride (PVC)



Polypeptide (protein)

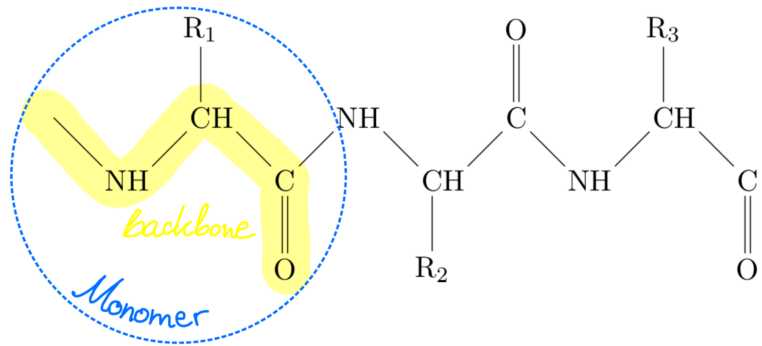


Figure 7.3: Polypeptide consisting of monomers with a backbone of an amino acid and specific side chains of the polymer R_i .

¹https://en.wikipedia.org/wiki/Polymer_architecture#/media/File:RAFT_Architecture.png

²https://en.wikipedia.org/wiki/Polymer_architecture#/media/File:Graphs.jpg

7.1.5 Definitions

In this course, we are focusing on conformation of ideal chains. In ideal polymers, there are no interactions between the monomers.

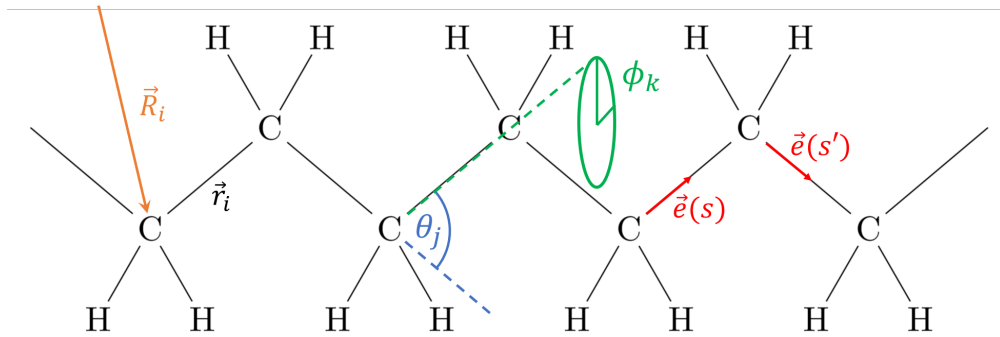


Figure 7.4: Bond vector \vec{r}_i , bond angle θ_j , torsion angle ϕ_k and unit tangent vector $\vec{e}(s)$ where s denotes the arc length for a given polymer.

First, we introduce the bond vector \vec{r}_i with a **bond length** of $l_b^{(i)} = |\vec{r}_i|$ as seen in Figure 7.4. In polyethylene, the bond length is $l_b \simeq 1.54\text{\AA}$.

θ_i denotes the **bond angle** which has a value of $\theta = 68^\circ$ for polyethylene and ϕ_i denotes the **torsion angle**. Typically, a change of ϕ is accompanied by a change in energy as seen in Figure 7.5.

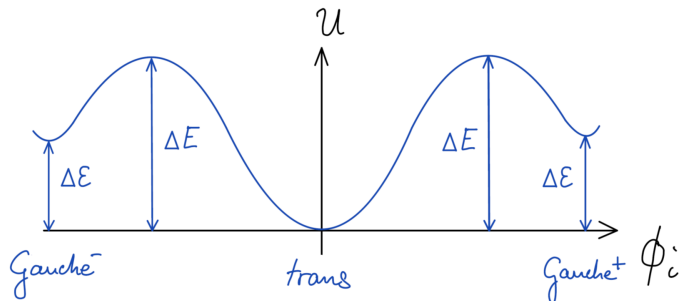


Figure 7.5: The energy landscape of a polymer depends on the torsion angle Φ .

The typical energy difference due to the torsion angle at the Gauche conformation for polyethylene is $\Delta\epsilon \sim 0.8k_B T$.

A change of the torsion angle ϕ_i leads to a change of flexibility of a chain on large scales. The flexibility or stiffness of a chain is characterized by the "persistence length" l_p which describes the decay length of directional correlations. Typically, correlations decay exponentially:

$$D(|s' - s|) = \langle \vec{e}(s) \vec{e}(s') \rangle = e^{-\frac{|s' - s|}{l_p}} \quad (7.1)$$

Some typical persistence lengths are:

- $l_p \simeq 1 \text{ nm}$ for unfolded proteins or single-stranded DNA
- $l_p \simeq 50 - 70 \text{ nm}$ for double-stranded DNA
- $l_p \simeq 10 - 20 \mu\text{m}$ for actin filaments

The **stiffness/flexibility** of a polymer is obtained by comparing the **persistence length** to the **contour length** which can be defined as the **end-to-end vector**, \vec{R}_n , given by

$$\vec{R}_n = \sum_{i=1}^n \vec{r}_i \quad \left(\text{cont. limit of } \vec{R}_n = \int_0^{l_c} \vec{e}(s) ds \right) \quad (7.2)$$

with the maximum $|\vec{R}_n|_{\max} = l_c$ being the **contour length** as seen in Figure 7.6.

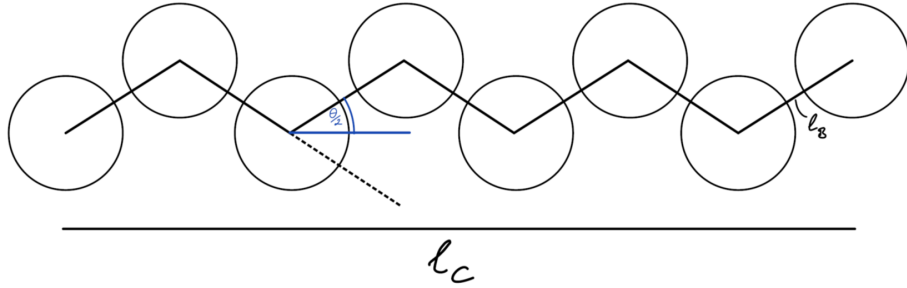


Figure 7.6: Contour length of a simple chain: For a constant bond length, l_b , and a constant bond angle, θ , the contour length is given as $l_c = nl_b \cos \frac{\theta}{2}$.

A polymer is **stiff** if $l_c \lesssim l_p$ and **flexible** if $l_c \gg l_p$.

How do we define the size (conformational length) of a polymer?

$$\langle \vec{R}_n \rangle = \sum_{i=1}^n \langle \vec{r}_i \rangle = 0 \quad (\text{in isotropy}), \quad (7.3)$$

but the **mean-square** is non-zero:

$$\langle \vec{R}_n^2 \rangle = \left\langle \sum_i \vec{r}_i \sum_j \vec{r}_j \right\rangle = \sum_i \langle \vec{r}_i^2 \rangle + \sum_{i \neq j} \langle \vec{r}_i \cdot \vec{r}_j \rangle = nl_b^2 + \sum_{i \neq j} \langle \cos \theta_{ij} \rangle l_b^2 \quad (7.4)$$

where the second contribution depends on the angular correlations (considering small θ). If the angular correlation is zero, the equation for the mean square reduces to:

$$\sqrt{\langle \vec{R}_n^2 \rangle} = \sqrt{nl_b} \quad (7.5)$$

This is however not a good measure for ring or branched polymers.

We define the **radius of gyration** R_g :

$$R_g^2 = \langle \vec{R}_g^2 \rangle = \frac{1}{n} \sum_{i=1}^n \langle (\vec{R}_i - \vec{R}_{\text{com}})^2 \rangle \quad (7.6)$$

The radius of gyration denotes the average square distance of monomers at position \vec{R}_i to the polymer center-of-mass as seen in Figure 7.7 where the center-of-mass is

$$\vec{R}_{\text{com}} = \frac{1}{n} \sum_i \vec{R}_i \quad (7.7)$$

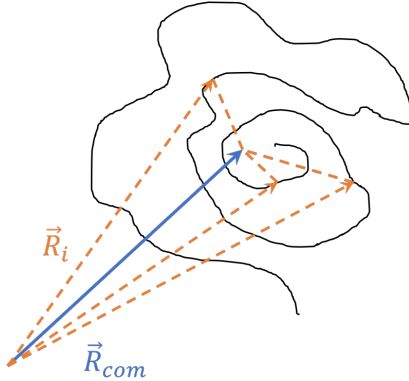


Figure 7.7: The center-of-mass of the polymer \vec{R}_{com} in relation to the distances of the monomer \vec{R}_i .

The radius of gyration can be rewritten as:

$$\begin{aligned}
 R_g^2 &= \frac{1}{n} \sum_i \langle \vec{R}_i^2 - 2\vec{R}_i \vec{R}_{\text{com}} + \vec{R}_{\text{com}}^2 \rangle \\
 &= \frac{1}{n} \sum_i \langle \vec{R}_i^2 - 2\frac{\vec{R}_i}{n} \sum_j \vec{R}_j + \frac{1}{n^2} \sum_{j,k} \vec{R}_j \vec{R}_k \rangle \\
 &= \langle \frac{1}{n} \sum_i \vec{R}_i^2 - \frac{1}{n^2} \sum_{i,j} \vec{R}_i \vec{R}_j \rangle \\
 &= \frac{1}{2n^2} \sum_{i,j} \langle (\vec{R}_i - \vec{R}_j)^2 \rangle \\
 &= \frac{1}{n^2} \sum_{i < j} \langle (\vec{R}_i - \vec{R}_j)^2 \rangle
 \end{aligned} \tag{7.8}$$

whereas $\frac{1}{2} \sum_{i,j} \langle (\vec{R}_i - \vec{R}_j)^2 \rangle = \sum_{i < j} \langle (\vec{R}_i - \vec{R}_j)^2 \rangle$ holds due to the symmetry in i and j .

7.2 Chain models

7.2.1 Freely jointed chain (FJC) model

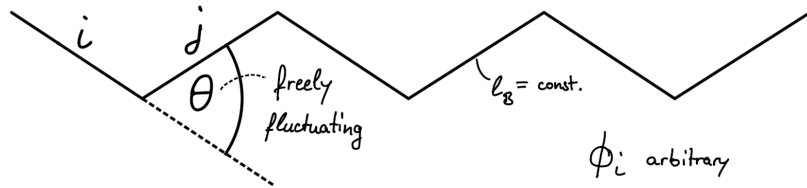


Figure 7.8: The freely jointed chain model with a freely fluctuating bond angle θ and an arbitrary torsion angle ϕ_i .

In this model, the bond angle is freely fluctuating as seen in Figure 7.8 which leads to no bond correlations, e.g. $\langle \cos \theta_{ij} \rangle = 0$ for $i \neq j$.

The root-mean-square end-to-end distance is then given by

$$\sqrt{\langle \vec{R}_n^2 \rangle} = \sqrt{n l_b^2 + \sum_{i \neq j} \langle \cos \theta_{ij} l_b^2 \rangle} = \sqrt{n} l_b \tag{7.9}$$

indicating a random walk behaviour.

For the **FJC**, the contour length is given as $l_c = nl_b$ and the persistence length equals the bond length $l_p = l_b$, leading to an end-to-end mean-square of

$$\langle \vec{R}_n^2 \rangle = l_c l_p. \quad (7.10)$$

The radius of gyration of the **FJC** model for the continuous limit $\sum_i^n \rightarrow \int_0^{l_c} ds$ results in:

$$\begin{aligned} R_g^2 &= \frac{1}{n^2} \sum_{i < j} \langle (\vec{R}_i - \vec{R}_j)^2 \rangle \\ &\rightarrow \frac{1}{l_c^2} \int_0^{l_c} ds \int_s^{l_c} \langle (\vec{R}(t) - \vec{R}(s))^2 \rangle \\ ... &= \frac{\langle \vec{R}_n^2 \rangle}{6} \end{aligned} \quad (7.11)$$

7.2.2 Freely rotating chain (FRC) model

In contrast to the **FJC** model, the bond angles of the **FRC** model are constant $\theta_i = \theta = \text{const.}$ as seen in Figure 7.9.

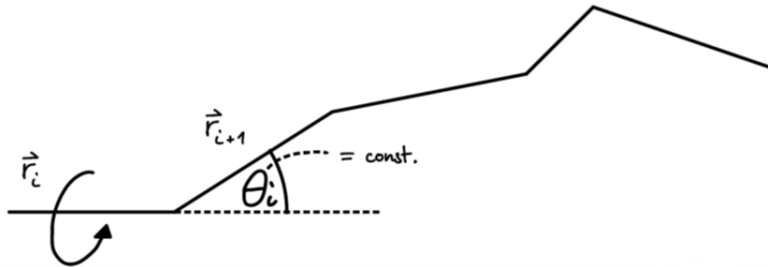


Figure 7.9: The freely rotating chain model with a constant bond angle θ and an arbitrary torsion angle ϕ_i .

This leads to angular correlations:

$$\begin{aligned} \langle \vec{r}_i \cdot \vec{r}_{i+1} \rangle &= \cos \theta l_b^2 \\ \langle \vec{r}_i \cdot \vec{r}_{i+2} \rangle &= \cos^2 \theta l_b^2 \\ \vdots \\ \langle \vec{r}_i \cdot \vec{r}_j \rangle &= l_b^2 \cos^{|i-j|} \theta \end{aligned} \quad (7.12)$$

The mean-square end-to-end distance is given by

$$\langle \vec{R}_n^2 \rangle = \sum_{i,j=1}^n \langle \vec{r}_i \cdot \vec{r}_j \rangle = \sum_{i=1}^n \sum_{k=-i+1}^{n-i} \langle \vec{r}_i \cdot \vec{r}_{i+k} \rangle \quad (7.13)$$

where $k = j - i$. For large n , we can neglect end effects:

$$\langle \vec{R}_n^2 \rangle \simeq \sum_{i=1}^{\infty} \sum_{k=-\infty}^{\infty} l_b^2 \cos^k \theta \quad (7.14)$$

This inner sum is a geometrical sum resulting in

$$\sum_{k=-\infty}^{\infty} l_b^2 \cos^k \theta = l_b^2 \left(1 + 2 \sum_{k=1}^{\infty} \cos^2 \theta \right) = l_b^2 \left(1 + 2 \left(\frac{1}{1 - \cos \theta} - 1 \right) \right) = l_b^2 \frac{1 + \cos \theta}{1 - \cos \theta} \quad (7.15)$$

The mean-square end-to-end distance of the **FRC** can thus be approximated as:

$$\boxed{\langle \vec{R}_n^2 \rangle = nl_b^2 \frac{1 + \cos\theta}{1 - \cos\theta}} \quad (7.16)$$

Another way of denoting the mean-square end-to-end distance is $\langle \vec{R}_n^2 \rangle = n\tilde{l}_b^2$ with \tilde{l}_b being the effective segment length $\tilde{l}_b = l_b \sqrt{\frac{1+\cos\theta}{1-\cos\theta}}$.

Comparing both the **FJC** and the **FRC** model, we see:

$$\begin{aligned} \textbf{FJC:} \quad & \langle \vec{R}_n^2 \rangle = nl_b^2 & l_c = nl_b \\ \textbf{FRC:} \quad & \langle \vec{R}_n^2 \rangle = nl_b^2 \frac{1 + \cos\theta}{1 - \cos\theta} & l_c = nl_b \cos \frac{\theta}{2} \end{aligned} \quad (7.17)$$

In a more general way, the mean-square end-to-end distance can be denoted as

$$\langle \vec{R}_n^2 \rangle = nl_b^2 C_n \xrightarrow{n \rightarrow \infty} nl_b^2 C_\infty \quad (7.18)$$

where C_∞ is called the (Flory) characteristic ratio of the **FRC**. It has an n dependence for finite chains because of end-effects but converges quickly to the limiting value C_∞ for increasing chain length. Introducing the Kuhn length, l_k , the mean-square end-to-end distance can be rewritten to

$$\langle \vec{R}_n^2 \rangle = nl_b^2 C_\infty = Nl_k^2 \quad (7.19)$$

with N being the renormalized degree of polymerization, such that the contour length is $l_c = Nl_k$. This way $\{N, l_k\}$ in the **FRC** model equals the $\{n, l_b\}$ in the **FJC** model. This is a very general finding in polymer physics. Polymers are self-similar, i.e., fractal objects with universal scaling behavior of conformations where microscopic DOFs (small scales) can be renormalized away. The Kuhn length is thus synonymous for the effective bond length, irrespective of any specific microscopic model details.

With the contour length, $l_c = Nl_k$, given, the Kuhn length can be determined:

$$l_k = \frac{\langle \vec{R}_n^2 \rangle}{l_c} = \frac{\langle \vec{R}_n^2 \rangle}{nl_b^2 \cos \frac{\theta}{2}} = l_b \frac{C_\infty}{\cos \frac{\theta}{2}} \quad (7.20)$$

| examples | C_∞ | $l_k [\text{\AA}]$ | $l_b [\text{\AA}]$ |
|--------------|-------------|--------------------|--------------------|
| Polyethylene | $\simeq 7$ | $\simeq 12$ | 1.5 |
| Poly Alanine | $\simeq 9$ | $\simeq 36$ | 4 |
| DNA (double) | $\simeq 90$ | $\simeq 300$ | $\simeq 3.5$ |

Table 7.1: Kuhn lengths and bond lengths for example polymers

The persistence length l_p of the FRC model can be derived via:

$$\begin{aligned} \langle \vec{r}_i \cdot \vec{r}_j \rangle &= l_b^2 \cos^{|j-i|} \theta \\ \cos^{|j-i|} \theta &= \exp\{|j-i| \ln \cos \theta\} = \exp\left\{-\frac{|j-i|}{s_p}\right\} \end{aligned} \quad (7.21)$$

with $s_p = -\frac{1}{\ln \cos \theta}$ being the persistence segment. The persistence length is then defined as

$$l_p = l_b \cdot s_p = \frac{l_b}{|\ln \cos \theta|} \quad \text{with} \quad \theta \leq \frac{\pi}{2} \quad (7.22)$$

Note: In literature, the stiffness is often defined as

$$\begin{aligned}\tilde{l}_p &= \left\langle \frac{\vec{r}_1}{|\vec{r}_1|} \cdot \vec{R}_n \right\rangle \\ &= \frac{1}{l_b} \left\langle \vec{r}_1 \cdot \sum_i^n \vec{r}_i \right\rangle = l_b \sum_{i=1}^n (\cos \theta)^{i-1} \\ &= l_b \frac{1 - (\cos \theta)^n}{1 - \cos \theta} \xrightarrow{n \rightarrow \infty} \tilde{l}_p = \frac{l_b}{1 - \cos \theta}\end{aligned}\quad (7.23)$$

7.2.3 Hindered rotation model

We consider freely rotating chains and a torsion angle ϕ_i that has a probability distribution of $P(\phi_i) = \phi_0 e^{-\beta U(\phi_i)}$.

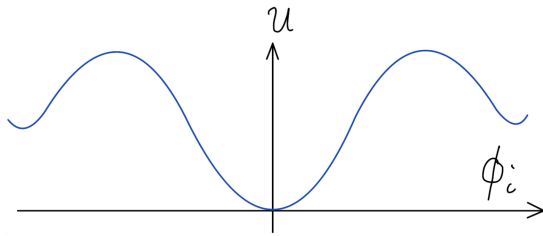


Figure 7.10: The energy landscape $U(\phi)$ as a function of the torsion angle of the polymer ϕ_i .

$$\langle \vec{R}_n^2 \rangle = n l_b^2 C_\infty \quad \text{with} \quad C_\infty = \frac{1 + \cos \theta}{1 - \cos \theta} \frac{1 + \langle \cos \theta \rangle}{1 - \langle \cos \theta \rangle} \quad (7.24)$$

The term $\langle \cos \theta \rangle$ is meant to be the ensemble average of the probability distribution.

7.2.4 The Gaussian (or Rouse) chain



Figure 7.11: The Gaussian chain model with harmonic springs between the monomers.

The Gaussian chain is a model of monomers connected to each other via a harmonic spring as seen in Figure 7.11.

The next neighbour potential is given as:

$$U(\vec{R}_i - \vec{R}_{i+1}) = \frac{1}{2} k (\vec{R}_i - \vec{R}_{i+1})^2 \quad \text{with} \quad k = \frac{3k_B T}{l_b^2} \quad (7.25)$$

In the Gaussian chain, the mean square distance equals the squared bond length: $\langle \vec{r}_i^2 \rangle = l_b^2$. This results in the mean-square end-to-end distance being random walk like:

$$\langle \vec{R}_n^2 \rangle = n l_b^2 \quad (7.26)$$

All distance distributions of the model are of Gaussian nature.

End-to-end distributions

The probability distribution $\phi(\vec{R}_{ee}, n)$ that the end-to-end distance of n segments is $|\vec{R}_{ee}|$:

$$\phi(\vec{R}_{ee}, n) = \frac{1}{(2\pi)^3} \int dk^3 e^{i\vec{k}\cdot\vec{R}_{ee}} \left[\frac{\sin kl_b}{kl_b} \right]^n \quad (7.27)$$

with l_b being the effective segment length. For long chains $n \rightarrow \infty$:

$$\phi(\vec{R}_{ee}, n) \simeq \left(\frac{3}{2\pi nl_b^2} \right)^{3/2} \exp \left\{ -\frac{3\vec{R}_{ee}^2}{2nl_b^2} \right\} \quad (7.28)$$

While being an approximation for the **FJC** and **FRC** model, it is the exact solution for the **Gaussian chain** model.

Note that the Gaussian probability distribution implies that the corresponding free energy is harmonic. As a result, the stretching response of the polymer (pulling the polymer by a constant force) is linear like Hook's law for simple linear elasticity, with a spring constant given by $k_B T/(nl_b^2)$. For ideal chains and low forces, this is indeed what one experimentally observes [7]. However, for non-ideal (real) chains and large stretching forces the response is very different. [Check our computational lab "nano-tug-of-war" https://www.compmat.uni-freiburg.de/Nano_Tug-of-War].

7.2.5 Form factor

The form factor of an ideal polymer (of non-interacting monomers), is defined as:

$$F(k) = N \cdot f(k^2 R_g^2) \quad \text{with} \quad f(x) = \frac{2}{x^2} (e^{-x} - 1 + x) \quad (7.29)$$

with $f(x)$ being the Debye function. For extreme values of kR_g , the form factor can be simplified to

$$F(k) = \begin{cases} N \left(1 - \frac{k^2 R_g^2}{3} \right) & \text{if } kR_g \ll 1 \\ 2N/k^2 R_g^2 & \text{if } kR_g \gg 1 \end{cases} \quad (7.30)$$

with R_g being the radius of gyration, which is directly accessible from low-temperature scattering of dilute solutions.

7.2.6 Real chains

In reality monomer-monomer interactions are present, e.g., excluded volume and dispersion attraction etc. Instead of the random walk behaviour of idealistic polymers, we see "self avoiding walk" behaviour or polymers or attractions that can even lead to collapses of the chain to a compact globule (like in protein folding).

We recall the virial expansion:

$$\frac{\beta P}{\rho} = 1 + B_2 \rho + \dots \quad \text{with} \quad B_2 = -\frac{1}{2} \int d^3 r f(r) = -\frac{1}{2} \int 4\pi r^2 dr (e^{-\beta V(r)} - 1) \quad (7.31)$$

where $V(r)$ denotes the effective monomer-monomer pair potential. We define the effective interaction volume as being $2B_2 = v$.

Typically, the effective monomer-monomer pair potential is split up in a repulsive and an attractive part:

$$V(r) = V_{\text{rep}} + V_{\text{att}} \quad (7.32)$$

$$B_2 = \int d^3r \left(1 - e^{-\beta V_{\text{rep}}} e^{-\beta V_{\text{att}}} \right) \quad (7.33)$$

Small attraction terms can be approximated as:

$$e^{-\beta V_{\text{att}}} \simeq (1 - \beta V_{\text{att}}) = \left(1 - \frac{V_{\text{att}}}{k_B T} \right) \quad (7.34)$$

which leads to

$$v = 2B_2 = A - \frac{B}{T} \quad (7.35)$$

where the terms A and B are temperature independent. A is the hard core contribution (entropic) whereas B is the attractive contribution (energetic). We can rewrite by defining v_0 , via

$$v = v_0 \left(1 - \frac{\theta}{T} \right) \quad (7.36)$$

Typically $v_0 \simeq l_b^3$ with $\theta = B/A$ and $v_0 = A$. When modeling with a Lennard-Jones potential, then $v_0 \simeq \sigma^3$. As we see, for $T = \theta$, the effective interaction volume vanishes, $v = 0$, and the chain behaviour becomes **ideal** (on a 2-body level). Hence, θ is an important temperature or solvent condition, because we can apply ideal chain statistics. The solvent at the θ temperature is called θ -solvent. Hence, in a θ -solvent, $R_n \propto n^{1/2}$. If the temperature is lower, we name the solvent 'poor solvent' because the polymer collapses and does not walk freely random. Here, rather $R_n \propto n^{1/3}$ because the monomers roughly fill a compact sphere. For higher temperatures, we call the solvent 'good', because the self-avoiding polymer swells and fluctuates happily around, more extended than an ideal random walk. Here, one finds the famous Flory scaling $R_n \propto n^{3/5}$ [7]. These scaling laws have been fundamental to describe structure and dynamics of polymeric systems in materials science and especially in biophysics.

Part II

Simulation methods

Chapter 8

Molecular dynamics (MD) computer simulations

8.1 Newton and forces

The idea of molecular dynamics (MD) simulations is extremely simple: propagate positions and velocities of all particles by numerically solving the classical equations of motion, that is, using Newton and forces, based on a given Hamiltonian. The challenging part is to cope with boundary conditions, finite system sizes and finite simulation times, as well as with a proper connection to what we know from statistical mechanics and thermodynamics. Good standard books to read to get into simulations are the newest edition of Allen & Tildesley [8] as well as the book by Smit & Frenkel [9]. A first introduction can also be found in many computational physics books, such as the one from Lesar [10].

For the beginning, consider N particles ($i = 1 \dots N$) at positions \vec{r}_i interacting with a pair potential $V(r)$ and the system has the total energy $H = \hat{E} = \hat{K} + \hat{U} = \text{const.}$. We assign the symbol $\hat{\cdot}$ to the variables to indicate they are instantaneous quantities, not averages. \hat{K} is the kinetic energy, while \hat{U} is the potential energy. The latter usually consists of particle-particle interaction energies and external potentials.

MD is a classical approach, therefore the motion of particles is governed by Newton's equation of motion:

$$\vec{F}_i = m_i \vec{a}_i = m_i \frac{d^2 \vec{r}_i}{dt^2} \quad (8.1)$$

$$\begin{aligned} \text{with } \vec{F}_i &= -\nabla_i \hat{U}(\vec{r}_1, \vec{r}_2, \dots, \vec{r}_N) \\ &= -\nabla_i \hat{U}(\{\vec{r}^N\}) \end{aligned} \quad (8.2)$$

where \vec{F}_i is freely acting on particle i .

For pair potentials $V(r)$ (which, keep in mind, is an approximation) and in the absence of any external fields, the potential energy is of the form

$$\hat{U} = \frac{1}{2} \sum_{i \neq j}^N \sum_j^N V(|\vec{r}_i - \vec{r}_j|) \quad (8.3)$$

This provides a force \vec{F}_i on particle i of

$$\vec{F}_i = \sum_{i \neq j} \vec{f}_{ij} = - \sum_{i \neq j} \frac{dV}{dr} \frac{\vec{r}_j - \vec{r}_i}{|\vec{r}_j - \vec{r}_i|} = - \sum_{i \neq j} \frac{dV}{dr} \frac{\vec{r}_{ij}}{r_{ij}} \quad (8.4)$$

with the pair forces \vec{f}_{ij} and the pair distance $r_{ij} = |\vec{r}_{ij}|$. (Forces from external potentials follow analogously, i.e., $\vec{F}_{i,\text{ext}} = -\nabla_i V_{\text{ext}}(\vec{r}_i)$ and have to be added to the total force per particle.) Note, according to Newton's third law, $\vec{f}_{ij} = -\vec{f}_{ji}$.

In Molecular Dynamics the acceleration

$$\vec{a}_i = \frac{d^2\vec{r}_i}{dt^2} = \frac{1}{m_i} \vec{F}_i = \frac{1}{m_i} \sum_{i \neq j} \vec{f}_{ij} \quad (8.5)$$

is then obtained numerically to propagate velocities and positions, which results in $3N$ coupled differential equations for $\vec{r}_i(t)$. Typical algorithms are provided in the following sections.

8.2 Numerical integration

Finite differences assume that the acceleration \vec{a} is constant in a very small time interval Δt . Then the velocity increment in such a small discrete time step can be estimated by a first order expansion

$$\vec{v}_i(t + \Delta t) \simeq \vec{v}_i(t) - \sum_{i \neq j} \vec{f}_{ij} \frac{\Delta t}{m} = \vec{v}_i(t) + \vec{a}_i(t) \Delta t \quad (8.6)$$

e.g., the velocity at time $t + \Delta t$ is acquired from the velocity and the forces at t . The position is then accessible via the integration of $\vec{v}_i(t + \Delta t)$

$$\vec{r}_i(t + \Delta t) \simeq \vec{r}_i(t) + \vec{v}_i(t) \Delta t + \frac{1}{2} \vec{a}_i \Delta t^2 \quad (8.7)$$

which equals a Taylor expansion of \vec{r}_i in t . This is usually called a first order **Euler** integration scheme. However, such first order integration scheme is not accurate enough as its error in $\vec{r}_i(t)$ is $\sim \Delta t^3$, and it is not time reversible.

To make it time reversible, we consider the backward Taylor expansion, for which we obtain

$$\vec{r}_i(t - \Delta t) \simeq \vec{r}_i(t) - \vec{v}_i(t) \Delta t + \frac{1}{2} \vec{a}_i \Delta t^2 \quad (8.8)$$

Adding Equation 8.7 and Equation 8.8 we get the **Classic Verlet algorithm**. The classic Verlet algorithm has an error in $\vec{r}_i(t)$ in the order of $\sim \Delta t^4$, and it is time reversible. The classic Verlet algorithm (Verlet, 1967) is summarized as:

$$\boxed{\vec{r}_i(t + \Delta t) = 2\vec{r}_i(t) - \vec{r}_i(t - \Delta t) + \vec{a}_i \Delta t^2} \quad (8.9a)$$

$$\boxed{\vec{v}_i(t) = \frac{[\vec{r}_i(t + \Delta t) - \vec{r}_i(t - \Delta t)]}{2\Delta t}} \quad (8.9b)$$

where also the velocities have now to be considered consistently as a second order, time reversible (i.e., invariant under $\Delta t \rightarrow -\Delta t$ transformation) finite difference derivative. Note that the velocities are not needed for the position integration, but they are of course important to evaluate for the calculation of energies and maybe other dynamic properties.

Since position \vec{r}_i and velocity \vec{v}_i are not obtained at the same time step, the total energy \hat{E} cannot be exactly evaluated at the same time. This little problem is solved by two-step algorithms such as the "**Velocity Verlet**" or the **half-step** scheme, presented in the following.

"Velocity Verlet" (Swope et al., 1982)

$$\boxed{\vec{r}_i(t + \Delta t) = \vec{r}_i(t) + \vec{v}_i(t) \Delta t + \frac{1}{2} \vec{a}_i(t) \Delta t^2} \quad (8.10a)$$

$$\boxed{\vec{v}_i(t + \Delta t) = \vec{v}_i(t) + \frac{1}{2} (\vec{a}_i(t) + \vec{a}_i(t + \Delta t)) \Delta t} \quad (8.10b)$$

The velocity Verlet is mathematically equivalent to the Verlet algorithm by a few simple transformations you can do as exercise, or see the Smit and Frenkel book [9]. It can be written in a more algorithmic 'code' fashion way by 'half-advancing' the velocities like this [8]:

$$\vec{v}_i(t + \frac{1}{2}\Delta t) = \vec{v}_i(t) + \frac{1}{2}\vec{a}_i(t)\Delta t \quad (8.11a)$$

$$\vec{r}_i(t + \Delta t) = \vec{r}_i(t) + \vec{v}_i(t + \frac{1}{2}\Delta t)\Delta t \quad (8.11b)$$

$$\vec{v}_i(t + \Delta t) = \vec{v}_i(t + \frac{1}{2}\Delta t) + \frac{1}{2}\vec{a}_i(t + \Delta t)\Delta t \quad (8.11c)$$

This can be directly implemented in a computer code.

Other mathematically equivalent versions are available, e.g. the half-step leap-frog version. It has the same accuracy but different advantages and disadvantages in the order how we evaluate the quantities. We show it here more for historical reasons because usually the Velocity Verlet is employed because it has the most advantages.

"Leap frog" (Kockney, 1970; Potter, 1972)

$$\vec{v}_i(t + \frac{1}{2}\Delta t) = \vec{v}_i(t - \frac{1}{2}\Delta t) + \vec{a}_i(t)\Delta t \quad (8.12a)$$

$$\vec{r}_i(t + \Delta t) = \vec{r}_i(t) + \vec{v}_i(t + \frac{1}{2}\Delta t)\Delta t \quad (8.12b)$$

The values are stored in every step $\vec{r}_i(t), \vec{a}_i(t), \vec{v}_i(t - \frac{1}{2}\Delta t)$. The velocity evaluation "leaps" over the current coordinates. The velocity $\vec{v}_i(t)$ is then derived by:

$$\vec{v}_i(t) = \frac{1}{2}(\vec{v}_i(t + \frac{1}{2}\Delta t) + \vec{v}_i(t - \frac{1}{2}\Delta t)) \quad (8.13)$$

The numerical benefit is that the finite differences are small ($\frac{1}{2}\Delta t$). The velocities on the other hand are not treated satisfactorily as they are not defined at the same time as the positions.

Note:

There is a more rigorous derivation of the Velocity Verlet algorithms possible by the *Liouville formulation* of classical mechanics [8]. There one can proof that the **Velocity Verlet** algorithm is time reversible and phase-space volume conserving as well as energy conserving for long times and sufficiently small Δt . Hence, the Verlet integrator is a '*symplectic*' (phase space volume conserving) integrator.

That is, H or $E = \text{const.}$ in the NVE ensemble (constant number of particles N , volume V and energy E ; "microcanonical ensemble").

8.3 Choice of time step & computing time

The optimal choice of Δt is a balance between accuracy & stability and computing time, but typically set by the fastest time scale in the system. This is for example the atomic vibration in atomic solid or bond systems of $\simeq 0.1$ ps = 10^{-13} s.

One can show [8], if f is the highest frequency, then the requirement for stability is $\Delta t \leq 1/(\pi f)$.

Hence, for a typical **Verlet** algorithm $\sim 10 - 100$ steps per vibrational period are typically chosen:

$$\Delta t \simeq (1 - 10) \text{ fs} = 10^{-15} \text{ s} - 10^{-14} \text{ s} \quad (8.14)$$

Thus, a standard **MD** simulation length is

- ca. 10^6 time steps for 1 ns simulation
- ca. 10^9 time steps for 1 μs simulation

8.4 Mean and standard derivation

Recall our notation:

\bar{x} = mean value from time average

$\langle x \rangle$ = mean value from ensemble average

and for ergodic systems, $\langle x \rangle = \bar{x}$, what is mostly *ad hoc* assumed but not always fulfilled. Another criterion for accuracy & stability (and the choice of time step) of simulations is to check for energy conservation and to scrutinize the magnitude of energy (or other properties') fluctuations. The mean value from a time average \bar{x} in the simulation is given by

$$\bar{x} = \frac{1}{\tau_{\max}} \sum_{\tau=1}^{\tau_{\max}} x(\tau) \quad \tau = n\Delta t \quad (8.15)$$

where n indicates the number of time steps. The mean energy \bar{E} of the system is thus given by

$$\bar{E} = \bar{U} + \bar{K} = \frac{1}{2} \overline{\sum_{i \neq j} V(|\vec{r}_i - \vec{r}_j|)} + \overline{\sum_i^N \sum_{\alpha=x,y,z} \frac{mv_{i,\alpha}^2}{2}} \quad (8.16)$$

and its standard derivation σ_E by

$$\sigma_E = \sqrt{(\bar{E}^2 - \bar{E}^2) / \bar{E}^2} \sim \Delta t^2 \quad (8.17)$$

From an empirical point of view, a time step Δt is reasonable if $\sigma_E \leq 10^{-3} - 10^{-4}$.

8.5 Connection to thermodynamics and velocity rescaling

For a many-body atomic system (in contrast to a planetary systems with only very few 'particles') we can obviously make connection to thermodynamics and try to define a temperature. Statistical mechanics told us that the thermodynamic average temperature in 3D can be expressed by the kinetic energy:

$$\bar{T} = \frac{2\bar{K}}{3Nk_B} \quad (8.18)$$

with the instantaneous temperature

$$\hat{T} = \frac{2\hat{K}}{3Nk_B} \quad \text{and} \quad \hat{K} = \hat{E} - \hat{U} \quad \text{with} \quad \hat{E} = \text{const.} \quad (8.19)$$

In an NVE ensemble \bar{T} is not constant in time. This is later imposed in the NVT ensemble where $\bar{T} = \text{const.}$

The kinetic energy can be expressed by particle velocities:

$$\hat{K} = \sum_i \frac{p_i^2}{2m_i} = \sum_i \frac{1}{2} m_i \vec{v}_i^2 = \sum_i \sum_{\alpha=x,y,z} \frac{1}{2} m_i v_{i,\alpha}^2 \quad (8.20)$$

A simple way to perform Molecular Dynamics at constant Temperature T_S in NVE (or to impose it as initial condition) is to start from a Maxwell-Boltzmann distribution Eq. (11.7) and in the process of the simulation rescale the particle velocities (e.g. every 10th or 100 MD step) according to the rule

$$v_{i,\alpha}^{\text{new}} = \sqrt{\frac{T_S}{\hat{T}}} v_{i,\alpha}^{\text{old}} \quad (8.21)$$

where \hat{T} is the instantaneous temperature obtained by Equation 8.19. We will discuss the limitations of this 'velocity rescaling' later when we talk about properly thermostating a simulation in *NVT*. In particular, this rescaling does not correspond to a real thermodynamic ensemble. It also leads to systematic problems, such as the 'flying ice cube' problem: the system freezes into a finite solid cube which translates with a high center-of-mass velocity in the simulation box. While the mean temperature may be ok (and as desired), this system is clearly not in an equipartitioned equilibrium! However, velocity rescaling can be used to initialize a system in *NVE* already close to an equilibrium ensemble at a desired temperature.

We note already here how in the *NVT* ensemble the average pressure can be calculated. We can use the virial, according to

$$\bar{P} = \frac{N}{V} k_B \bar{T} - \frac{1}{3V} \overline{\sum_{i=1}^N r_{ij} \nabla_i U} \quad (8.22)$$

In the case of isotropic pair potential, this reduces to

$$\bar{P} = \frac{N}{V} k_B \bar{T} - \frac{1}{3V} \overline{\frac{1}{2} \sum_{i=1}^N r_{ij} \frac{dV}{dr_{ij}}} \quad (8.23)$$

Hence, we can easily access the equation of state in a simulation by calculating the pressure in dependence of, for example, the volume (at fixed temperature). We will discuss this in more detail when we talk about barostatting a simulation to simulate at constant pressure.

8.6 Initial conditions and steps to set up a MD simulation

- define your model: (pair) potentials, external fields, i.e., the 'force field'
- define the simulation cell and appropriate boundary conditions (e.g. the cell shape and volume, particle density, confining external fields such as walls, etc.); more details on boundary conditions come in the next sections.
- in an *NVE* ensemble the initial configuration (\vec{r}_i, \vec{p}_i) defines the energy $E = \text{const.}$
The initial configuration should avoid overlaps and extreme "non-equilibrium" configurations as extreme forces will cause the simulation to crash.
A good approach is energy minimization where atoms are displaced by Δr until the force F is lower than a threshold.
- define initial velocities

They are typically chosen from a Maxwell-Boltzmann distribution for the Cartesian velocities

$$P(v_{i,\alpha}) = \frac{1}{\sigma \sqrt{2\pi}} e^{-\frac{v_{i,\alpha}^2}{2\sigma^2}} \quad (8.24)$$

where $\sigma = \sqrt{\frac{k_B T}{m_i}}$ and $\alpha = x, y, z$. Alternatively we can start with random velocities and let them equilibrate into a Maxwell-Boltzmann distribution using velocity rescaling.

- for n_{equi} time steps
 - solve equations of motion for $\{\vec{r}_i, \vec{v}_i\}$
 - calculate \hat{K} , \hat{U} , $\bar{K}(t)$, $\bar{U}(t)$
 - check for drift, conservation etc,
 - if needed, rescale velocities $v_{i,\alpha}^{\text{new}} = \sqrt{\frac{T_S}{\hat{T}}} v_{i,\alpha}^{\text{old}}$

- if equilibrated, for n time steps do
 - solve the equations of motion
 - calculate \hat{K} , \hat{U} and things of interest (every m steps with $\frac{m}{n} = 10\dots 100$)
 - accumulate values for \bar{K} , \bar{U} etc.
- organize input and output files
- analyze data, averages, correlations, etc.
- find physical model and equations that describe your computer experiment

Chapter 9

Particle-resolved simulations of finite systems

9.1 Computational boxes and periodic boundary conditions

In simulations, we can only consider finite systems in space and time. Hence, we need appropriate boundary conditions and computational 'boxes'. Let us consider N particles in a simulation box of volume V_{box} in 3D. The number of particles ranges typically between $10^2 \leq N \leq 10^4$, but varies a lot depending on the respective hardware and software, ranging as far as up to $N \sim 10^7$. One problem is that the computational time to evaluate (pair) forces is $\sim N^2$ (or $\sim N \log N$ using special techniques).

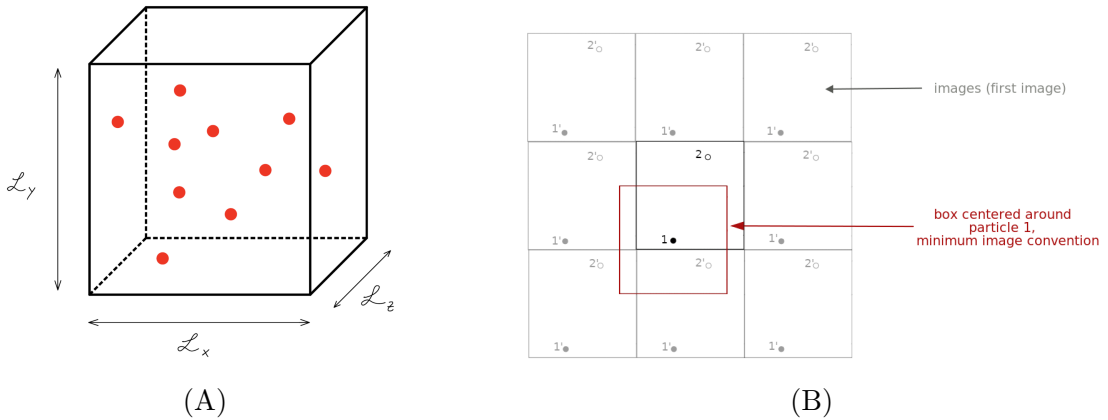


Figure 9.1: Simulation cell with boundary walls. Most particles inside the volume $V_{\text{box}} = \mathcal{L}_x \mathcal{L}_y \mathcal{L}_z$ feel the boundaries imposed by the box surface. Better is to make the box periodic (B): if one particles exits on the 'right' side, it will re-enter on the 'left' side. These are periodic boundary conditions (PBC).

The simulation cell of a finite system is shown in Figure 9.1-A. A main problem of finite systems are the surfaces, as most particles feel the box surface. One way to solve this problem is to introduce periodic boundary conditions (**PBC**) (see Figure 9.1-B). This creates infinites replicas of the main calculation box. Therefore we have an infinite number of periodic 'images' of every particle. The images in the boxes in vicinity of the main box are the 'first' image, and so forth and so on.

The form of the box volume is not restricted to cubic boxes, but instead any crystal lattice can serve as a unit cell. It is only important that it can be periodically repeated in a 100%

space-filling way in the desired space dimension. Depending on the geometry of the model system (e.g., a protein in water) for example truncated polyhedrons can be more efficient than cubic boxes for simulations because only the most relevant hydration layer is considered, not many water molecules far away from the protein. Also, for the simulation of crystals, non-cubic boxes are important to respect the periodicity ("commensurability") of the crystal in all space directions.

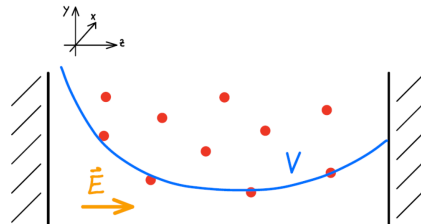


Figure 9.2: Simulation cell with applied external potential by an external electric field \vec{E} .

If an external potential is present, the cell and the periodic boundary conditions need to be adapted as shown in Figure 9.2. Here, a field induces density inhomogeneities in one direction, say z . An equilibrium can be established by introducing confining walls in that direction. The perpendicular directions, x, y , can be periodic.

Periodic boundary conditions in code [8]: consider a 1D box with coordinate axis x and the box size L and $x = 0$ being the center of the box:

- if $x > L/2$ then $x = x - L$
- if $x < L/2$ then $x = x + L$

A bit more general

- if $x > L/2$ then $x = x - L * \text{INT}(x/L)$
- if $x < L/2$ then $x = x + L * \text{INT}(x/L)$

The `INT()` function returns the nearest integer. This way, also longer 'jumps' ($> L$) bring back the particle to the main computational box with $-L/2 < x < L/2$.

Important concept in PBCs: Minimum image convention (see Appendix for illustrations): Calculate interactions/forces f_{ij} only using the 'minimum image', that is, take the particle image of j for the calculation which is in nearest distance to particle i , even if it is not in the main box. Code: Distance $x_2 - x_1 = \Delta x \rightarrow \Delta x = \Delta x - L * \text{INT}(\Delta x/L)$

Problems of periodic boundary conditions (PBCs)

- long ranged potentials have to be dealt with via truncation and cut-offs
- no long-wavelength fluctuations are possible, which leads to quantitative and qualitative errors for phase transitions
- commensurability for crystals is not always possible
- corrections to transport properties or charging free energies due to simulation of periodic lattice

- in general, finite size effects are still present (check: how do simulation averages depend on box size? ← systematic 'finite size scaling study'; always recommended!)
- quasi-ergodicity and kinetic trapping

9.2 Implementation of short-ranged pair potentials: cutoffs and truncation

Cutoffs need to be introduced with $r_{\text{cut}} < \frac{L}{2}$, where L is the smallest box dimension, to avoid overlaps of periodic images (see Appendix). Hence, energies and forces

$$\text{potential energy} \quad \hat{U} = \frac{1}{2} \sum_{i \neq j} V(r_{ij}) \quad (9.1a)$$

$$\text{forces} \quad f_{ij} = \frac{1}{2} \sum_{i \neq j} \left(-\frac{dV}{dr_{ij}} \right) \quad (9.1b)$$

are only calculated for $r < r_{\text{cut}}$. Typically the potentials are shifted then to make sure $V(r_{\text{cut}}) = 0$ and there is no jump at the cut-off. Even better is to shift the force, see Fig. 9.3, then the force does not jump at r_{cut} and the slope of the potential goes smoothly to zero there. However, this changes your model potentials, in particular when r_{cut} is quite short relative to the range of the potential (see illustrations in Appendix).

The cutoff value r_{cut} should not be too small of course, otherwise we make a big error. The error ΔU can be calculated via

$$\Delta U \simeq 4\pi \frac{N}{V_{\text{box}}} \int_{r_{\text{cut}}}^{\infty} V(r) r^2 dr \quad (9.2)$$

for three dimensions. For potentials of the form $V(r) \sim r^{-n}$, the respective error is $\Delta U \sim r_{\text{cut}}^{3-n}$. In the case of the Lennard-Jones potential, the error vanishes with r_{cut}^{-3} as $n = 6$. For potentials with $n \leq 3$ though, the error diverges! This is the case for long-ranged pair potentials as the Coulomb potential where $n = 1$. (These require special methods that we will discuss later on.)

1. **Calculate potentials (or forces)** according to "minimum image convention" (hand-out/appendix)
2. **Use cut-off r_{cut}**
It is very important to avoid numerical artefacts by making cut potentials (or forces) continuous at r_{cut} as shown in Figure 9.3.

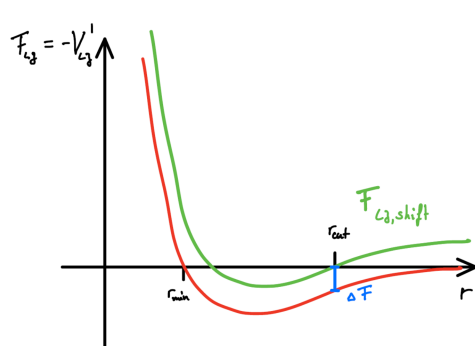


Figure 9.3: The given Lennard-Jones pair force (red) is shifted by ΔF (green) before applying the cut-off at r_{cut} in order to satisfy continuity

9.3 Solutions to speed-up particle-based codes

In particle-based simulations, both the number of atoms needed to model a representative volume element, and the number of time steps required to simulate a real time in the μs range are limiting factors. For example:

- it takes 150000 atoms to model a volume of 1000 nm^3 using a bcc crystal with a lattice parameter of 2.5 \AA ,
- it takes 100000 atoms to model a volume of 1000 nm^3 of water with a density $\rho \approx 0.096 \text{ atoms}/\text{\AA}^3$
- with a time step $\delta t \approx \text{fs}$, it takes 10^9 time steps to simulate a real time in the μs range

without any algorithms to speedup a molecular dynamics engine, 95% of the computing time is used for the force calculation. The remaining 5% are used for the update of the atoms positions/velocities, thermostating, barostating, ... It is therefore necessary to develop algorithm to speedup the force calculations.

The possible methods to speedup particle-based scheme are:

- Verlet list/neighbor list
- Link-cell
- Parallel solution for the force calculation

9.3.1 Verlet/neighbor list

main idea: For each atom i , a list of nearest neighbors included in a sphere of radius $r_s = r_c + \delta$, where r_c and δ are the potential cutoff and a shell thickness, respectively, is constructed and maintained (see Fig. 9.4). The list is used to evaluate the forces acting on atom i . The list is updated before any atoms could have moved farther than δ .

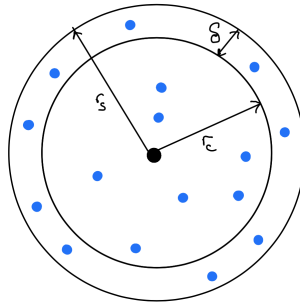


Figure 9.4: Definition of the Verlet list centered on atom i . δ is the shell thickness.

In practice, the shell thickness, δ is much lower than the cutoff radius, r_c .

The shell thickness depends on the physical properties such as the temperature, the density of the system, the diffusivity. As a rule of thumb, $\delta \approx r_c/5$.

Let us consider a system of N atoms interacting with short range potential. For notation purposes, "Number" is an array containing the number of atoms included in the verlet list centered on atom i , and "VerletList" is an array containing the corresponding atom's ids. The algorithms to evaluate the forces on atoms i , without and with the Verlet list are given in Table 9.1

| Without the Verlet list | With the Verlet list |
|--|---|
| <pre>do i = 1, N - 1 do j = i+1, N F_i = force due to atoms j on i F_j = $-F_i$</pre> | <pre>do i = 1, N - 1 do j = 1, Number(i) jj = VerletList(i,j) F_i = force due to atoms jj on i</pre> |

Table 9.1: Algorithms to evaluate the forces on atoms i without and with the Verlet list. "Number" is an array containing the number of atoms included in the Verlet list centered on atom i , and "VerletList" is an array containing the corresponding atom's ids.

Although the computing time is reduced while using the Verlet list, the overall gain is not significant since the array "VerletList" must be updated every few time steps, and the corresponding computing time to maintain the list is still proportional to N^2 .

9.3.2 Link-cell

main idea: The simulation box is decomposed in (N_x, N_y, N_z) boxes of length $d > r_c$, along the x , y , and z directions (see Fig. 9.5).

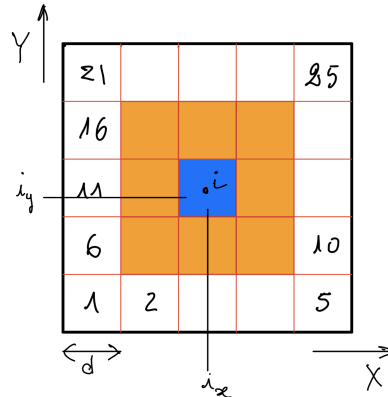


Figure 9.5: 2D representation of the domain decomposition used for the link-cell algorithm.

At each time step, the atoms i with coordinates (x_i, y_i, z_i) are assigned to a box, n_{box} according to $n_{box} = i_x + N_x(i_y - 1 + N_y(i_z - 1))$ where $i_{x,y,z} = \text{floor}((x, y, z)_i/d) + 1$ with $\text{floor}(x)$ being the operator returning the largest integer not greater than x . To calculate the force on atoms i included in the box n_{box} , only the atoms included in the nearest boxes need to be considered. The algorithm to calculate the force F_i on atoms i is summarized in Table 9.2.

| |
|--|
| do i = 1, number of boxes |
| do j = 1, number of atoms in box i |
| jj = Cell(i,j) # atom id of atom j included in the box i |
| do k = 1, 27 |
| kk = Ncell(i,k) |
| do l = 1, number of atoms cell k |
| ll = Cell(kk, l) # atom id of atom l included in the nearest box |
| force between atom ll and atoms jj |

Table 9.2: Algorithm to evaluate the forces on atoms jj with the link cell. "Cell" is an array containing the atom's ids included in cell i . "Ncell" is an array containing the nearest neighboring box.

Although the link-cell must be update every time steps, since its computational time is proportional to the number of atoms N , the computational time for the force calculations is reduced from N^2 to $N\log(N)$.

Notes:

- the size the boxes must be larger than the radius cutoff of the short-ranged potential ($d > r_c$),
- the domain decomposition must be larger than (4, 4, 4) to be efficient,
- interesting if the number of atoms, N , is larger than 1000,
- update the link-cell list at each time step.

Combining the link-cell list with the Verlet list leads to a significant computational gain over conventional link-cell method since the number of atoms in spheres of volume $V = \frac{4}{3}\pi r_s^3$ is much lower than in cube of volume $V = 27r_c^3$.

9.3.3 Parallel solutions

Let us define T_1 and T_N the elapsed time of 1 and N workers (processors), respectively, and f the fraction of the code that cannot be parallelized.

The speedup, S , is defined by the Amdahl's law as:

$$S = \frac{T_1}{T_N} < \frac{T_1}{(f - \frac{1-f}{N})T_1} < \frac{1}{f} \text{ as } N \rightarrow \infty \quad (9.3)$$

If 90% of the code is parallel, and 10% not, a speedup of 10 at best can be obtained with a lot of workers.

The efficiency is defined as the ratio between the speedup and the number of workers. For a code to scale linearly, the efficiency is 1, and thus the number of workers must be equal to speedup. If the efficiency is larger than 1, one has a super-linear scaling, and it is associated to a cache effect.

There is a difference between task-parallel algorithm and data-parallel algorithm. Task-parallel program is the parallel execution of different tasks on each computing code. Data-parallel program is the execution of the same tasks on each node.

examples: Let us assume a list $N = [...]$, and two different tasks $\sum i$ and $\sum i^2$

data-parallel for 2 cores: # 0: $\sum_{i=0}^{N/2-1}$ and #1: $\sum_{i=N/2}^N$

task-parallel for 2 cores: # 0: $\sum_{i=0}^N i$ and #1: $\sum_{i=0}^N i^2$

A key factor for parallel code is the communication time between processors. The communication time includes the data transfers and the startup of the parallel environment. It reduces the parallel efficiency.

Strategy for the parallelism of particle-based engine

In molecular dynamics, the forces, velocities, and positions update is done simultaneously in parallel. Thus one has to divide the force calculation among processors. It exists two classes of algorithm to parallelize a MD code. i.e. *atom-decomposition* vs *domain-decomposition* (see Fig. 9.6).

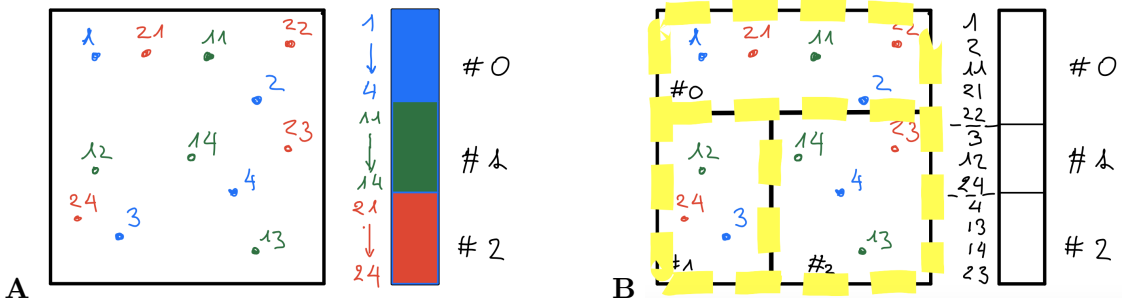


Figure 9.6: **A** Atom-decomposition, and **B** Domain-decomposition.

When considering the atom-decomposition strategy, a predetermined set of atoms is given to each processors. With such an approach, one can reach a perfect load balancing if each processors have the same amount of atoms. Since each processors need the information of all atoms to calculate the forces, such a strategy is adequate for shared memory architecture, and thus for replica exchange type of calculations.

When considering the domain-decomposition strategy, the entire simulation box is decomposed in sub-regions and buffer regions, the buffer regions being used to transfer information between processors. While the method can be easily interpreted as an extension of the link-cell method, a parallelization of the MD code using a domain-decomposition method has the advantage that the domain size can now be lower than the radius cutoff used for the short-range interactions. However, for highly inhomogeneous systems, dynamics load balancing must be considered, which drastically complicates the communication strategy to implement between domains.

Notes:

In python language, one can use the package `numba` combined with the decorator `@njit(parallel=True)` to perform an implicit parallelization of the force calculation. In that case, the outer loop of the force calculation will be parallelized, and the code will become a task-parallel program.

9.4 Errors

9.4.1 Systematic errors

- finite size effects
- long-ramped interaction effects
- poor equilibration or poor initial step
- force field
- using software as black box
- lack of knowledge of statistical mechanics and approximations

9.4.2 Statistical errors

The (absolute) standard error of the mean f_x is defined as

$$f_x = \frac{\sigma_x}{\sqrt{n}} \quad (9.4)$$

with n being the number of measurements. The relative error is then given by $\epsilon_x = \frac{f_x}{\langle x \rangle}$.

The Propagation of errors is approximated by the upper bounds. Some simple Propagation rules are displayed here:

| | | |
|-----------------------------|---------------|--------------------------------------|
| $y = x_1 + x_2 - x_3 \dots$ | \rightarrow | $f_y = \sum_i f_{x_i}$ |
| $y = x_1 * x_2 / x_3 \dots$ | \rightarrow | $\epsilon_y = \sum_i \epsilon_{x_i}$ |
| $y = c * x_1$ | \rightarrow | $f_y = c * f_{x_1}$ |
| $y = x_1^n$ | \rightarrow | $\epsilon_y = n * \epsilon_{x_1}$ |

Table 9.3: Some fundamental error propagation rules

In simulations:

In simulation the average over time τ is given by

$$\bar{x}_\tau = \frac{1}{\tau} \int_0^\tau dt x(t) \quad (9.5)$$

and the standard derivation σ_x by

$$\sigma_x^2 = \frac{1}{\tau} \int_0^\tau dt (x(t) - \bar{x}_\tau)^2 \quad (9.6)$$

If all $x(t)$ are uncorrelated, then $f_{x_\tau}^2 = \frac{\sigma_x^2}{n}$ with $\tau = n\Delta t$.

It is important to note though, that for small time $\tau < \tau_c$ $x(t)$ and $x(t+\tau)$ are correlated. In this case the standard derivation is given by

$$\tilde{\sigma}_x^2 = \frac{1}{\tau^2} \int_0^\tau \int_0^\tau dt dt' (x(t) - \bar{x})(x(t') - \bar{x}) \quad (9.7)$$

$$\simeq \frac{1}{\tau} \int_0^\infty dt C_{xx}(t) = \frac{\tau_c}{\tau} C_{xx}(0) = \frac{\tau_c}{\tau} \sigma_x^2 = \frac{\sigma_x^2}{N} \quad (9.8)$$

using the invariance and $t > \tau_c$ whereas τ_c denotes the correlation time or "memory time" of the system. $N = \frac{\tau}{\tau_c}$ is then the number of independent measurements. It is therefore useful to calculate block averages to determine the error as seen in Figure 9.7.

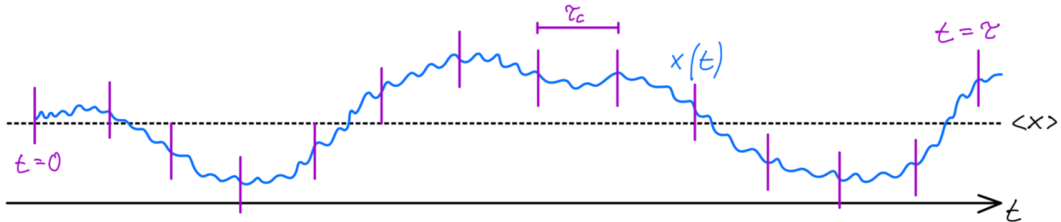


Figure 9.7: To determine the error, $N = \frac{\tau}{\tau_c}$ independent blocks can be identified. The number $\frac{1}{N}$ is also a measurement for the "statistical inefficiency" of the system.

Slow dynamics equal in general a long memory of the system. It is important to be careful with the error analysis, in particular when multiple time scales (and multiple τ_c) play a role.

9.5 Units

Units in your particle-based simulation (MD, MC, Brownian Dynamics) can be either "real" or "reduced", for example

| unit | scale | reduction factor | reduced unit |
|-------------|---------------------------|---------------------------------|-------------------------|
| mass | kg or u | m_0 | $m^* = m/m_0$ |
| length | m or nm | σ | $L^* = L/\sigma$ |
| time | s or ps | $t_0 = \sigma \sqrt{m_0/k_B T}$ | $t^* = t/t_0$ |
| energy | kJ/mol | $k_B T$ | $E^* = E/k_B T$ |
| temperature | K | " | " |
| density | 1/mm ³ | $1/\sigma^3$ | $\rho^* = \rho\sigma^3$ |
| pressure | kJ/(mol mm ³) | $k_B T/\sigma^3$ | $P^* = P\sigma^3/k_B T$ |

Table 9.4: Units used in particle-resolved simulation techniques (such as Molecular Dynamics, Monte-Carlo or Brownian Dynamics), and their respective reduced units.

Chapter 10

Long range interactions: Electrostatics in molecular physics

Typically, ions, molecules and macromolecules carry charges and move in a polar environment. Examples are ions in water, proteins and DNA in aqueous electrolytes, ionic crystals, cell membranes, micelles and charged colloids (see Figure 10.1 and Figure 10.2).

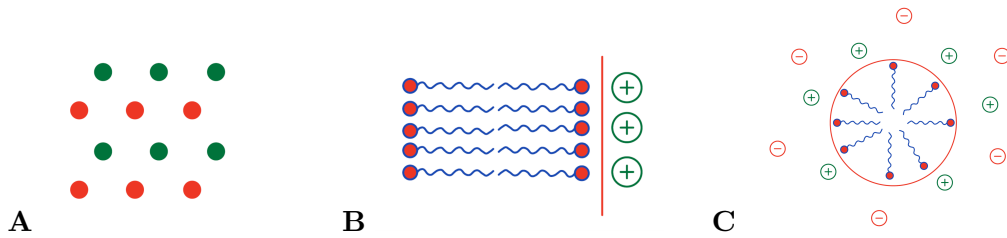


Figure 10.1: Examples for charged structures are **A** ionic crystals **B** cell membrane or **C** micelles from left to right.



Figure 10.2: Examples for charged structures are **A** charged colloids or **B** charged rods as a model for DNA.

All charges interact with the Coulomb pair potential given by:

$$V_C(r) = \frac{Z_1 Z_2 e^2}{4\pi\epsilon_0\epsilon_r r} \quad (10.1)$$

with Z_i being the valency and ϵ_r being the dielectric constant of the background (e.g., a continuum of water).

Deriving the charge density distributions $\rho_{\pm}(r)$, the electrostatic potential $\Phi(r)$ and the electric field $E(r) = -\nabla\Phi$ though is not trivial because of the mobility and fluctuations of charges and their long range of $\sim \frac{1}{r}$. Usually there are at least two components (+ and -), like in salt

to ensure electroneutrality. The charges attract and lead to ion pairing and alternating signs of charge. The summation of Coulomb interaction is cumbersome because of the long range every contribution is important. In particular, in periodic system in principle one has to add up all contributions to infinity because the Coulomb sum over all images is only slowly and conditionally converging (classic Madelung problem for ionic crystals in solid state physics). This can be solved by Ewald summation introduced later. Usually simple cut-offs are too inaccurate and not well-controlled. But let us first look at some simple theory to understand also the basic action of mobile electrostatic charges, which leads to the very important Debye-Hückel screening effect.

The theoretical treatment is usually done by the **Poisson-Boltzmann** equation:

The Poisson-Equation is given by

$$\nabla[\epsilon(\vec{r})\nabla\Phi(\vec{r})] = -\frac{\lambda(\vec{r})}{\epsilon_0} \quad (10.2)$$

where $\epsilon(\vec{r})$ is the position-dependent dielectric constant and $\lambda(\vec{r})$ is the charge density per volume. If λ and ϵ are known, then the integration of the Poisson-Equation yields the solution for the field and the potential. Often $\epsilon(\vec{r}) = \text{const.} = \epsilon_r$ is assumed for simplicity.

Now what happens if we consider mobile salt ions? Assuming the Boltzmann distribution ("mean-field" approximation) of the charge density, we get the distribution of charges in the potential Φ , as

$$\lambda(\vec{r}) = \lambda_{\text{ext}}(\vec{r}) + \sum_{i=+,-} Z_i \rho_i e^{-\beta Z_i e \Phi(\vec{r})} \quad (10.3)$$

whereas the first term describes the external, fixed charge distribution and the second term describing the Boltzmann assumption for ions, $\lambda_{\text{ion}}(\vec{r}) = \sum Z_i \rho_i(\vec{r})$. This is 'mean-field' because steric and electrostatic spatial correlations between the ions are neglected. (The ion-ion $g(r)$ shown in the Appendix show these correlations.)

Including the Boltzmann assumption for ions in the Poisson-Equation, we get a nonlinear differential equation for Φ and $\rho_{\pm}(\vec{r})$, the Poisson-Boltzmann equation.

For small electrostatic potentials the exponential Boltzmann distribution can be linearized. For symmetric salt, the linearized version results into the **Debye-Hückel** (DH) theory, given as:

$$\boxed{\Delta\Phi(\vec{r}) = \kappa^2 \Phi(\vec{r})} \quad (10.4)$$

The DH theory introduces generally (without assuming any specific charge distribution) the **screening length** κ^{-1} , defined by

$$\kappa = \sqrt{4\pi\lambda_B \sum_i Z_i^2 \rho_i} \quad (10.5)$$

For a monovalent symmetric salt of bulk (or reservoir) concentration c_s , this reduces to

$$\kappa_s = \sqrt{8\pi\lambda_B c_s} \quad (10.6)$$

where $\lambda_B = \frac{e^2}{4\pi\epsilon_0\epsilon_r k_B T}$ is the **Bjerrum length**, which is an electrostatic coupling parameter. It tells us at which distance the electrostatic interaction between two elementary charges is the same as the thermal energy $k_B T$. For example, $\lambda_B = 0.71$ nm for water under normal conditions.

However, the Debye-Hückel screening length $\lambda_D = \kappa^{-1}$ is the decisive parameter that tunes the range of electrostatic interaction. It can vary from millimeter to $\lambda_D \rightarrow 0$, depending on the salt

concentration. A reference size is the screening length of $c_s = 0.1 \text{ mol/l}$ salt in water at 300 K which is $\lambda_D \simeq 1\text{nm}$.

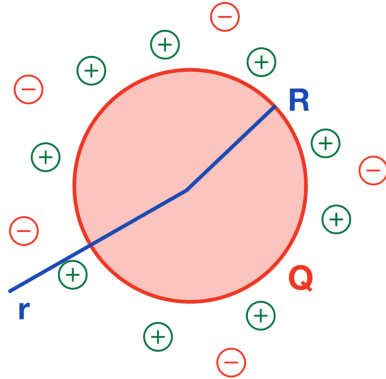


Figure 10.3: Salt ions screening a charged colloidal sphere of radius R . The electrostatic potential in radial distance r is exponentially screened to a range defined by the Debye-Hückel screening length $\lambda_D = \kappa^{-1}$.

The solution to the Debye-Hückel theory for a charged sphere is given by:

$$\Phi(r) = \frac{Q}{4\pi\epsilon_0\epsilon_r r} \frac{e^{-\kappa(r-R)}}{1 + \kappa R} \sim \frac{e^{-\kappa r}}{r} \quad (10.7)$$

where the first factor is the usual Coulomb contribution and the second factor describes the exponential screening from the ions, cf. Fig. 10.3.

Note, the Poisson-Boltzmann (PB) equation and the linearized PB form (DH-theory) can be solved for various geometries analytically, such as ions between charged walls or for interacting spherical macromolecules. For interested reader we refer to the literature, for example [3].

Important for simulations:

Make sure that $\kappa^{-1} = \lambda_D \ll \text{box size}$, as otherwise artefacts due to finite size will be created.

10.0.1 Molecular Dynamics simulations of ions and charged particles

The long range nature of the Coulomb pair potential ($\sim \frac{1}{r}$) is intrinsically problematic with finite or periodic systems.

Consider the total Coulomb energy:

$$U_C = \frac{1}{2} \sum_{i \neq j} \frac{Z_i Z_j e^2}{4\pi\epsilon_0\epsilon_r |\vec{r}_i - \vec{r}_j|} = \frac{1}{\beta} \frac{1}{2} \sum_{i \neq j} \frac{Z_i Z_j \lambda_B}{|\vec{r}_i - \vec{r}_j|} \quad (10.8)$$

We recall that due to the $\sim \frac{1}{r}$ behavior, the error of the cut-off is substantial!

Consider summing over all images \vec{m} across the **PBC**:

$$\beta U_C = \frac{1}{\beta} \frac{1}{2} \sum_{\vec{m}} \sum'_{i=j} \frac{Z_i Z_j \lambda_B}{|\vec{r}_{ij} + \vec{m}L|} \quad (10.9)$$

where we sum over all images $\vec{m} = (m_x, m_y, m_z), \vec{m} \in \mathbb{Z}^3$ and L denoting the cubic box length and $\vec{r}_{ij} = \vec{r}_j - \vec{r}_i$.

This solution is only conditionally convergent and the result substantially depends on the order of \vec{m} ! Direct sums prove to be risky and problematic. Typical treatments are for example:

1. **Truncation**/Reaction field/Multipole methods: A good discussion is given in Allen & Tildesley [8] including the seminal work by Wolf [13].
2. **Ewald method** and extensions: the "gold standard"

10.0.2 Truncation methods

Generally, one can attempt to cut the electrostatic potential to treat explicitly the interactions in the main simulation box, and then try to approximate the action of the surrounding charges by expanding their potential in multipole moments.

Simple first order truncation For example, we consider charged particles in a spherical volume with a cut-off radius of r_c as seen in Figure 10.4.

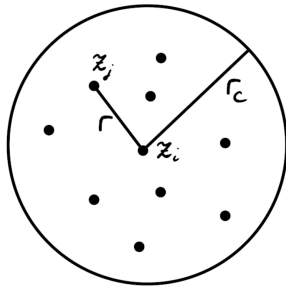


Figure 10.4: Spherical volume with cut-off radius r_c and charged particles with charge valencies Z_i .

The Coulomb energy is then given by

$$\beta E_c = \sum_{i=1}^N \left(\sum_{j \neq i}^{r_{ij} < r_c} \frac{Z_i Z_j \lambda_B}{r_{ij}} - Z_i \Delta U(r_{ij}) \right) \quad (10.10)$$

where $\Delta U(r_{ij})$ is the correction factor, e.g., the first order correction to respect to charge neutrality of the whole system

$$\Delta U = Z_i \frac{\lambda_B}{r_c} \quad \text{with} \quad Z_i = \sum_j^{r_{ij} < r_c} Z_j \quad (10.11)$$

We then get a Coulomb energy of:

$$\beta E_c = \sum_{i=1}^N \left(\sum_{j \neq i}^{r_{ij} < r_c} \beta V_{\text{Shift}}^c(r_{ij}) - \frac{\lambda_B}{r_c} Z_i^2 \right) \quad (10.12)$$

with a shifted Coulomb potential of

$$\beta V_{\text{Shift}}^c(r_{ij}) = \begin{cases} Z_i Z_j \lambda_B \left(\frac{1}{r_{ij}} - \frac{1}{r_c} \right) & \text{if } r_{ij} < r_c \\ 0 & \text{if } r_{ij} > r_c \end{cases}. \quad (10.13)$$

For further reading, e.g., how to include higher moments, see the literature [8, 14].

Damped Coulomb Coulomb interaction is damped by an error function close to truncation. Suppresses artificial oscillations of the potential of truncated Coulomb systems [13]. Good efficient methods for dense Coulomb systems such as ionic crystals.

Multipole methods: fast numerical evaluation of higher multipole moments [8].

Reaction field method: assumes medium with effective dielectric constant outside the truncation sphere. Results in a further shift of the cut Coulomb potential [8].

This results in a further shift of the interaction potential by

$$\beta \Delta V_{\text{RF}}(r_{ij}) = Z_i Z_j \lambda_B \frac{\epsilon_{\text{RF}} - 1}{2\epsilon_{\text{RF}} + 1} \frac{r_{ij}^2}{r_c^3} \quad (10.14)$$

where ϵ_{RF} denotes the dielectric constant outside the range of r_c .

This method is in general a good approach for $N > 10^5$ particles because it involves Fourier transforms.

10.0.3 Ewald method

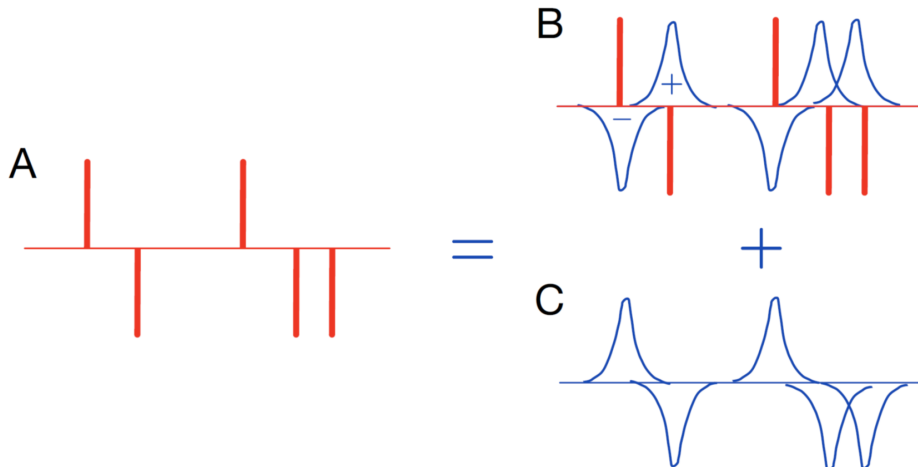


Figure 10.5: Gaussian screening the discrete charge distribution: A set of point charges **A** defined as $\rho(\vec{r}) = \sum_i q_i \delta(\vec{r} - \vec{r}_i)$ with $q_i = z_i e$ can be decomposed into a set of **B** + **C**. The set **B** adds Gaussian neutralizing clouds around the charges, so that all interactions become short-ranged (in the regions where the Gaussian overlap). The inverted Gaussians in **C** then present a 'smooth' (with only long wavelength variation) screening background. Hence, **B** and **C** represent short- and long-range interactions, respectively.

The general idea of this approach is to split the problem into short- and long-ranged action of charges and evaluate with separate, rapidly converging sums in real and k-space, respectively. This is achieved by a so called Gaussian screening as seen in Figure 10.5. The Gaussian functions taken for mathematical convenience. They are given as:

$$\rho_G(\vec{r}) = \sum_{i=1}^N q_i \left(\frac{\alpha}{\pi} \right)^{3/2} e^{-\alpha(\vec{r} - \vec{r}_i)^2} \quad (10.15)$$

where $\alpha^{-1/2}$ is the distribution width, also referred to as Ewald screening length. The charges are $q_i = z_i e$.

Then **B** has a total charge density:

$$\rho_{\text{tot}}(\vec{r}) = \sum_i q_i \left(\delta(\vec{r} - \vec{r}_i) - \left(\frac{\alpha}{\pi} \right)^{3/2} e^{-\alpha(\vec{r} - \vec{r}_i)^2} \right) \quad (10.16)$$

The electrostatic potential of a Gaussian is $\phi_G \sim \frac{\text{erf}(\alpha r)}{r}$. As a result [8], the Coulomb energy of the short-ranged part is

$$\beta U_B = \frac{1}{2} \sum_{i=j} z_i z_j \frac{\text{erfc}(\sqrt{\alpha} |\vec{r}_{ij} + \vec{m}L|)}{|\vec{r}_{ij} + \vec{m}L|} \quad (10.17)$$

with $\text{erf}(x) = \frac{2}{\sqrt{\pi}} \int e^{-x^2} dx$ being the error function and the complementary error function $\text{erfc} = 1 - \text{erf}$.

For sufficiently large α and a real space cut-off of $r_c < L$, then only considering $\vec{m} = \vec{0}$ in the sum is sufficient as the sum is very quickly converging.

The **long-ranged** interactions **C** result in the total Coulomb energy

$$\beta U_C = \frac{2\pi\lambda_B}{V} \sum_{\vec{k} \neq 0} \frac{1}{k^2} |\rho(\vec{k})|^2 e^{-\frac{k^2}{4\alpha^2}} \quad (10.18)$$

with $\vec{k} = \frac{2\pi\vec{m}}{L}$ and employing the Fourier space density fluctuations

$$|\rho(\vec{k})|^2 = \sum_i \sum_j q_i q_j e^{-i\vec{k}(\vec{r}_j - \vec{r}_i)} \equiv S(\vec{k}), \quad (10.19)$$

which equals the charge-charge structure factor $S(\vec{k})$. The latter expressions are derived by Fourier transforming the Poisson equation with Gaussian charge distributions [8]. The low k (large wavelength)-expansion in Fourier space is meaningful as we want to include the long range effects of the smooth distribution **C**.

For too large values of α , many terms of the k -space are needed. Therefore we would like to optimize the choice of α . Here, empirical choices and rules of thumb are available [8].

The total Ewald energy is then given by:

$$U_{\text{Ewald}} = U_A + U_B - \sqrt{\frac{\alpha}{\pi}} \sum_{i=1}^N q_i^2 \quad (10.20)$$

with the last term being the self-energy correction. The simulation time of the Ewald method scales $\tau_{\text{sim}} \sim N^{3/2}$.

The Ewald forces are given by the derivation $\vec{F}_i = -\nabla U_{\text{Ewald}}$.

Note: *PPPM* (particle-particle particle-mesh Ewald method):

The *PPPM* is an algorithmic implementation on a discrete grid (mesh) using FFT routines which results in $\tau_{\text{sim}} \sim N \log N$

Chapter 11

MD simulation in different ensembles

In the majority of the lessons discussed thus far and especially in the simulations implemented in the exercises, we have studied the (natural) time evolution of a system of N particles confined to a volume V and interacting only with one another through pairwise forces. In other words, we have studied the dynamical evolution of systems in the "isolated", microcanonical (N, V, E) ensemble where neither heat gets exchanged with the environment (via a bath), nor is external work done by or on the system. This is, however, almost never the 'realistic' ensemble in which experiments are performed. More realistic scenarios are portrayed in Figure 11.1.

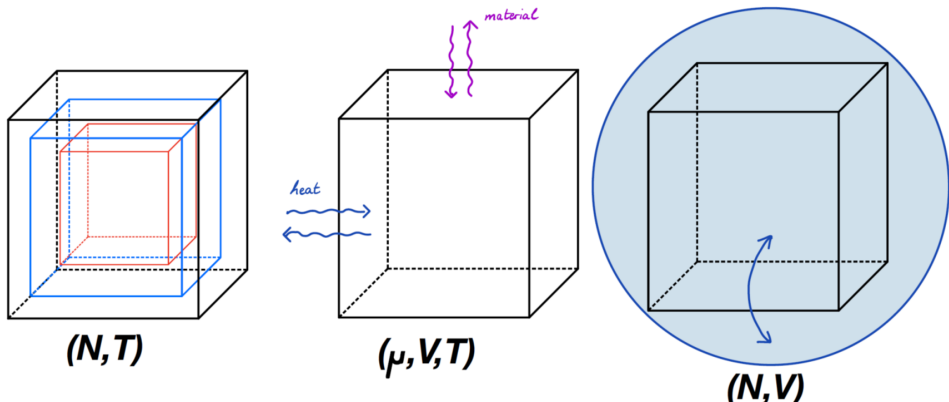


Figure 11.1: In the **Isothermal-Isobaric ensemble on the left**, heat flow is allowed and mechanical work can be done on or by the system. The pressure P has small fluctuations about a mean value and the volume responds to the difference between external and internal pressure. In the **Grand Canonical ensemble** in the middle, the chemical potential μ is conserved. The **Canonical ensemble** on the right does not conserve energy E anymore. Heat flow is allowed and small fluctuations about a constant mean value may occur in the temperature T .

11.1 Canonical (NVT) ensemble

In the canonical ensemble, the mean temperature T has a specified average (macroscopic) value, while both the total energy ($E = U + K$) and the instantaneous kinetic energy can fluctuate. Furthermore, these fluctuations are system-size dependent.

Considering the canonical partition function

$$Z_N = \int \frac{d^{3N}r d^{3N}p}{h^{3N} N!} e^{-\beta H(r,p)} \quad (11.1)$$

whereas the total energy is given by

$$\langle E \rangle = -\langle H \rangle = -\frac{1}{Z_N} \frac{\partial Z_N}{\partial \beta} \quad (11.2)$$

$$\langle E^2 \rangle = \frac{1}{Z_N} \frac{\partial^2 Z_N}{\partial \beta^2} \quad (11.3)$$

and the isochoric heat temperature by

$$\begin{aligned} c_V &= T \frac{\partial^2}{\partial T^2} (k_B T \ln Z_N) \\ &= \frac{\partial}{\partial T} \left(k_B \ln Z_N - \frac{1}{T} \frac{1}{Z_N} \frac{\partial Z_N}{\partial \beta} \right) \end{aligned} \quad (11.4)$$

one can show that the canonical fluctuations of the total energy follows

$$\sigma_E^2 = \langle E^2 \rangle - \langle E \rangle^2 = k_B T^2 c_V \quad (11.5)$$

As such, relative fluctuations are

$$\boxed{\frac{\sqrt{\sigma_E^2}}{\langle E \rangle} \sim \frac{1}{\sqrt{N}}} \quad (11.6)$$

as both c_V and E are extensive properties. As $N \rightarrow \infty$, the fluctuations vanish, which equals ensemble equivalence.

Considering the Maxwell-Boltzmann distribution of particle velocities in the canonical equilibrium,

$$f(v) d^3v = \frac{m}{2\pi k_B T}^{\frac{3}{2}} e^{-\frac{mv^2}{2k_B T}} d^3v \quad (11.7)$$

It can be shown from the moments of the momenta $\vec{p} = m\vec{v}$, that the instantaneous temperature follows a similar fluctuation (see section 15.6):

$$\boxed{\frac{\sigma_T^2}{\langle T \rangle^2} \sim \frac{1}{N}} \quad (11.8)$$

These are **physical** fluctuations of a system in equilibrium with a heat bath. As such, a proper thermostat (def.: a machinery to control the temperature of a system) should allow such fluctuations of a 'finite-sized' system.

We shall see in the following that this is a rather non-trivial task!

In fact, until ~ 1980 , simulations were limited to either microcanonical NVE or "isothermal" schemes.

Let us start with such an "ad-hoc" thermostat.

Ad-hoc schemes for thermostats

1. Velocity rescaling: simplest ad-hoc scheme

The instantaneous temperature $T(t)$ is calculated as

$$\sum_i \frac{1}{2} m_i v_i^2 = \frac{3N}{2} k_B T(t) \quad (11.9)$$

If we define a rescaling function of velocities λ such that

$$\sum_i \frac{1}{2} m_i (\lambda v_i)^2 \equiv \frac{3N}{2} k_B T^0 \quad (11.10)$$

where T^0 is the desired temperature:

$$\lambda = \sqrt{\frac{T^0}{T(t)}} \quad (11.11)$$

As discussed before, this scheme has a couple of issues:

- samples not NVT but rather isokinetic ensemble NVK
- not time-reversible, not ergodic, incorrect fluctuations, can lead to the 'flying ice cube' problem
- Not NVT , but useful as 'warm-up'
- deterministic thermostat (not stochastic in its dynamics)
- Can be extended to proper NVT by drawing kinetic energies randomly from a canonical distribution (Bussi et al, JCP 126, 014101 (2007)), similar as in the stochastic Andersen thermostat, see below.

2. Berendsen thermostat:

In Berendsen thermostating the velocities are rescaled ($v_i \rightarrow \lambda v_i$) in such a way that the rate of change of temperature is proportional to the deviation of temperature:

$$\frac{dT(t)}{dt} = \frac{1}{\tau} (T^0 - T(t)) \quad (11.12)$$

where τ describes the coupling strength to the heat bath and the scaling for T is given by a Leap-Frog scheme:

$$\lambda = \left(1 + \frac{\Delta t}{\tau} \left(\frac{T^0}{T} - 1 \right) \right) \quad (11.13)$$

From a given instant. the system's temperature decays exponentially towards the desired temperature T^0 with a time scale τ . For small $\tau \rightarrow 0$ the fluctuations are suppressed (approaching the NVE ensemble) whereas for $\tau \rightarrow \infty$ no thermostating is possible. For $\Delta t/\tau = 1$ we essentially recover velocity rescaling.

This thermostat is deterministic and similar than velocity rescaling, but with weaker coupling to the bath. The changes of temperature decay exponentially with τ , i.e., it has advantageously less abrupt changes than in velocity rescaling. However, it is also not time reversible, and also does not sample a correct NVT ensemble. Good for 'warm up', not recommended for production.

Stochastic Methods: The Andersen Thermostat [11]

The Andersen Thermostat can be thought of as a hybrid MC (Monte Carlo) and MD (Molecular Dynamics) method. In this method, the system is considered to be coupled to a heat bath. The coupling is through stochastic 'impulsive' forces acting randomly on a subset of particles in a system which instantaneously change their velocity. These can be interpreted as 'collisions' of these particles with the heat bath. These collisions cause the energy of the system to change stochastically, which is akin to MC moves. Between two such 'collisions', the system evolves following a standard NVE MD.

The strength of coupling with the heat bath is determined by the frequency ϑ of such stochastic collisions. If successive collisions are considered uncorrelated, the probability that a particle will collide with the heat bath in the interval $[t, t + dt]$ is given by the Poisson process:

$$P(t, \vartheta)dt = \vartheta e^{-\vartheta t}dt \quad (11.14)$$

At a given time step during the simulation, if a particle is identified to undergo a collision, its velocity v is acquired from a Maxwell-Boltzmann distribution at the desired temperature T :

$$f(v_n)dv_n = \left(\frac{m}{2\pi k_B T}\right)^2 e^{-\frac{mv_n^2}{2\pi k_B T}} dv_n \quad (11.15)$$

Schematic algorithm

If Δt is the time step of the simulation and ϑ is the collision frequency, the probability that a particle will undergo collision during a time-step evaluation is $\vartheta \Delta t$.

The integration routine then changes to loop over time:

```

begin loop over time
    1. calculate forces
    2. update positions
    3. update velocities*
    4. t' = t + Δt
end loop over time

```

* Check using a random number of generations and collision probability $\vartheta \Delta t$ if a given particle should collide. If yes, assign v from the Maxwell-Boltzmann distribution at T , if no, do nothing.

In short, any standard integration routine can be used in which a subset of particles is selected and their velocities redefined.

Some comments:

- The Andersen thermostat does produce a canonical distribution (see handout in section 15.6).
- The combination of MC and MD turns the simulation to a Markov process.
- Neither energy, nor momentum is conserved in this approach (and thus is not invariant under Galilean transformation)
- The Andersen thermostat is good at computing static properties, but not at computing dynamic properties as the choice of ϑ critically dictates the diffusion.
- For too slow frequencies, too weak coupling, long time before a canonical distribution is sampled; too fast frequencies, too tight coupling, perturbs strongly the microscopic dynamics. Empirical choices are known [8].

Stochastic Langevin approach

Like Andersen, the Langevin approach defines also the coupling of the particles' motion to an external heat bath by friction and fluctuation forces. It actually defines an independent simulation method, see section 13. Like Andersen, it interferes with the dynamics of a Newtonian (ballistic) system where there is no bath friction. However, the Langevin approach is physically appropriate for coarse-grained systems, where the solvent (and other microscopic) degrees of freedom have been integrated out, and fluctuations and friction/dissipation effectively remain for the macromolecules on large time scales.

Extended Lagrangian approach

A quick recap of Lagrangian and Hamiltonian mechanics:

The Lagrangian of a system is defined as

$$\mathcal{L}(q, \dot{q}) = K(\dot{q}) - U(q). \quad (11.16)$$

The generalized momentum p is associated with the generalized coordinate q via

$$p = \frac{\partial \mathcal{L}(q, \dot{q})}{\partial \dot{q}} \quad (11.17)$$

Lagrange equation of motion

$$\begin{aligned} \frac{d}{dt} \left(\frac{\partial \mathcal{L}}{\partial \dot{q}} \right) - \frac{\partial \mathcal{L}}{\partial q} &= 0 \\ \Rightarrow \frac{\partial \mathcal{L}}{\partial q} &= \dot{p} \end{aligned} \quad (11.18)$$

The Hamiltonian of a system is defined via the Legendre transformation of the Lagrangian:

$$\mathcal{H}(p, q) = p\dot{q} - \mathcal{L}(q, \dot{q}). \quad (11.19)$$

Hamilton equation of motion

$$\begin{aligned} \frac{\partial \mathcal{H}}{\partial p} &= \dot{q} \\ \frac{\partial \mathcal{H}}{\partial q} &= -\dot{p} \end{aligned} \quad (11.20)$$

The standard Lagrangian for a system of N particles, which form an isolated NVE system, would be

$$\mathcal{L} = \sum_{i=1}^N \frac{m_i}{2} \dot{\vec{r}}_i^2 - U(\{\vec{r}_i\}) \quad (11.21)$$

Nosé-Hoover Thermostat

Nosé in 1983 introduced a clever extension to generalize the formalism to perform MD simulations in the canonical (NVT) ensemble. The basic idea of this Extended Lagrangian is the following:

An additional 'external' coordinate s which represents the coupling to an external system with which heat can be exchanged is introduced. The coupling is through rescaling of the velocity such that

$$\vec{v}_i = s\dot{\vec{r}}_i \quad (11.22)$$

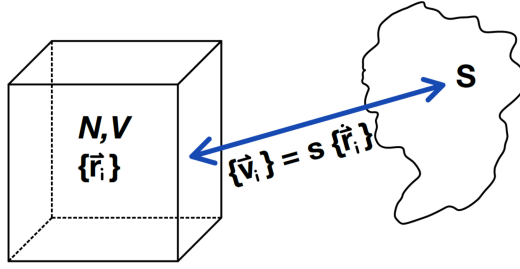


Figure 11.2: Coupling to an external system with which heat can be exchanged

The extended Lagrangian for the coupled system $(\{\vec{r}_i\}, \{\dot{\vec{r}}_i\}, s, \dot{s})$ is then written as [17]

$$\boxed{\mathcal{L}_{\text{Nosé}} = \sum_{i=1}^N \frac{m_i}{2} s^2 \dot{\vec{r}}_i^2 - U(\{\vec{r}_i\}) + \frac{Q}{2} \dot{s}^2 - gk_B T \ln s} \quad (11.23)$$

with Q being the thermal mass associated with s , and g denoting a parameter that needs to be fixed later on.

The conjugate momenta associated with \vec{r}_i and s are:

$$\begin{aligned} \vec{p}_i &= \frac{\partial \mathcal{L}_{\text{Nosé}}}{\partial \dot{\vec{r}}_i} = m_i s^2 \dot{\vec{r}}_i \\ p_s &= \frac{\partial \mathcal{L}_{\text{Nosé}}}{\partial \dot{s}} = Q \dot{s} \end{aligned} \quad (11.24)$$

The extended Hamiltonian can then be formulated as

$$\boxed{\mathcal{H}_{\text{Nosé}} = \sum_{i=1}^N \frac{\dot{\vec{p}}_i^2}{2m_i s^2} + U(\{\vec{r}_i\}) + \frac{p_s^2}{2Q} + gk_B T \ln s} \quad (11.25)$$

Considering the 'scaled momenta' for the particles

$$\vec{p}'_i = \frac{\vec{p}_i}{s} \quad (11.26)$$

and an Hamiltonian involving the scaled momenta, but without the additional terms

$$\mathcal{H}_{NVT}(\{\vec{p}'_i\}, \{\vec{r}_i\}) = \sum_{i=1}^N \frac{\dot{\vec{p}}'_i^2}{2m_i} + U(\{\vec{r}_i\}) \quad (11.27)$$

It can be shown that the canonical average over \mathcal{H}_{NVT} is the same as the microcanonical average over $\mathcal{H}_{\text{Nosé}}$, given that

$$g = 3N + 1. \quad (11.28)$$

This is exactly what we are looking for, since in the NVT ensemble
closed system + environment with heat exchange = closed system at constant energy.
As such, the scaled momenta \vec{p}'_i are the 'real' realizable momenta in the canonical ensemble.
We now define real (primed) and virtual (unprimed) variables for the other quantities too such that

$$\begin{aligned} \vec{r}'_i &= \vec{r}_i \\ \vec{p}'_i &= \vec{p}_i / s \\ s' &= s \\ \Delta t' &= \Delta t / s \\ p'_s &= p_s / s \end{aligned} \quad (11.29)$$

It is then clear that the variable s can be conceptually visualized as a scaling for time. Also, in the virtual variable implementation, the simulation's integration time step has to be variable (and not fixed) to obtain the appropriate momenta.

Equations of motion in virtual variables

$$\begin{aligned}\dot{\vec{r}}_i &= \frac{\partial \mathcal{H}_{\text{Nosé}}}{\partial \vec{p}_i} = \frac{\vec{p}_i}{m_i s^2} \\ \dot{\vec{p}}_i &= -\frac{\partial \mathcal{H}_{\text{Nosé}}}{\partial \vec{r}_i} = -\frac{\partial U(\{\vec{r}_i\})}{\partial \vec{r}_i} \\ \dot{s} &= \frac{\partial \mathcal{H}_{\text{Nosé}}}{\partial p_s} = \frac{p_s}{Q} \\ \dot{p}_s &= -\frac{\partial \mathcal{H}_{\text{Nosé}}}{\partial s} = \frac{1}{s} \left(\sum_i \frac{\vec{p}_i'^2}{m_i s^2} - gk_B T \right)\end{aligned}\quad (11.30)$$

Equations of motion in real variables

$$\begin{aligned}\dot{\vec{r}}'_i &= \frac{d\vec{r}'_i}{dt'} = s \frac{d\vec{r}'_i}{dt} = \frac{\vec{p}_i}{m_i s^2} = \frac{\vec{p}'_i}{m_i} \\ \dot{\vec{p}}'_i &= s \frac{d}{dt} \left(\frac{\vec{p}_i}{s} \right) = \frac{d\vec{p}_i}{dt} - \frac{1}{s} \vec{p}_i = -\frac{\partial U(\{\vec{r}'_i\})}{\partial \vec{r}'_i} - \vec{p}'_i \frac{s' p'_s}{Q} \\ \dot{s}' &= \frac{ds'}{dt'} = s \frac{ds}{dt} = \frac{s'^2 p'_s}{Q} \\ \dot{p}'_s &= \frac{dp'_s}{dt'} = s \frac{d}{dt} \left(\frac{p_s}{s} \right) = \frac{dp_s}{dt} - \frac{1}{s} p_s \frac{ds}{dt} = \frac{1}{s'} \left(\sum_i \frac{\vec{p}'_i^2}{m_i} - gk_B T \right) - s' \frac{p'^2_s}{Q}\end{aligned}\quad (11.31)$$

These equations of motion do not require variable time steps and the Hamiltonian given by Equation 11.25 can be written in real variables as:

$$\mathcal{H}'_{\text{Nosé}} = \sum_{i=1}^N \frac{\vec{p}'_i^2}{2m_i} + U(\{\vec{r}'_i\}) + \frac{s'^2 p'^2_s}{2Q} + gk_B T \ln s' \quad (11.32)$$

Although \mathcal{H}' is not a 'Hamiltonian' because the equations of motion can not be derived from it. The Hamiltonian written in real variables is a conserved quantity.

Hoover showed that the real-variable equations can be simplified by introducing [15]

$$\xi = \frac{s' p'_s}{Q} \quad (11.33)$$

which leads to the **Nosé-Hoover thermostat**:

$$\begin{aligned}\dot{\vec{r}}'_i &= \frac{\vec{p}'_i}{m_i} \\ \dot{\vec{p}}'_i &= -\frac{\partial U(\{\vec{r}'_i\})}{\partial \vec{r}'_i} - \xi \vec{p}'_i \\ \dot{\xi}' &= \frac{1}{Q} \left(\sum_i \frac{\vec{p}'_i^2}{m_i} - gk_B T \right) \\ \frac{\dot{s}'}{s'} &= \frac{d \ln s'}{dt'} = \xi\end{aligned}$$

(11.34)

The first three equations are sufficient to generate particle trajectories whereas the last equation is included to check the conservation of energy.

From the third equation actually follows

$$\dot{\xi}' = g \frac{k_B}{Q} (T - T_{\text{desired}}) \quad (11.35)$$

which is a feedback mechanism to make T oscillate around the desired temperature as:

$$\begin{aligned} T > T_{\text{desired}} &\rightarrow \xi' \text{ increases} \\ T < T_{\text{desired}} &\rightarrow \xi' \text{ decreases} \end{aligned}$$

11.2 The isobaric/isothermal (NPT) ensemble

We now consider a simulation in an isobaric ensemble NPT . Thus, the volume, V , is able to change and fluctuate to maintain a constant mean pressure in the system. V is therefore introduced as a dynamical variable.

The thermodynamic definition of pressure from the Helmholtz thermodynamic potential F is given as

$$P = - \left(\frac{\partial F}{\partial V} \right) \Big|_{T,N} \quad (11.36)$$

whereas the isobaric-isothermal definition of the volume in the Gibbs thermodynamic potential is given via

$$V = \left(\frac{\partial G}{\partial P} \right) \Big|_{N,T}. \quad (11.37)$$

In classical mechanics, the mean kinetic energy $\langle K \rangle$ via the Clausius virial theorem can be described as

$$\langle \hat{K} \rangle = -\frac{1}{2} \sum_i \langle \vec{F}_i^{\text{tot}} \vec{r}_i \rangle = -\frac{1}{2} \sum_i \langle \vec{F}_i^{\text{int}} \vec{r}_i \rangle - \frac{1}{2} \sum_i \langle \vec{F}_i^{\text{ext}} \vec{r}_i \rangle = -\frac{1}{2} \theta_{\text{int}} - \frac{1}{2} \theta_{\text{ext}} \quad (11.38)$$

with θ_{int} and θ_{ext} defining the internal and external interactions. The external interactions are imposed on the system through a pressure P_0 as can be seen in Figure 11.3. This results in

$$\begin{aligned} d\vec{F}_i^{\text{ext}} &= -P_0 \vec{n} dA \\ \sum_i \vec{F}_i^{\text{ext}} \vec{r}_i &= -P_0 \int \vec{n} \vec{r} dA \end{aligned} \quad (11.39)$$

where \vec{n} is the normal vector in respect to the surface.

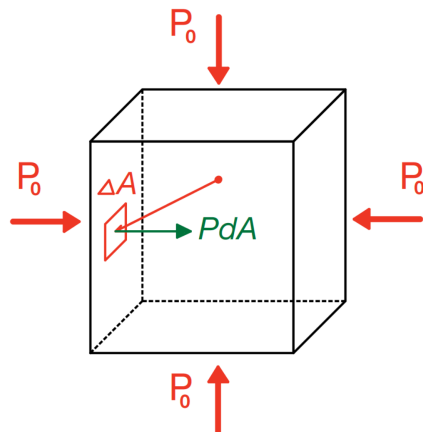


Figure 11.3: Applied external interactions on the volume V by the pressure P_0 .

If we apply the Gauss theorem to the above statement

$$\int \vec{n} \cdot \vec{r} dA = \int \nabla \cdot \vec{r} dV = 3V, \quad (11.40)$$

the external interactions are given by

$$\langle \theta_{\text{ext}} \rangle = -3P_0 V \quad (11.41)$$

This derivation is very general and independent of the box shape!

The kinetic energy can also be defined via the equipartitioning theorem as

$$\langle K \rangle = N \frac{1}{2} m \langle v^2 \rangle = \frac{3}{2} N k_B T \quad (11.42)$$

and since the pressure is everywhere the same: $P = \langle P \rangle$, we can derive the virial equation using Equation 11.41:

$$P = \frac{N}{V} k_B T - \frac{1}{3V} \sum_{i=1}^N \vec{r}_i \nabla_i U \quad (11.43)$$

In equilibrium all pressures $P \equiv P_0 \equiv P_{MD}$ are the same.

The pair forces $F_{ij} = -\frac{dV}{dr_{ij}}$ can be rewritten as:

$$\sum_i \vec{r}_i \vec{F}_i = \sum_i \sum_{i \neq j} \vec{r}_i \vec{F}_{ij} = \frac{1}{2} \sum_i \sum_{i \neq j} (\vec{r}_i \vec{F}_{ij} + \vec{r}_j \vec{F}_{ji}) \quad \text{with} \quad \vec{F}_{ji} = -\vec{F}_{ij} \quad (11.44)$$

Combining the two single sum terms in one double sum term

$$\frac{1}{2} \sum_i \sum_{i \neq j} \vec{r}_{ij} \vec{F}_{ij} = \sum'_{i>j} \vec{r}_{ij} \vec{F}_{ij} \quad \text{with} \quad \vec{r}_{ij} = \vec{r}_j - \vec{r}_i, \quad (11.45)$$

the pressure P in Equation 11.43 can be written as the virial equation

$$P = \frac{N}{V} k_B T + \frac{1}{3V} \sum'_{i>j} r_{ij} \frac{dV}{dr_{ij}}. \quad (11.46)$$

Note that in general the pressure is not a scalar quantity, but a second order tensor:

$$\underline{\underline{P}} = \begin{pmatrix} P_{xx} & P_{xy} & P_{xz} \\ P_{yx} & P_{yy} & P_{yz} \\ P_{zx} & P_{zy} & P_{zz} \end{pmatrix} = P_{ij} \quad (11.47)$$

Thus a generalization of this method to anisotropic systems and box geometries is possible. Only in isotropic systems, i.e., $P_{xx} = P_{yy} = P_{zz}$ and $P_{i \neq j} = 0$, the pressure is a scalar:

$$P = \text{Tr}(\underline{\underline{P}})/3 \quad (11.48)$$

It is then referred to as the "hydrostatic pressure".

To maintain the pressure of a MD simulation, one has to couple the simulation box to a barostat.

Berendsen barostat [12]

At first we define analogous to the Berendsen thermostat

$$\frac{dP_{MD}}{dt} = \frac{P_0 - P_{MD}}{\tau_P} \quad (11.49)$$

with the time constant τ_P . Now we introduce a scaling factor η , such that:

$$x_{\text{new}} = (1 + \eta \Delta t) x_{\text{old}} \quad (11.50)$$

$$x(t + \Delta t) = x(t) + x(t) \eta \Delta t + v(t) \Delta t \quad (11.51)$$

From this definition, we can derive the expressions

$$\dot{\vec{r}} = \vec{v} + \eta \vec{r} \quad \text{and} \quad \dot{V} = 3\eta V \quad (11.52)$$

Using the isothermal compressibility equation $\chi_T = -\frac{1}{V} \frac{\partial V}{\partial P}$, \dot{P} can be expressed linearly in respect to the scaling factor η :

$$\frac{dP}{dt} = -\frac{1}{\chi_T V} \frac{dV}{dt} = -\frac{3\eta}{\chi_T} \quad (11.53)$$

With the help of Equation 11.49, the scaling factor is finally expressed as:

$$\eta = -\frac{\chi_T (P_0 - P_{MD})}{3\tau_P}. \quad (11.54)$$

Notes:

- In an anisotropic scaling, the scaling factor is also "tensorial" $\eta_{ij} \sim P_{ij}$
- The isothermal compressibility χ_T is fixed (e.g. to the compressibility of water), but is not critical, as the barostat behavior depends on the value of $\frac{\chi_T}{\tau_P}$
- A large time constant τ_P equals weak coupling in the model
- The Berendsen thermostat is good for equilibration, but does not produce the correct statistical ensemble!

Andersen barostat [11]

The approach of the Andersen barostat is also based on an extended Lagrangian like the Nosé-Hoover thermostat. The method introduces an imaginary piston with a pseudo-"mass" W and a pseudo "velocity" V being the volume of the system (see Figure 11.4), resulting in a kinetic energy of the piston of

$$K_P = \frac{1}{2} W \dot{V}^2, \quad (11.55)$$

and a potential energy of

$$U_P = P_0 V. \quad (11.56)$$

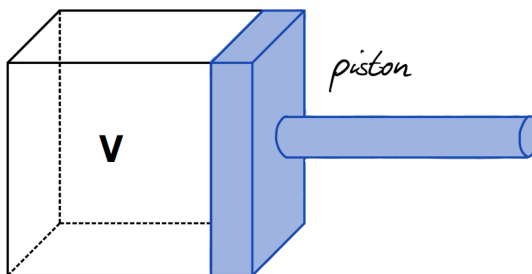


Figure 11.4: An imaginary piston working on the system with a pseudo mass W and a pseudo velocity V .

The scaled variables

$$\begin{aligned}\vec{\tau}_i &= \frac{\vec{r}_i}{V^{1/3}} \\ \dot{\vec{\tau}}_i &= \frac{\dot{\vec{r}}_i}{V^{1/3}}\end{aligned}\quad (11.57)$$

are chosen in order to ensure a coupling between the volume of the system and the coordinates \vec{r}_i .

The Lagrangian of the system uses then $\vec{\tau}$ and V as generalized coordinates:

$$\mathcal{L}(\vec{\tau}, \dot{\vec{\tau}}, V, \dot{V}) = \frac{1}{2}m \sum_{i=1}^N |\dot{\vec{\tau}}_i|^2 + \frac{1}{2}W\dot{V}^2 - U(V^{1/3}\vec{\tau}) - P_0V \quad (11.58)$$

The equations of motion are derived from the Euler-Lagrange equations, $\frac{\partial}{\partial t} \frac{\partial \mathcal{L}}{\partial \dot{q}_i} = \frac{\partial \mathcal{L}}{\partial q_i}$, and read as:

$$\ddot{\vec{\tau}}_i = \frac{\vec{F}_i}{mV^{1/3}} - \frac{2}{3V}\dot{V}\dot{\vec{\tau}}_i \quad (11.59)$$

with the first term being the Newtonian from the pair forces and the second term being a correction resulting from the piston coupling, as well as

$$W\ddot{V} = \frac{m}{3V^{1/3}} \sum_{i=1}^N |\dot{\vec{\tau}}_i|^2 + \frac{1}{3V^{2/3}} \sum_{i=1}^N \vec{\tau}_i \vec{F}_i - P_0 \quad (11.60)$$

Notes:

- The Hamiltonian is conserved in the Andersen barostat: $H = K + U + K_P + U_P$
- The approach generates trajectories in the isobaric-isoenthalpic ensemble (*NPH*)
- In order to simulate the *NPT* ensemble, we need to combine the approach, e.g., with the Nosé-Hoover thermostat (there exist extensions by Hoover or Melchionna)

The most accurate formulation is given by **Martyna et al.** [16]:

The *NPT* equations are given as

$$\begin{aligned}\dot{\vec{r}}_i &= \frac{\vec{p}_i}{m_i} + \frac{p_\epsilon}{W}\vec{\tau}_i \\ \dot{\vec{p}}_i &= \vec{F}_i - \left(\frac{p_\epsilon}{W} + \frac{p_\xi}{Q} \right) \vec{p}_i,\end{aligned}\quad (11.61)$$

where p_ϵ and p_ξ denote the coupled momenta of the barostat and the thermostat respectively and W and Q being the pseudo "masses" of the barostat and the thermostat.

The generalized coordinates are then defined as

$$\dot{V} = \frac{3p_\epsilon}{W}V \quad \text{and} \quad \dot{p}_\epsilon = 3V(P_{MD} - P_0) - \frac{p_\xi}{Q}p_\epsilon \quad (11.62)$$

for the barostat and as

$$\dot{\xi} = \frac{p_\xi}{Q} \quad \text{and} \quad \dot{p}_\xi = \sum_i \frac{\vec{p}_i^2}{2m} \frac{p_\epsilon^2}{W} p_\epsilon + (N+1)k_B T \quad (11.63)$$

for the thermostat.

Notes:

- This approach conserves the Jacobian and generates properly the isobaric-isothermal ensemble
- A robust integration scheme for this method can be seen in Tuckerman et al. [20]

Paranello-Rahman (anisotropic barostat)

The Paranello-Rahman barostat represents an extension of the Andersen barostat for arbitrary box shapes. The shape of the box can thus vary within certain constraints of the box angle and the elongation.

Notes:

- This certain approach is useful for crystalline solids
- The original publication can be found in [18]
- Also here, a coupling to a thermostat, e.g., the Nosé-Hoover thermostat, is required for an *NPT* ensemble

Chapter 12

Force field for molecules and polymers

It is strongly recommended to check the illustrations in the Appendix on this chapter.

12.1 Molecular force fields

For molecules and polymer, typically the classical Hamiltonian formally splits into bonded and nonbonded interactions (for simplicity we neglect kinetic terms and any external potentials in the following):

$$\mathcal{H} = \mathcal{H}_{\text{bonded}} + \mathcal{H}_{\text{nonbonded}} \quad (12.1)$$

Of course, quantum-mechanically the interactions are governed by electrons by under certain conditions the effects like bonding, rotation, and polarization can be separated (see e.g., the McQuarrie book on statistical mechanics). The nonbonded Hamiltonian $\mathcal{H}_{\text{nonbonded}}$ contains, for example, the Lennard-Jones and the Coulomb potential for atom-atom and charge-charge interactions, respectively, whereas the bonded Hamiltonian typically consists of

$$\mathcal{H}_{\text{bonded}} = \mathcal{H}_{\text{bonds}} + \mathcal{H}_{\text{angles}} + \mathcal{H}_{\text{torsions}}, \quad (12.2)$$

corresponding to classical treatments of bonds between atoms and angular and torsional constraints. The quantum-to-classical limit justifying such an additive splitting is described for example in the McQuarrie book [6]. We have learned about these internal constraints already in, e.g., the FJC and FRC models in the polymer chapter in the first part of the script.

$\mathcal{H}_{\text{bond}}$ is typically expressed in an expansion as $\mathcal{H}_{\text{bond}} = \sum_{ij} U_{\text{bond}}(r_{ij})$:

$$U_{\text{bond}}(r_{ij}) = \frac{k_{ij}}{2}(r_{ij} - r_{ij}^0)^2 + \frac{l_{ij}}{3}(r_{ij} - r_{ij}^0)^3 + \dots \quad (12.3)$$

Often, only the harmonic expansion, given by the first term of the Taylor expansion, of the 'real' bonding potential is calculated, or simply used as an ad-hoc approximation. The 'real' potential could be of a Morse-type or calculated numerically by quantum DFT. Then the spring constant can be estimated from the underlying potentials. Figure 12.1 illustrates the energy as a function of the distance of a simple bonded model, for which the zero-temperature bond length is r_0 . At elevated temperatures the latter will be close to the equilibrium mean bond length, but in general not exactly due to asymmetries in the molecule.

A disadvantage of harmonic bonds is that the potential is not sufficiently bound. This is a problem in situations when forces (stretching) of the molecule is applied and unrealistic large stretches are resulting. Importantly a polymer is finite (has a maximum contour length). For polymers then, for example, the FENE (finite extensible nonlinear elastic) potential is

used <https://en.wikipedia.org/wiki/FENE>, which for low temperatures can also be approximated by a harmonic potential but for larger fluctuations is stronger bounded. The other extreme are constrained rigid bonds (numerical implementation discussed below and in the Appendix, taken from [10]) which are also a good approximation for small stiff molecules, like water, and can save computational time.

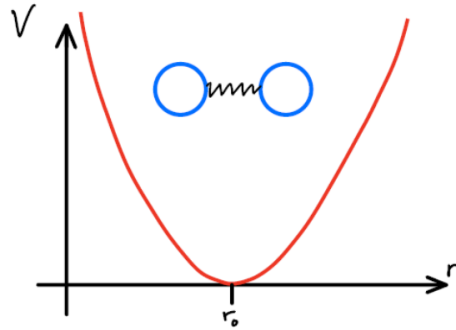


Figure 12.1: Sketch of a bonded potential with minimum at equilibrium point r_0

Analogously, $\mathcal{H}_{\text{angle}}$ is also expressed in an expansion as $\mathcal{H}_{\text{angle}} = \sum_{ijk} U_{\text{angle}}(\theta_{ijk})$:

$$U_{\text{angle}}(\theta_{ijk}) = \frac{k_{ijk}}{2} (\theta_{ijk} - \theta_{ijk}^0)^2 \quad \text{with} \quad \theta_{ijk} = \cos^{-1} \left(\frac{\vec{r}_{ij} \cdot \vec{r}_{ik}}{|\vec{r}_{ij}| |\vec{r}_{ik}|} \right) \quad (12.4)$$

The torsions (or "dihedral angles") are defined as (see illustration in Appendix):

$$\phi = \cos(\hat{n}_{ijk} \cdot \hat{n}_{ikm}) \quad (12.5)$$

where \hat{n}_{ijk} and \hat{n}_{ikm} are normal vector on the area defined as:

$$\hat{n}_{ijk} = \frac{\vec{r}_{ij} \times \vec{r}_{ik}}{|\vec{r}_{ij} \times \vec{r}_{ik}|} \quad \hat{n}_{ikm} = \frac{\vec{r}_{ki} \times \vec{r}_{km}}{|\vec{r}_{ki} \times \vec{r}_{km}|} \quad (12.6)$$

Typically, the torsion potential is calculated as $U(\phi_{ikm}) = A \cos(\phi_{ikm} + \delta)$, but many forms are used and implemented that are very molecule-specific.

It is important to remember that all **potentials and force fields are models!**

The big challenge in material science is to find the right "force-field" $\vec{F}_i = -\nabla_i \hat{U}$ and parameter determination.

This is often done by so called "training sets" which are today boosted by *Machine Learning* and *Data-driven approaches*. Parametrization can be achieved by both

- **"bottom-up":**
parameters from *ab-initio* QM-approaches
- **"top-down":**
fit parameters such that the material reproduces some macroscopic, experimental observables

and even combining both approaches to complete the definition of all missing parameters.

12.2 Mixing rules

For a system that consists of different species A and B , mixing rules are typically assumed to reduce the parameter space. With a given pair potentials defined by $(\sigma_{AA}, \epsilon_{AA})$ and $(\sigma_{BB}, \epsilon_{BB})$ we thus assume a mixed potential $(\sigma_{AB}, \epsilon_{AB})$.

For two arbitrary potentials i, j popular mixing rules for Lennard-Jones interactions are:

- **Lorentz-Berthelot rules**

$$\sigma_{ij} = \frac{\sigma_{ii} + \sigma_{jj}}{2} \quad \epsilon_{ij} = \sqrt{\epsilon_{ii}\epsilon_{jj}} \quad (12.7)$$

- **Geometric rules**

$$\sigma_{ij} = \sqrt{\frac{\sigma_{ii}\sigma_{jj}}{2}} \quad \epsilon_{ij} = \sqrt{\epsilon_{ii}\epsilon_{jj}} \quad (12.8)$$

There exist many more mixing rules. Often these convenient (but purely empirical) assumptions are not good and σ_{ij} , ϵ_{ij} ("cross interactions") have to be defined individually, e.g., from a more thorough 'first principles' coarse-graining, or 'top-down' fits to reproduce macroscopic experiments.

12.3 Constrained dynamics

One can speed-up simulations by avoiding fast vibrations and neglecting bonds or replacing a flexible bond by a rigid bond.

As a simple fix, often H -atoms in molecules are not resolved, see Figure 12.2. This leads to the so-called 'United Atom' (UA) models.

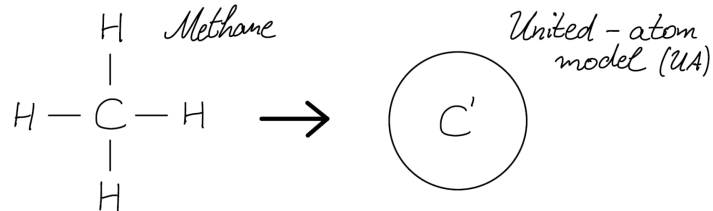


Figure 12.2: Instead of resolving the H -atoms, methane is reduced to a united-atom (UA) model.

Alternatively, one can constrain the degrees of freedom, e.g., bond and/or angle by rigid body **MD** simulation. One example is the SPC/E water model where the bond length, r_{OH} , and the bond angle, θ_{HOH} , are fixed:

$$r_{OH} = 0.1\text{nm} \quad \theta_{HOH} = 109.47^\circ \quad (12.9)$$

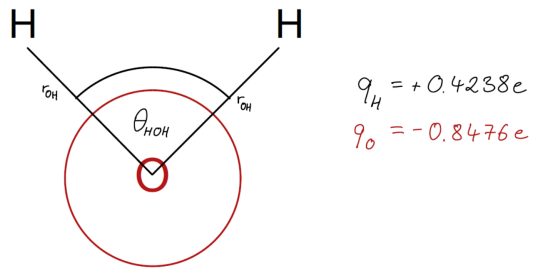


Figure 12.3: The SPC/E water model is a constrained model of the H_2O -molecule with fixed r_{OH} and θ_{HOH} .

Additionally, only the Lennard-Jones potential between O -atoms are calculated with:

$$\epsilon_{OO} = 0.650 \quad \sigma_{OO} = 0.3166\text{nm} \quad (12.10)$$

(The Wikipedia page "Water model" is a good reference here. A good discussion on the topic of constraints in general is found in Chapter 3.4 of [8], see also the corresponding appendix in this script.)

Briefly, one can formulate holonomic constraints using Lagrange Multipliers (see appendix, taken from [10]) and solve couple linear equations for these Lagrange Multipliers.

Methods using Lagrange Multipliers are for example: SETTLE, RATTLE, **SHAKE**, LINCS in GROMACS

This is mostly performed on bonds. While angles can also be constrained, this approach is too restrictive for molecular motion (as well as for torsion).

Another alternative for fast vibrations is the "multiple time-step algorithms" presented in Chapter 3.5 of [8].

Chapter 13

Langevin and Brownian Dynamics

Brownian motion (Brown, 1827; Einstein, 1905; Smoluchowski, 1906) describes the random movement of particles such as colloids, polymers, proteins etc. in a liquid or gas due to thermal "kicks" from solvent particles on "intermediate" time scales. This results in movement patterns like the one displayed in Figure 13.1.

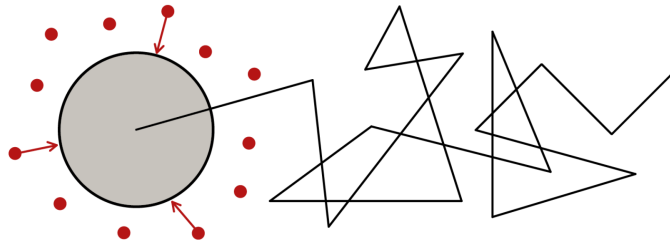


Figure 13.1: Brownian motion as the random movement of a particle due to thermal kicks of the solvent.

If we consider the one dimensional random walk where a distance L is travelled at each step, the covered distance in relation to the origin is given as

$$\langle x_N^2 \rangle = NL^2 \quad (13.1)$$

after $N = \frac{t}{\Delta t}$ steps. For the time continuous case, $\Delta t \rightarrow 0$, the diffusion constant, D , is introduced:

$$\langle x^2 \rangle = \frac{L^2}{\Delta t} t = 2Dt \quad (13.2)$$

In three dimension, the "diffusion law" is given as:

$$\langle r^2 \rangle = 6Dt \quad (13.3)$$

The diffusion of a metabolite (molecule) through a cell, for example, is

$$D \simeq 10^{-6} \frac{\text{cm}^2}{\text{s}} = 0.1 \frac{\text{nm}^2}{\text{ns}} \quad (13.4)$$

which equals an average distance $\sqrt{\langle x^2 \rangle}$ of

$$\begin{aligned} t = 5\text{ms} &\rightarrow \sqrt{\langle x^2 \rangle} \simeq 1\mu\text{m} \\ t = 50\text{ms} &\rightarrow \sqrt{\langle x^2 \rangle} \simeq 3.2\mu\text{m} \end{aligned} \quad (13.5)$$

13.1 Langevin equation

In the Langevin picture, the stochastic trajectory $\vec{r}_i(t)$ of a particle i is described by a stochastic equation of motion:

$$m\ddot{\vec{r}}_i(t) + \xi\dot{\vec{r}}_i(t) = \vec{F}_i^{\text{tot}}(t) + \vec{R}_i(t) \quad (13.6)$$

It looks like Newton, only that the action of the background solvent 'thermal bath' appear as additional friction and fluctuation force terms. The Langevin equation is derivable by coarse-graining fast time scales by projector-operator techniques [21]. Fast processes of small solvent appear as instantaneous stochastic or friction terms. \vec{F}_i^{tot} is the combined force from particle interactions and the external field and \vec{R}_i is a random force present due to solvent "kicks". This random force has a zero mean $\langle \vec{R}_i(t) \rangle = 0$, but a non-zero variance:

$$\langle \vec{R}_{i\alpha}(t) \cdot \vec{R}_{i\beta}(t') \rangle = \sigma_R^2 \delta_{\alpha\beta} \delta(t - t') \delta_{ij} \quad (13.7)$$

The variables $\alpha, \beta = x, y, z$ denote the respective dimension of movement and δ_{ij} (or $\delta_{\alpha\beta}$) is the Kronecker- δ and $\delta(t - t')$ is the Dirac- δ . The latter reflects that solvent force fluctuations are typically much faster than the Langevin particle's motion, i.e., there is no 'memory' and the process is Markovian. (Recall, memory and friction can be calculated from solvent-particle force ACFs in an all-atom MD simulation.) The yet unknown σ_R is the variance of the fluctuations.

The friction is given by the friction coefficient ξ which describes the friction force due to the presence of solvent around the moving particle ("viscous drag"). We saw when discussing the Smoluchowski (diffusion-drift) equation that the friction is related to the free particle diffusion constant, D , by the "Einstein relation":

$$D = \frac{k_B T}{\xi} \quad (13.8)$$

with a given variance of the random force of $\sigma_R^2 = 2\xi k_B T$. The latter must be true in equilibrium as we will proof below. Both equations are realisations of the more general fluctuation-dissipation theorem of statistical physics. Given $\sigma_R^2 = 2\xi k_B T$, we can derive the Einstein relation for a free particle ($F^{\text{tot}} \equiv 0$) in one dimension in the long-time limit (e.g. we neglect inertia as $m \ll \Delta t \xi$):

$$\begin{aligned} \xi \dot{x}(t) &= R(t) \quad \text{with} \quad x(t=0) = x_0 \\ x(t) &= x_0 + \frac{1}{\xi} \int_0^t dt' R(t') \\ \langle (x(t) - x_0)^2 \rangle &= \frac{1}{\xi^2} \int_0^t dt' \int_0^t dt'' \langle R(t'') R(t') \rangle \\ &= \frac{1}{\xi^2} \int_0^t dt' \int_0^t dt'' 2\xi k_B T \delta(t'' - t') \\ &= 2 \frac{k_B T}{\xi} t = 2Dt \end{aligned} \quad (13.9)$$

One can easily see that the velocity ACF for overdamped BD is only the δ -function

$$\langle \vec{v}(t) \vec{v}(t') \rangle = \langle \vec{R}(t) \vec{R}(t') \rangle \propto \delta(t - t') \quad (13.10)$$

The complete solution for $m \neq 0$ of the free particle Langevin equation can be derived as follows. We now assume that *priori* we do not know σ_R and will fix it from stationarity and equilibrium conditions. The formal solutions of the LE is

$$v(t) = v_0 \exp\{-\xi t/m\} + \exp\{-\xi t/m\} \int_0^t ds \exp\{\xi s/m\} R(s)/m \quad (13.11)$$

Then we can calculate considering $t' > t$

$$\begin{aligned}\langle \vec{v}(t) \vec{v}(t') \rangle &= \langle v_0^2 \rangle \exp\{-\xi(t'+t)/m\} \\ &+ \frac{2\sigma_R^2}{m^2} \exp\{-\xi(t'+t)/m\} \int_0^t ds \int_0^{t'} ds' \exp\{-\xi(s'+s)/m\} \delta(s-s') \\ &= \langle v_0^2 \rangle \exp\{-\xi(t'+t)/m\} + \frac{2\sigma_R^2}{m^2} \exp\{-\xi(t'+t)/m\} \int_0^t ds \int_0^{t'} \exp\{-\xi(2s)/m\} \\ &= \exp\{-\xi(t'+t)/m\} \left(\langle v_0^2 \rangle - \frac{2\sigma_R^2}{m\xi} \right) + \frac{2\sigma_R^2}{m\xi} \exp\{-\xi(t'-t)/m\}\end{aligned}\quad (13.12)$$

The term in the large parenthesis must vanish in the stationary case and we obtain $\sigma_R^2 = m\xi\langle v_0^2 \rangle$, and it further follows

$$\langle \vec{v}(t) \vec{v}(t') \rangle = \frac{3k_B T}{m} \exp\left\{-\frac{\xi}{m}|t-t'|\right\} \quad (13.13)$$

for the velocity auto-correlation function (ACF). From equipartitioning we in turn know that $\langle v_0^2 \rangle = k_B T/m$, hence in equilibrium it must hold

$$\sigma_R^2 = \xi k_B T \quad (13.14)$$

which is a simple realization of the fluctuation-dissipation theorem (see also some sections below). Hence, eq.(13.7) we can now fix to

$$\langle \vec{R}_{i\alpha}(t) \cdot \vec{R}_{i\beta}(t') \rangle = 2\xi k_B T \delta_{\alpha\beta} \delta(t-t') \delta_{ij} \quad (13.15)$$

The ansatz for the calculation of the MSD (in 1D) is

$$\begin{aligned}\langle x^2(t) \rangle &= \left\langle \int_0^t v(s) ds \int_0^t v(s') ds' \right\rangle \\ &= \int_0^t \int_0^t ds ds' \langle v(s)v(s') \rangle\end{aligned}\quad (13.16)$$

Some calculus (IN HANDWRITTEN SCRIPT, STILL TO BE TEXED but also see [3], I think) leads to the solution in 3D (only a factor 6 in 3D instead of 2 for 1D):

$$\langle (\vec{r}(t) - \vec{r}(t'))^2 \rangle = \frac{6k_B T}{\xi} \left(|t-t'| + \frac{m}{\xi} \left(\exp\left\{-\frac{\xi}{m}|t-t'|\right\} - 1 \right) \right) \quad (13.17)$$

for the mean-square distance (MSD) which yields the known diffusion law $\langle (\vec{r}(t) - \vec{r}(t'))^2 \rangle \rightarrow 6Dt$ for $t \rightarrow \infty$ (see Figure 13.2).

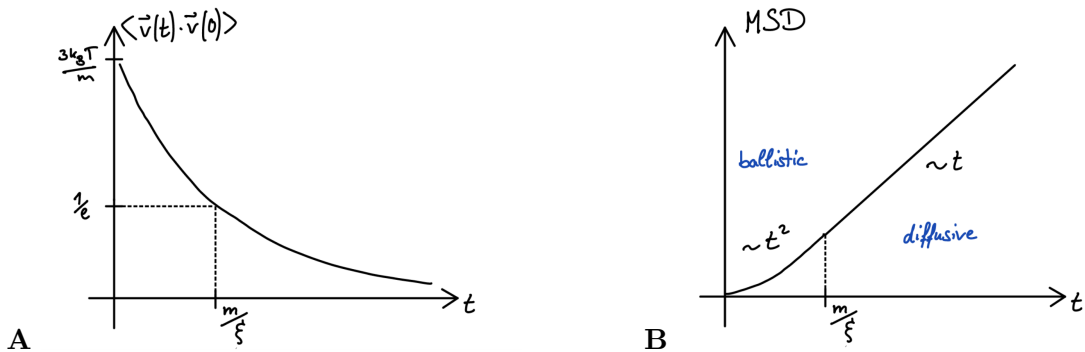


Figure 13.2: The **A** velocity ACF and the **B** MSD of the Langevin equation over the distance r .

An algorithmic implementation of the Langevin equation (LE) using velocity-verlet is displayed in Chapter 12 of Allen and Tildesley [8].

13.2 Brownian Dynamics computer simulations

The term Brownian Dynamics (BD) is often used to describe the overdamped Langevin Dynamics ($m = 0$):

$$\xi \dot{\vec{r}}_i(t) = \vec{F}_i^{\text{tot}}(t) + \vec{R}_i(t) \quad (13.18)$$

The finite difference algorithm is given as:

$$\vec{r}_i(t + \Delta t) \simeq \vec{r}_i(t) + \underbrace{\frac{\Delta t}{\xi} \left(-\nabla V_i^{\text{tot}} \right)}_{\vec{F}_i^{\text{tot}}} + \underbrace{\frac{1}{\xi} \int_t^{t+\Delta t} dt' \vec{R}_i(t')}_{\vec{\Delta r}(t)} \quad (13.19)$$

where the total force is the sum of the external pair forces as coarse-grained mean forces and the sum of internal pair forces $\vec{F}_i^{\text{tot}} = \vec{F}_i^{\text{ext}} + \sum_j \vec{F}_{ij}$. $\Delta \vec{r}(t)$ has a random Gaussian distribution with:

$$\langle \Delta \vec{r}(t) \rangle = 0 \quad \langle \Delta \vec{r}(t) \cdot \Delta \vec{r}(t') \rangle = \frac{2k_B T}{\xi} \Delta t = 2D \Delta t \quad (13.20)$$

which results in the finite difference algorithm being (Ermak & Yek, 1974)

$$\vec{r}_i(t + \Delta t) = \vec{r}_i(t) + \frac{D}{k_B T} \vec{F}_i^{\text{tot}}(t) + \sqrt{2D \Delta t} \vec{G} \quad (13.21)$$

where \vec{G} is the Gaussian random variable with $\langle G_{i\alpha} \rangle = 0$ and $\langle G_{i\alpha} G_{i\beta} \rangle = \delta_{ij} \delta_{\alpha\beta}$.

The steps to implement a Brownian Dynamics computer simulation are:

1. pick particle
2. calculate forces (like in MD)
3. pick random number (force) from Gaussian of variance $2D \Delta t$
4. integrate **BD** by moving particle according to finite difference algorithm as in Equation 13.19

Notes:

- No memory effects are included, as $\langle \vec{R}(t) \vec{R}(t') \rangle \sim \delta(t - t')$ and **BD** can be treated by generalized **LE**.
- Typically, hydrodynamic interactions are neglected, and only $\xi = 6\pi\eta R$ is calculated with η being the solvent viscosity (see Figure 13.3).

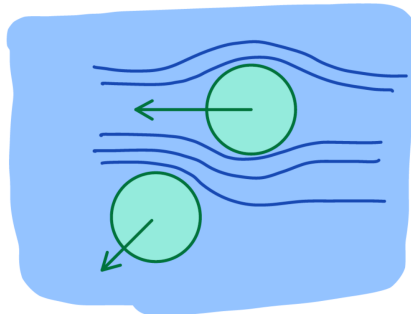


Figure 13.3: Friction force due to Stokes' drag in fluid of viscosity η .

- An approximate inclusion of hydrodynamic interactions is achieved by introducing a diffusion tensor $\underline{\underline{D}}$ of Rank 2.

$$\vec{r}_i(t + \Delta t) = \vec{r}_i(t) + \frac{\underline{\underline{D}}(t)}{k_B T} \vec{F}_i^{\text{tot}}(t) + \nabla \cdot \underline{\underline{D}}(t) \Delta t + \vec{R} \quad \text{with} \quad \langle \vec{R} \otimes \vec{R} \rangle = 2\underline{\underline{D}} \Delta t \quad (13.22)$$

For instance, the far-field approximation of two-body hydrodynamic interaction by the Oseen-Tensor is given as:

$$D_{ij} = \begin{cases} \frac{k_B T}{6\pi\eta R} \mathbb{1} & \text{for } i = j \\ \frac{k_B T}{8\pi\eta r_{ij}} \left(\mathbb{1} + \frac{\vec{r}_{ij} \otimes \vec{r}_{ij}}{|r_{ij}|^2} \right) & \text{for } i \neq j \end{cases} \quad (13.23)$$

with the unity matrix $\mathbb{1}$ and $r_{ij} = |\vec{r}_i - \vec{r}_j|$.

- If we consider Equation 13.21 and change the variables to be $D = \frac{k_B T}{2m} \Delta t$, we get

$$\vec{r}_i(t + \Delta t) = \vec{r}_i(t) + \frac{1}{2} \frac{\Delta t^2}{m} \vec{F}_i^{\text{tot}} + \sqrt{\frac{k_B T}{m}} \Delta \vec{G} \quad (13.24)$$

which equals the Velocity-Verlet algorithm with velocities randomly selected from the Maxwell-Boltzmann distribution as in the Andersen thermostat. For equilibrium properties, both techniques are formally equivalent. However, dynamic properties (such as diffusion) may have different interpretations and may need corrections.

- In interacting systems, we can talk about short- and long-time selfdiffusion of particles. At short times, they do not interact and diffusive with D_0 which is essentially input to the BD equation. However, at long times mutual interactions (crowding, sticking) will slow down the dynamics and the long-time diffusion $D_l < D_0$ will appear. There will be a cross-over behavior in the MSD at relevant times, roughly determined by the mean time between the interactions (density-dependent).

Chapter 14

Sampling methods and reaction coordinates

14.1 Free energy calculations and entropy

The free energy is not directly accessible as simple averages from simulations (i.e., trajectory data), but is fundamental to characterize the material properties, phases and states! There are various more or less sophisticated methods to calculate $F = U - TS$ available.

Let's consider some of the standard ones:

14.1.1 Thermodynamic Integration

Consider the potential energy function of a known reference system U_0 and the potential energy function of a known target system U_1 . Let's introduce a parameter λ such that:

$$U(\lambda = 0) = U_0 \quad U(\lambda = 1) = U_1 \quad (14.1)$$

where both constraints are interpolates through a λ -path.

The Helmholtz free energy is given as:

$$F = -k_B T \ln Z \quad (14.2)$$

with the partition sum being

$$Z(\lambda) = \frac{1}{\Omega^{3N} N!} \int d^{3N}r e^{-\beta U(\lambda)} \quad (14.3)$$

From the free energy, we can calculate the derivative with respect to the λ -parameter:

$$\left(\frac{\partial F(\lambda)}{\partial \lambda} \right)_{N,V,T} = \frac{1}{Z} \int d^{3N}r \frac{\partial U}{\partial \lambda} e^{-\beta U(\lambda)} = \langle \frac{\partial U}{\partial \lambda} \rangle_\lambda \quad (14.4)$$

with the thermodynamic "force" $\frac{\partial U}{\partial \lambda}$. The energy difference is then given as:

$$F(\lambda = 1) - F(\lambda = 0) = \int_{\lambda=0}^{\lambda=1} d\lambda \langle \frac{\partial U}{\partial \lambda} \rangle_\lambda \quad (14.5)$$

For example, if simply we interpolate linearly between two potentials, $V(r, \lambda) = \lambda V(r) + (1 - \lambda)V_0(r)$, with the reference pair potential $V_0(r)$ and the target pair potential $V(r)$, then we need to average $V(r) - V_0(r)|_\lambda$, i.e., the energy difference of the system interacting with $V(r, \lambda)$ vs. $V_0(r)$ and integrate it up.

Another example, If $\lambda = r$ (i.e., simply the distance between two particle), then $\frac{\partial U}{\partial \lambda}$ is simply the mean force. Integration of the latter provides the free energy along r , also often called the *potential of mean force* (PMF), see also section 6.1.

In practice, the λ -path should be chosen in such a way to be numerically convenient. This can prove to be tricky for (discrete in λ) simulation sampling due to badly behaving $U(\lambda)$ (see Figure 14.1 for example). λ could also be a physical 'reaction coordinate', see section 14.1.4 further below. Then one obtains from TI directly the 'free energy landscape' as a function of λ which could be useful to study equilibrium populations and kinetics along λ .

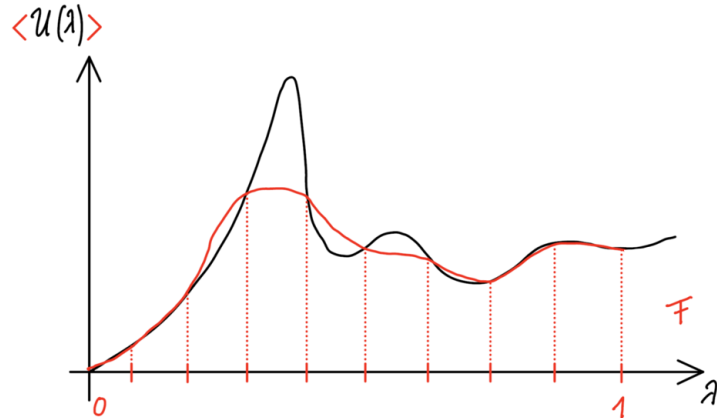


Figure 14.1: An example for a badly behaving sample of the potential $U(\lambda)$.

This happens for instance if $\lambda = \sigma$ or $\lambda = \epsilon$ for "blowing" up (solvation) of a Lennard-Jones sphere in water (see Figure 14.2)

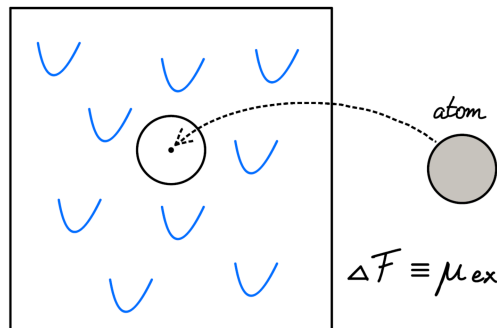


Figure 14.2: Solvation of a Lennard-Jones sphere in water with the chemical potential μ_{ex} being the free energy difference.

Free energy of a solvation of a Lennard-Jones sphere:

Consider the free energy of charging a LJ atom in water to an ion of charge Q at $\vec{r}_c \equiv 0$.

$$U = U_0 + U_C(\lambda) \quad U_C = \sum_i^{N_{H2O}} \frac{\lambda Q q_i \lambda_B}{|\vec{r} - \vec{r}_i|} \quad \frac{\partial U_C}{\partial \lambda} = \Phi(\vec{r} \equiv 0) - \Phi \quad (14.6)$$

This results in a free energy F of:

$$F = F_0 + Q \int d\lambda \langle \Phi(\vec{r} \equiv 0) \rangle_\lambda \quad (14.7)$$

from the average of the electrostatic potential at $\vec{r} \equiv 0$.

14.1.2 Particle insertion method

(Also called Widom's insertion method). The particle insertion methods is a very useful and convenient method to calculate the free energy of inserting a particle into a complex medium. With that we can obtain the probability that a particle enters a systems. It is a convenient method because it can done in a 'post'processing way for many systems, i.e., it can be used already with pre-stored available trajectory data of an ergodic equilibrium system.

We consider the excess chemical potential μ_{ex} as the free energy of solvation when adding a particle to the system (see Figure 14.3):

$$\mu_{\text{ex}} = F^{\text{ex}}(N+1, V, T) - F^{\text{ex}}(N, V, T) \quad (14.8)$$

$F^{\text{ex}} = F - F_{\text{ideal}}$ is the "excess" over the ideal gas.

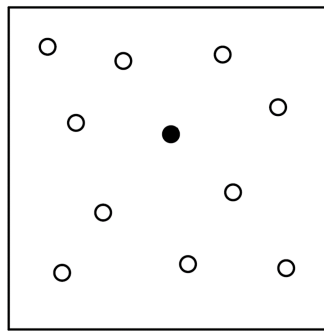


Figure 14.3: Insertion of a particle to the reference system consisting of N particles.

Consider the excess chemical potential

$$\mu_{\text{ex}} = k_B T \ln \frac{V \tilde{Z}_N}{\tilde{Z}_{N+1}} \quad (14.9)$$

where \tilde{Z}_N is the configurational integral for N particles:

$$\frac{\tilde{Z}_{N+1}}{\tilde{Z}_N} = \frac{\int \exp\{-\beta U_{N+1}(\vec{r}_1, \dots, \vec{r}_{N+1})\} d^{3(N+1)}r}{\int \exp\{-\beta U_N(\vec{r}_1, \dots, \vec{r}_N)\} d^{3N}r} \quad (14.10)$$

Now the potential energy equals

$$U_{N+1}(\vec{r}_1, \dots, \vec{r}_{N+1}) = U_N(\vec{r}_1, \dots, \vec{r}_N) + \epsilon(\vec{r}_1, \dots, \vec{r}_N) \quad (14.11)$$

where ϵ is the interaction energy of particle $(N+1)$ fixed at $\vec{r}_{N+1} \equiv 0$ with all others ("test particle limit").

$$\frac{\tilde{Z}_{N+1}}{\tilde{Z}_N} = \frac{\int \exp\{-\beta \epsilon\} \exp\{-\beta U_N\} d^{3(N+1)}r}{\int \exp\{-\beta U_N\} d^{3N}r} \quad (14.12)$$

For a homogeneous solution, this reduces to:

$$\frac{\tilde{Z}_{N+1}}{\tilde{Z}_N} = \frac{V \int \exp\{-\beta \epsilon\} \exp\{-\beta U_N\} d^{3N}r}{\int \exp\{-\beta U_N\} d^{3N}r} = V \langle e^{-\beta \epsilon} \rangle \quad (14.13)$$

"Widom's test particle insertion" approach:

$\mu_{\text{ex}} = -k_B T \ln \langle \exp\{-\beta \epsilon\} \rangle_0$

(14.14)

where 0 is in reference to N particles of the system. In practice, one does average over many random insertions of "test particles" into the ensemble of trajectories of N particles as seen in Figure 14.4. The ensembles can be generated before, hence the whole procedure can be performed as post-processing. This is particularly convenient if one wants to sample different particles (i.e. solutes of different size or charge): one can always use the same pre-generated trajectories of the underlying liquid.

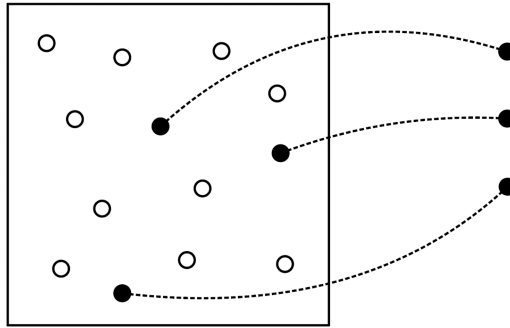


Figure 14.4: Insertion of many test particles to a reference system consisting of N particles.

14.1.3 Free energy perturbation approach

Consider the perturbation of a reference Hamiltonian \mathcal{H}_1 by $\Delta\mathcal{H}$:

$$\mathcal{H}_1 = \mathcal{H}_0 + \Delta\mathcal{H} \quad (14.15)$$

This results in a difference in free energy of:

$$\begin{aligned} -\beta\Delta F &= \ln \frac{Z_1}{Z_2} = \ln \frac{\int d^{3N}r e^{-\beta(\mathcal{H}_0+\Delta\mathcal{H})}}{\int d^{3N}r e^{-\beta\mathcal{H}_0}} \\ &= \ln \langle \exp\{-\beta\Delta\mathcal{H}\} \rangle_0 = \underbrace{\ln \langle \exp\{-\beta\Delta U\} \rangle_0}_{\text{for equal masses}} \end{aligned} \quad (14.16)$$

$$\simeq \underbrace{-\beta\langle\Delta U\rangle}_{\beta\Delta U \ll 1} \sim \left(\frac{\partial U_0}{\partial \lambda} \right)_{\Delta\lambda} \quad (14.17)$$

This method is directly related to the Thermodynamic Integration as well as the Particle Insertion for $\Delta U = \epsilon$. The average of quantity A in the perturbed system is calculated as:

$$\langle A \rangle_{\text{pert}} = \frac{\int d^{3N}r A e^{-\beta(\mathcal{H}_0+\Delta\mathcal{H})}}{\int d^{3N}r e^{-\beta(\mathcal{H}_0+\Delta\mathcal{H})}} = \frac{\langle A \exp\{-\beta\Delta\mathcal{H}\} \rangle_0}{\langle \exp\{-\beta\Delta\mathcal{H}\} \rangle_0} \quad (14.18)$$

One might wonder why this is a 'perturbation' approach because Eqs. 14.16 and 14.18 are in principle exact for every perturbation. Practical problems in evaluating the integrals appear in fact for larger perturbations: the significant contributions of phase space of the perturbed systems then lie in the very rarely sampled tails of the equilibrium distribution. Hence, a FEP simulation with large perturbations will in practice never converge. This also relates to important sampling in Monte-Carlo where Markov chains are generated to move in phase space to well represent the to-be-sampled system (and not just randomly throwing darts).

A good book for more details and more free energy calculation methods is Chipot and Pohorille, "Free energy calculations", Springer.

Example: Charging free energy of a sphere of radius R

$$\Delta U(0 \rightarrow q) = \Phi_0 q \quad (14.19)$$

with ϕ_0 being the electrostatic potential at q .

$$\begin{aligned} \Delta F &= -k_B T \ln \langle \exp\{-\beta \Delta U\}_0 \rangle \\ &\underset{\beta \Delta U \ll 1}{\approx} -k_B T \ln \left\langle 1 - \beta \Delta U + \frac{\beta^2}{2} \Delta U^2 \right\rangle_0 \\ &\simeq \langle \Delta U - \frac{\beta}{2} \Delta U^2 \rangle_0 = \langle \phi_0 \rangle_0 q + \frac{\beta}{2} \langle \phi_0^2 \rangle_0 q^2 \end{aligned} \quad (14.20)$$

Thus if we calculate the potential and fluctuations in the reference system, we get the charging free energy for small charges q .

14.1.4 Reaction coordinate

An important concept for free energy calculations, and thus characterizing a complex system, is the projection of the many degrees of freedom of the original system to a very small number (low dimension) of coordinates, so called *Reaction Coordinates*.

A simple example of such a reaction-coordinate would be the end-to-end distance of a random-walk (or ideal polymer), where many different realizations of the walk can lead to the same distance. Another prominent example is the distance of a molecule to a protein binding pocket in water, where also many solvation and protein conformational states are possible for a fixed distance.

Consider the *NVT* ensemble. The partition sum Z , leading to $F = E - TS = -k_B T \ln Z$, sums over all states Γ in phase space. Now project the states on a 'collective variable' or 'reaction coordinate' $\hat{q}(\Gamma)$. Many states $\{\Gamma\}_q$ can lead to the same value q .

Formally, the probability of finding a state Γ in *NVT* is $P(\Gamma) = \exp\{-\beta H(\Gamma)\}/Z$. Then the probability of finding q is:

$$P(q) = \frac{1}{Z} \int d\Gamma \exp\{-\beta H(\hat{q})\} \delta(q - \hat{q}(\Gamma)) \quad (14.21)$$

The Dirac- δ function serves as a projection operator, collecting all states with prescribed value $q = \hat{q}$. Hence, we can write $P(q) = \langle \delta(q - \hat{q}) \rangle_{NVT}$. Note that from this follows the Boltzmann entropy of the ensemble of value q : $S(q) = +k_B \ln P(q) + S_0$, and the total entropy

$$S = k_B \int dQ P(q) \ln P(q) + S_0 = k_B \langle \ln P(q) \rangle_P + S_0 \quad (14.22)$$

is of Gibbs/Shannon form and we require normalization $\int dq P(q) = 1$. The entropy difference between two distributions is then

$$\Delta S(q) = k_B \ln P(q) - k_B \ln P_0(q) = k_B \ln \frac{P(q)}{P_0(q)} \quad (14.23)$$

The total 'relative entropy' follows from the 'Kullback-Leibler divergence':

$$\Delta S = k_B \int dq P(q) \ln \frac{P(q)}{P_0(q)} \quad (14.24)$$

Also the energy can be projected on q , via

$$E(q) = \frac{1}{Z} \int d\Gamma H(\hat{q}) \exp\{-\beta H(\hat{q})\} \delta(q - \hat{q}(\Gamma)) = \langle H(\hat{q}) \delta(q - \hat{q}) \rangle_{NVT} \quad (14.25)$$

$F(q) = E(q) - TS(q)$ is then the 'free energy landscape' along reaction coordinate q . The $F(q)$ is also often called the '*potential of mean force*' (PMF), because it can be obtained from integrating a mean thermodynamic force along the q -pathway like we showed in the λ -integration in the Thermodynamic Integration (TI) approach above. (We will also see this in the next chapter when we define effective potentials which are also free energies along distance coordinates.) $F(q)$ is important but not always easy to get!

14.1.5 Importance sampling & Umbrella sampling

Now consider the free energy along a "reaction coordinate" or "order parameter" q . The free energy along q is then calculated as:

$$F(q) = -k_B T \ln P(q) = k_B T \ln \frac{1}{Z} \int d^{3N} \delta(q - \hat{q}\{\vec{r}_1, \dots, \vec{r}_N\}) e^{-\beta\{\vec{r}_1, \dots, \vec{r}_N\}} \quad (14.26)$$

where $P(q)$ is the probability distribution and the function is integrated over all $\{\vec{r}_i\}$ for which $q = \hat{q}\{\vec{r}_1, \dots, \vec{r}_N\}$ with $\hat{q} = \sum_i q_i \delta(\vec{r} - \vec{r}_i)$.

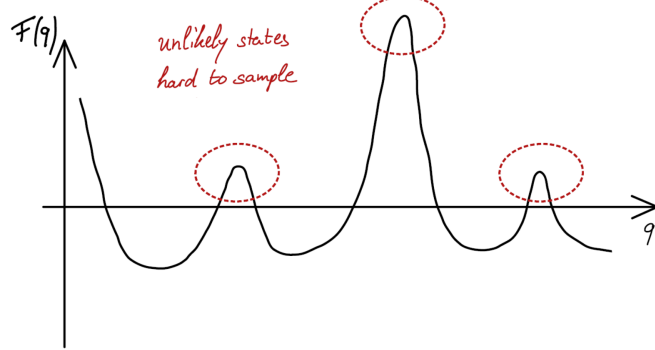


Figure 14.5: Sampling unlikely states can prove to be challenging as they are very sensitive to q .

Importance sampling

$$\Delta F(q) = F(q) - F(q_0) = -k_B T \ln \frac{P(q)}{P(q_0)} \quad (14.27)$$

$$P(q) = \frac{\text{Tr} \delta(q - \hat{q}\{\vec{r}_i\}) e^{-\beta U(\{\vec{r}_i\})}}{\text{Tr} e^{-\beta U(\{\vec{r}_i\})}} \quad (14.28)$$

with the trace being $\text{Tr} = \frac{1}{Q^{3N} N!} \int d^3 r_1 \dots \int d^3 r_N$. If we add a biasing potential $V(\hat{q})$ to facilitate sampling, we get an adjusted probability distribution of

$$P'(q) = \frac{\text{Tr} \delta(q - \hat{q}) e^{-\beta(U + V(\hat{q}))}}{\text{Tr} e^{-\beta(U + V(\hat{q}))}} = \frac{e^{-\beta V(q)} \text{Tr} \delta(q - \hat{q}) e^{-\beta U}}{\text{Tr} e^{-\beta(U + V(\hat{q}))}} \quad (14.29)$$

The calculation of $P'(q_0)$ is analogous and the solution between $P'(q)$ and $P'(q_0)$ is then:

$$P'(q) = \frac{e^{-\beta V(q)}}{e^{-\beta V(q_0)}} \frac{P(q)}{P(q_0)} P'(q_0) \quad (14.30)$$

Applying this formula to Equation 14.27, we finally get:

$$\boxed{\Delta F(q) = -k_B T \left(\ln \frac{P'(q)}{P'(q_0)} + V(q_0) - V(q) \right)}$$

(14.31)

The desired free energy function can be obtained by sampling the "non-Boltzmann" distribution $P'(q)$ and subtracting the bias $V(q)$ afterwards. A challenge is the fact, that a good choice of $V(q)$ is a priori not known. Often the system is piecewise constrained with an "umbrella potential" (typically harmonic) at values q_i as seen in Figure 14.6.

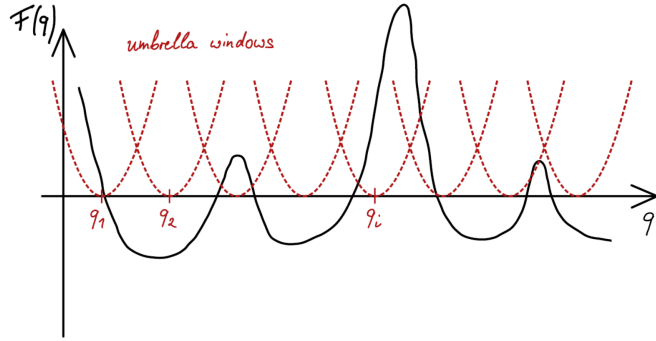


Figure 14.6: Umbrella sampling by piecewise constraining the system with umbrella potential at q_i .

The sampling is done over all **overlapping** umbrella windows. Using Equation 14.31 for every window and matching overlapping branches, the free energy $F(q)$ can be reconstructed. (In practice, one would use WHAM¹ = weighted histogram analysis method)

The fact that equidistant windows may not be efficient or sufficient may be challenging and the procedure needs iterations (adding stiff windows with long sampling) to obtain the accurate $F(q)$!

14.2 From free energies to phase diagrams

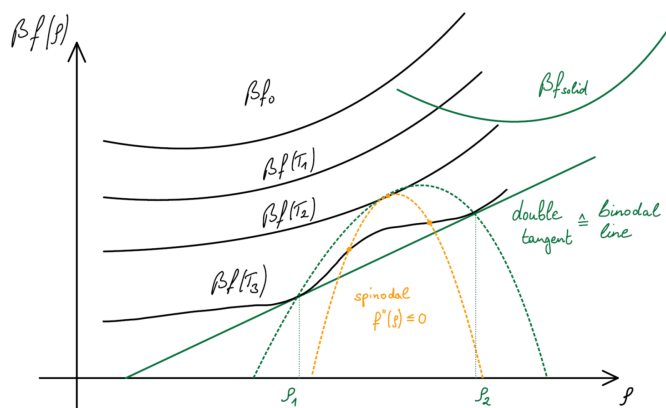


Figure 14.7: The free energy per volume $f = F/V$ in dependence of the density ρ at different temperatures $T_3 < T_2 < T_1$.

Free energies of a system can be used to calculate a system's stability, coexisting phases, and phase diagrams. For this, we define the free energy per volume:

$$f = \frac{F}{V} = \frac{F_{\text{id}}}{V} + \frac{F_{\text{exc}}}{V} = f_{\text{id}} + f_{\text{ex}} \quad (14.32)$$

For hard spheres (being in the following a reference '0' system) this is given as:

$$\beta f_{\text{exc}}^0 = \rho \left(\ln \Lambda^3 \rho - 1 \right) + \underbrace{\frac{6}{\pi \sigma^3} \frac{\eta^2 (4 - 3\eta)}{(1 - \eta)^2}}_{\text{Carnahan-Starling eq. of state}} \quad (14.33)$$

¹<https://www.youtube.com/watch?v=E8gmARGvPfI>

with σ being the diameter of the sphere, $\eta = \frac{\pi}{6}\rho\sigma^3$ being the packing fraction and $\rho = \frac{N}{V}$ being the density.

Now we consider a pair potential of

$$V_\lambda(r) = V_{\lambda_0}(r) + W_\lambda(r) \quad (14.34)$$

with the switching parameter λ like in the TI approach we introduced above. Let V_{λ_0} be our known reference system and W_λ be some (attractive) potential like for example a van-der-Waals or depletion potential. The energy $U(\lambda)$ of the system is:

$$U(\lambda) = \sum_{i < j} V_\lambda(|\vec{r}_i - \vec{r}_j|) \quad (14.35)$$

Applying the thermodynamic integration

$$\frac{\partial \beta F_{\text{exc}}}{\partial \lambda} = \frac{1}{Z(\lambda)} \int d^3 r_1 \dots \int d^3 r_N e^{-\beta U(\lambda)} \beta U'(\lambda) = \beta \langle U'(\lambda) \rangle_\lambda \quad (14.36)$$

we get the ensemble average for a system interacting with V_λ with $U'(\lambda) = \frac{\partial U}{\partial \lambda}$.

How we use λ as a switching parameter should not be important, free energy differences are not path-dependent. Hence, we can chose the λ -integration as convenient as possible: let us assume simply that $W_\lambda(r) = \lambda W(r)$, i.e., λ switches on the potential linearly:

$$V_\lambda(r) = V_0(r) + \lambda W(r) \quad (14.37)$$

with $\lambda_0 = 0$ and $\lambda_1 = 1$. This results in

$$U'(\lambda) = \frac{\partial U}{\partial \lambda} = \sum_{i < j} W(|\vec{r}_i - \vec{r}_j|). \quad (14.38)$$

The integration of Equation 14.36 yields:

$$\beta F_{\text{exc}}(\lambda = 1) = \beta F_{\text{exc}}^0 + \beta \int_0^1 d\lambda \langle \sum_{i < j} W(|\vec{r}_i - \vec{r}_j|) \rangle_\lambda \quad (14.39)$$

The Taylor expansion up to the first order of $U'(\lambda)$ is given as:

$$\langle U'(\lambda) \rangle_\lambda \simeq \langle U'(\lambda) \rangle_0 + (\lambda - \lambda_0) \frac{\partial}{\partial \lambda} \langle U'(\lambda) \rangle_0 + \mathcal{O}(\lambda^2) \quad (14.40)$$

with

$$\langle U'(\lambda) \rangle = \frac{\int d^3 r U'(\lambda) e^{-\beta U(\lambda)}}{\int d^3 r e^{-\beta U(\lambda)}} \quad (14.41)$$

$$\frac{\partial}{\partial \lambda} \langle U'(\lambda) \rangle = \langle U''(\lambda) \rangle - \beta \left(\langle U'^2(\lambda) \rangle - \langle U'(\lambda) \rangle^2 \right) \quad (14.42)$$

Applying the Taylor expansion to Equation 14.39, we get the **high temperature expansion**:

$$\beta F_{\text{exc}}(\lambda = 1) = \beta F_{\text{exc}}^0 + \underbrace{\beta \langle \sum_{i < j} W(|\vec{r}_i - \vec{r}_j|) \rangle_0}_{\text{mean of perturbation}} - \frac{1}{2} \beta \underbrace{\left(\langle \sum_{i < j} W(|\vec{r}_i - \vec{r}_j|)^2 \rangle_0 - \langle \sum_{i < j} W(|\vec{r}_i - \vec{r}_j|) \rangle_0^2 \right)}_{\text{variance of perturbation}} \quad (14.43)$$

The F_{exc}^0 term can be identified with the hard sphere reference system, which we perturb by W . The pairwise additivity yields:

$$\left\langle \sum_{i < j} W(|\vec{r}_i - \vec{r}_j|) \right\rangle_\lambda = \left\langle \sum_{i < j} \int d^3 r \delta(r - |\vec{r}_i - \vec{r}_j|) W(r) \right\rangle_\lambda = \frac{\rho N}{2} \int d^3 r g_\lambda(r) W(r) \quad (14.44)$$

with $g_\lambda(r) = g(r)$ for a system interacting with V_λ . This results in:

$$\beta F_{\text{exc}} = \beta F_{\text{exc}}^0 + \frac{\beta \rho N}{2} \int_0^1 d\lambda \int d^3 r g_\lambda(r) W(r) \quad (14.45)$$

Also the pair density can be expanded in powers of λ :

$$\rho g_\lambda(r) = \rho_\lambda^{(2)}(r) = \rho_0^{(2)}(r) + \lambda \left(\frac{\partial \rho_\lambda^{(2)}(r)}{\partial \lambda} \right)_{\lambda=0} + \mathcal{O}(\lambda^2) \quad (14.46)$$

First-Order perturbation theory:

$$\boxed{\frac{\beta F_{\text{exc}}}{V} \simeq \frac{\beta F_{\text{exc}}^0}{V} + \frac{\beta \rho^2}{2} \int d^3 r g_0(r) W(r)} \quad (14.47)$$

Let's now assume that $W(r)$ is a long-ranged potential and its contribution dominates over the correlations of $g(r)$. We can neglect the effect of correlations. This mean-field approximation then yields:

$$\begin{aligned} \beta f_{\text{exc}} &= \frac{\beta F_{\text{exc}}}{V} \simeq \frac{\beta F_{\text{exc}}^0}{V} + \frac{\beta \rho^2}{2} \int d^3 r W(r) \\ &= \frac{\beta F_{\text{exc}}^0}{V} + \beta \rho^2 a \end{aligned} \quad (14.48)$$

where the parameter $a < 0$ for an attractive potential $W(r)$. Thermodynamics ($P = -\partial F/\partial V$) tells us that the equation of state can be obtained from $f_{\text{exc}} = F_{\text{exc}}/V = (F - F_{\text{id}})/V$ through

$$\frac{\beta P}{\rho} - 1 = \rho \frac{\partial}{\partial \rho} \frac{\beta f_{\text{exc}}}{\rho} \quad (14.49)$$

For hard spheres of diameter σ and small packing fractions $\eta = (\pi/6)\sigma^3 \rho$, the Carnahan Starling expression Eq. (14.33) reduces to the second virial contribution only, and $F_{\text{exc}}^0 \simeq (2/3)\pi\sigma^3 \rho$. Inserted in Eqs. (14.48) and (14.49) one can bring the latter (by using $1/(1-x) \simeq 1+x$ for small x) into the form:

$$\frac{\beta P}{\rho} \simeq \frac{1}{1 - \underbrace{\frac{2}{3}\pi\sigma^3 \rho}_{4\eta=b\rho}} + a\beta\rho \quad (14.50)$$

Finally, substituting $v = \rho^{-1}$ and rearranging, we get the real gas equation (van-der-Waals equation of state):

$$\boxed{\left(P + \frac{a}{v^2} \right) (v - b) = k_B T} \quad (14.51)$$

In general, attraction can lead to concave paths in the free energy in dependence of the density, ρ , meaning $f''(\rho) \leq 0$. But as $\chi_T \sim f''^{-1}(\rho)$, this can lead to a diverging compressibility for $f''(\rho) = 0$ and thus instability! The loci of $f''(\rho) = 0$ defines the **spinodal line**.

Equilibrium for coexisting phases: $(T, \mu, P = -\frac{\Omega}{V})$

Let's assume two states in mechanical, chemical, and thermal equilibrium:

$$P_1 = P_2 \quad \mu_1 = \mu_2 \quad T_1 = T_2 = T \quad (14.52)$$

The pressure P and the chemical potential μ can be written in terms of $f = \frac{F}{V} = f(\rho)$:

$$P = -\left(\frac{\partial F}{\partial V}\right)_{N,T} = -\frac{\partial}{\partial V} \left(V f\left(\frac{N}{V}\right)\right)_{N,T} = -f - V f'(\rho) \left(-\frac{N}{V^2}\right) = -f - \rho f' \quad (14.53)$$

$$\mu = \left(\frac{\partial F}{\partial N}\right)_{T,V} = \frac{\partial}{\partial N} \left(V f\left(\frac{N}{V}\right)\right)_{T,V} = f' \quad (14.54)$$

The conditions imposed on the free energy $f(\rho)$ are:

$$f'_1(\rho_1) = f'_2(\rho_2) \quad f_1(\rho_1) - \rho_1 f'_1(\rho_1) = f_2(\rho_2) - \rho_2 f'_2(\rho_2) \quad (14.55)$$

This implies that for the same slope f' and the same f -axis interception point, there are two coexisting densities ρ_1 and ρ_2 . With the so-called Maxwell's double-tangent construction, ρ_1, ρ_2 define the **binodal line** (see Figure 14.7 and Figure 14.8).

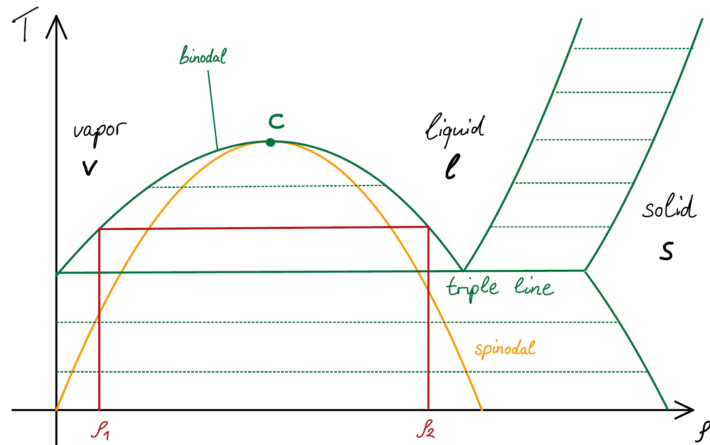


Figure 14.8: Phase diagram with binodal and spinodal curves. There may be coexisting states indicated by the horizontal lines with a density difference $\Delta\rho \neq 0$ (e.g. $\Delta\rho = \rho_2 - \rho_1$ for the red line between liquid and vapor).

Chapter 15

Appendix

15.1 Complexity diagram

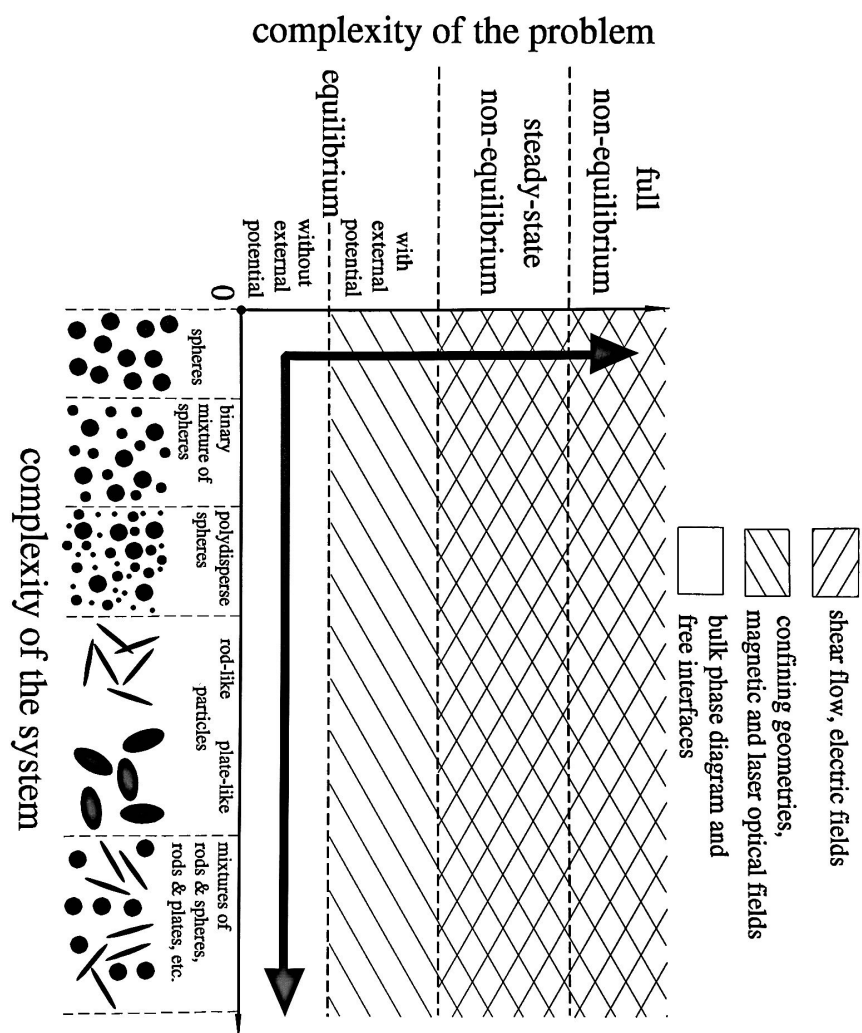


Figure 1. Schematic diagram of complexity: the x -axis shows the complexity of the system, the y -axis the complexity of the problem. The two arrows indicate possible research directions. The problems associated with different kinds of external field are also indicated.

15.2 Overview of interatomic potentials

Table 5.1 Values of the Lennard-Jones parameters for the rare gases [32]

| Ne | Ar | Kr | Xe |
|-----------------|--------|--------|--------|
| ϵ (eV) | 0.0031 | 0.0104 | 0.0140 |
| σ (Å) | 2.74 | 3.40 | 3.65 |



Figure 5.4 Solid curve is the experimental Ar-Ar potential while the dashed curve is the best Lennard-Jones fit to that potential (adapted from [16]).

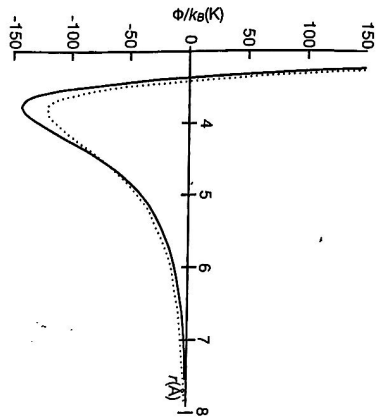


Fig. 1.3 Argon pair potentials. We illustrate (solid line) a recent pair potential for argon calculated by ab initio methods (see Palkowski and Szalewicz, 2010). Also shown is the Lennard-Jones 12-6 potential (dashed line) used in computer simulations of liquid argon.

Table 1.1 Atom-atom interaction parameters

| Atom | Source | ϵ/k_B (K) | σ (nm) |
|------|-----------------------------|--------------------|---------------|
| H | Murad and Gubbins (1978) | 8.6 | 0.281 |
| He | Maitland et al (1981) | 10.2 | 0.228 |
| C | Tildesley and Madden (1981) | 51.2 | 0.335 |
| N | Cheung and Powles (1975) | 37.3 | 0.331 |
| O | English and Venables (1974) | 61.6 | 0.295 |
| F | Singer et al. (1977) | 52.8 | 0.283 |
| Ne | Maitland et al. (1981) | 47.0 | 0.272 |
| S | Tildesley and Madden (1981) | 183.0 | 0.352 |
| Cl | Singer et al. (1977) | 173.5 | 0.335 |
| Ar | Maitland et al (1981) | 119.8 | 0.341 |
| Br | Singer et al. (1977) | 257.2 | 0.354 |
| Kr | Maitland et al (1981) | 164.0 | 0.383 |

Figure 5.6 Comparisons between pair potentials, all calculated with the potential minimum at $r_m = 3$ and the Lennard-Jones $\sigma = 2^{1/6}r_m$. The well depth was $\epsilon = 1$ for all cases. Shown are the Lennard-Jones potential (solid curve), the Mie potential with $m = 10$ and $n = 6$ (the long-dashed curve), the Morse potential with $\alpha = 2.118$ (dot-dashed curve), and the Born-Mayer potential with $\alpha = 4.38$ (dotted curve). (a) The well region. The potentials are all forced to have the same minimum and all go to zero at $r = \sigma$. (b) The short-range part of the potentials.

Table 6.1 Reduced units in Lennard-Jones systems

| Value | In reduced units |
|------------------|--|
| Potential energy | $U^* = U/\epsilon$ |
| Temperature | $T^* = k_B T/\epsilon$ |
| Density | $\rho^* = \rho \sigma^3$ |
| Pressure | $P^* = P \sigma^3/\epsilon$ |
| Time | $t^* = t/t_0$, where $t_0 = \sigma \sqrt{m/\epsilon}$ |

ϵ and σ are defined in Eq. (6.21). All energies are in units of ϵ , e.g., $E^* = E/\epsilon$, $K^* = K/\epsilon$.

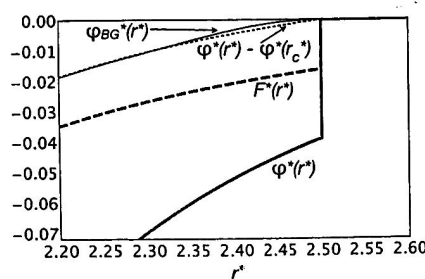


Figure 6.4 Force F^* , potential ϕ^* , and shifted potential $\phi^*(r^*) - \phi^*(r_c^*)$ for an LJ potential cutoff at $r_c = 2.5\sigma$. Note that there is a discontinuity in both the potential and force at the cutoff. $\phi_{BG}^*(r^*)$ is a potential that smoothly interpolates the potential and derivative to zero at $r_c^* = 2.5$, avoiding the discontinuities [43].

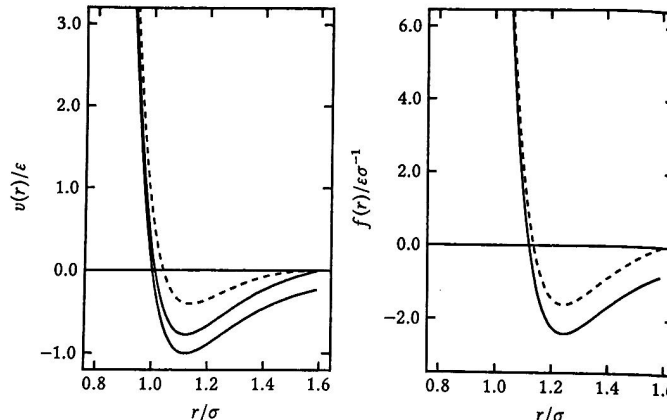


Fig. 5.2 Magnitude of the pair potential $v(r)$ and the force $f(r)$, for the Lennard-Jones and shifted Lennard-Jones potentials (solid lines), and the shifted-force modification (dashed lines). Note that, for illustration, we have chosen a very short cutoff distance, $r_c = 1.6\sigma$.

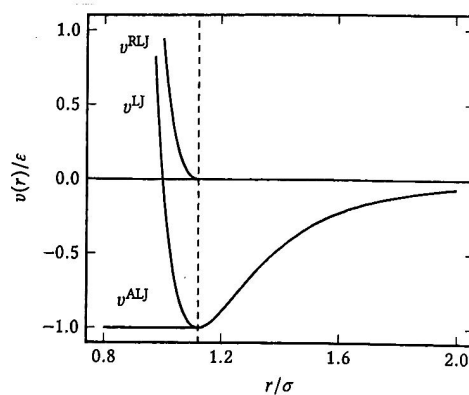


Fig. 1.5 The separation of the Lennard-Jones potential v^LJ into attractive and repulsive components, $v^A LJ$ and $v^R LJ$, respectively. The vertical dashed line shows the position of r_{min} .

15.3 Numerical integration and energy conservation

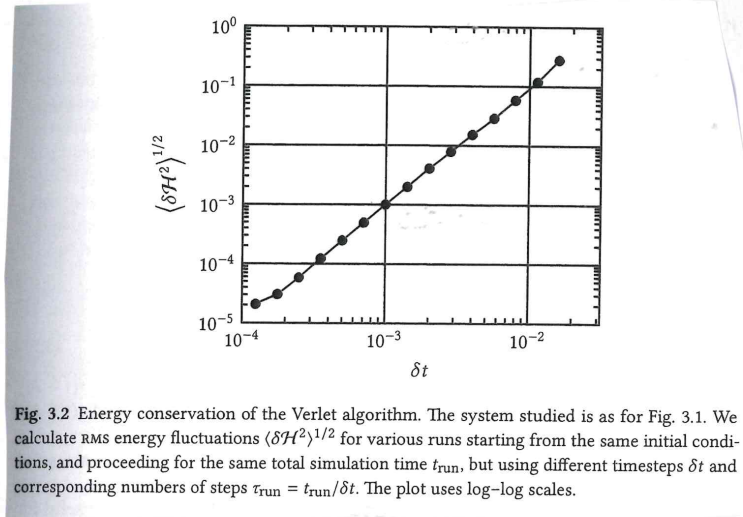


Fig. 3.2 Energy conservation of the Verlet algorithm. The system studied is as for Fig. 3.1. We calculate RMS energy fluctuations $\langle \delta H^2 \rangle^{1/2}$ for various runs starting from the same initial conditions, and proceeding for the same total simulation time t_{run} , but using different timesteps δt and corresponding numbers of steps $\tau_{\text{run}} = t_{\text{run}}/\delta t$. The plot uses log-log scales.

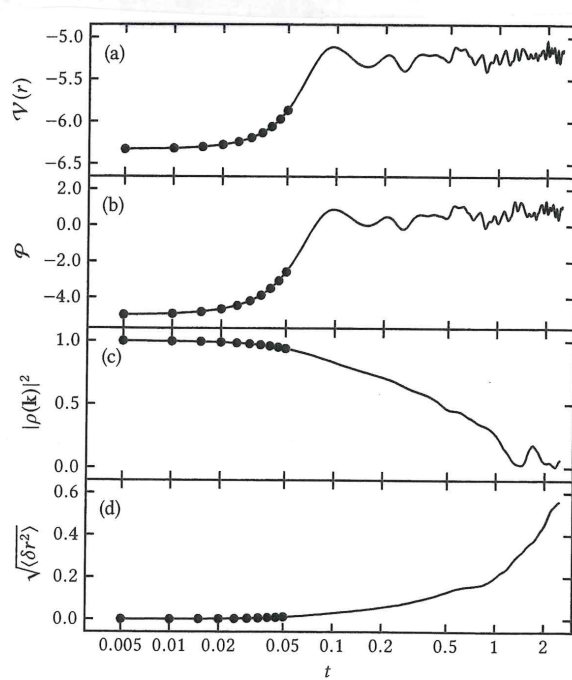


Fig. 5.7 The equilibration phase of an MD simulation. The horizontal scale is logarithmic; the first ten steps are shown explicitly. We show the evolution of: (a) the potential energy; (b) the instantaneous pressure; (d) the square modulus of the translational order parameter; and (c) the root-mean-square displacement from the initial positions. The system consists of 108 atoms interacting via the shifted Lennard-Jones pair potential, $r_c^* = 2.5$, no long-range corrections applied. The simulation starts from an FCC lattice with a Maxwell-Boltzmann velocity distribution. The system is near the triple point ($\rho^* = 0.8442$, $T^* = 0.722$, $P^* = 0.610$, $E^*/N = -4.129$). The simulation is in the constant-energy ensemble, using the velocity Verlet algorithm, with $\delta t^* = 0.005$.

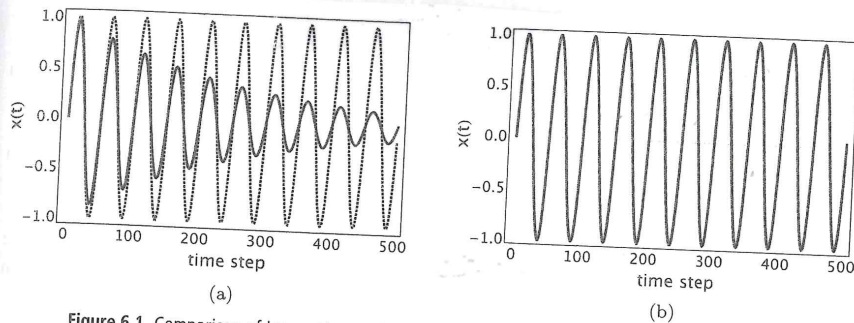


Figure 6.1 Comparison of integration methods for the one-dimensional harmonic oscillator with $k = m = \omega = 1$, $x(0) = 0$, and $v(0) = 1$. Exact result from Appendix D.3 is given as the dotted curves. $\delta t = 2\pi/50$, i.e., there are 50 points per period of the oscillation. (a) The solid curve is from a calculation based on the simple solution in Eq. (6.8) and Eq. (6.9). (b) The solid curve is from a calculation based on the Verlet algorithm in Eq. (6.11). The solid curve overlays the exact solution.

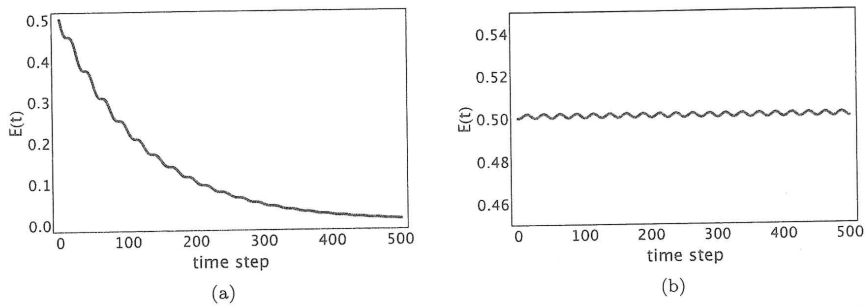


Figure 6.2 Comparison of energy conservation between calculations with the two integration methods of Figure 6.1. The exact energy, E_{exact} , equals $1/2$. (a) $E(t)$ versus t for the calculation in Figure 6.1a. (b) $E(t)$ versus t for the calculation in Figure 6.1b and is based on the Verlet algorithm.

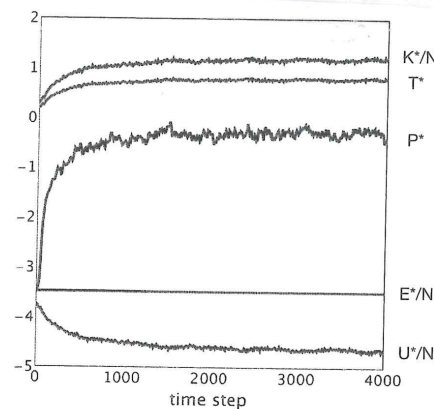


Figure 6.5 Initial equilibration of the Lennard-Jones system described in the text. Shown are instantaneous values for K^*/N , T^* , P^* , E^* , and U^*/N . Note that while K^* and U^* vary greatly over the course of the first 1500 time steps or so, the energy E^* is constant.

15.4 Simulations of finite systems: simulation boxes, periodic boundary conditions and periodic images

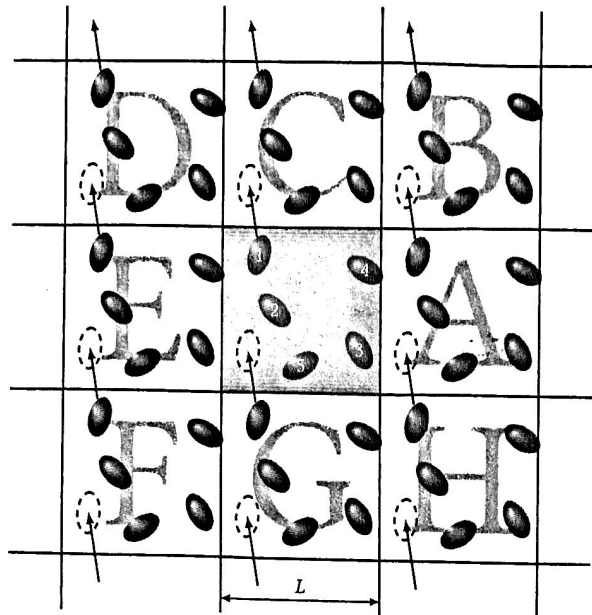


Fig. 1.13 A two-dimensional periodic system. Molecules can enter and leave each box across each of the four edges. In a three-dimensional example, molecules would be free to cross any of the six cube faces.

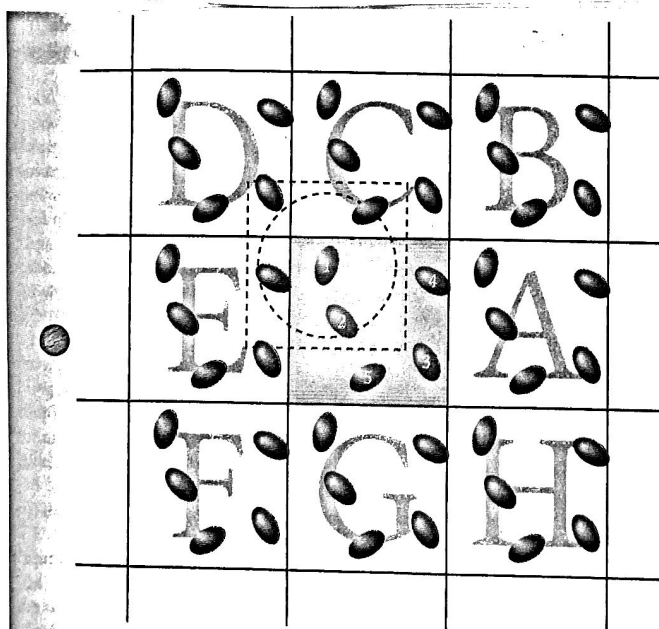


Fig. 1.16 The minimum image convention in a two-dimensional system. The central 'box' contains five molecules. The dashed 'box' constructed with molecule 1 at its centre also contains five molecules. The dashed circle represents the cutoff.

A&T

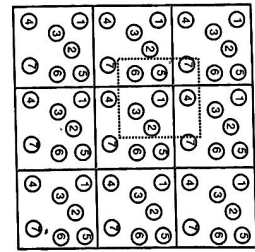


Figure 3.4 Periodic boundary conditions. The central cell is replicated to fill space. As a particle in the central cell moves, its images move in the same way. The dashed box indicates the effective cutoff for the nearest-image convention for particle 1.

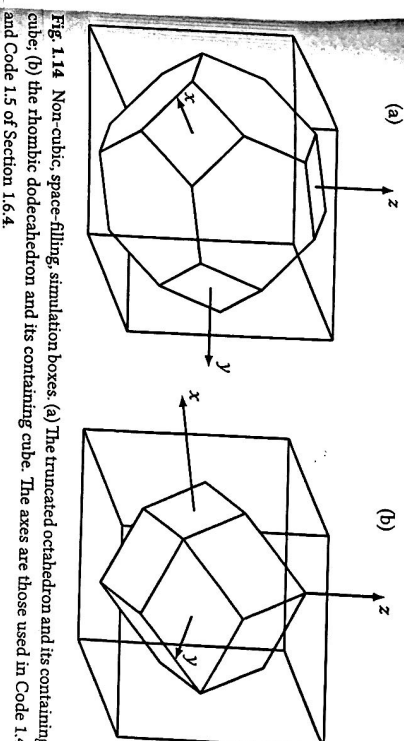


Fig. 1.14 Non-cubic, space-filling, simulation boxes. (a) The truncated octahedron and its containing cube; (b) the rhombic dodecahedron and its containing cube. The axes are those used in Code 1.4 and Code 1.5 of Section 1.6.4.

Table 6.1 Reduced units in Lennard-Jones systems

| Value | In reduced units |
|------------------|--|
| Potential energy | $U^* = U/\epsilon$ |
| Temperature | $T^* = k_B T/\epsilon$ |
| Density | $\rho^* = \rho \sigma^3$ |
| Pressure | $P^* = P \sigma^3/\epsilon$ |
| Time | $t^* = t/t_0$, where $t_0 = \sigma \sqrt{m/\epsilon}$ |

ϵ and σ are defined in Eq. (6.21). All energies are in units of ϵ , e.g., $E^* = E/\epsilon$, $K^* = K/\epsilon$.

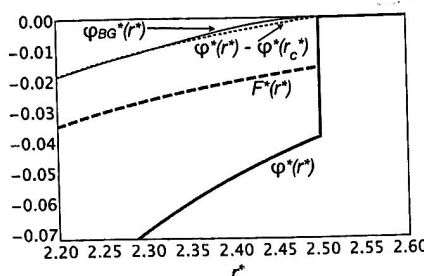


Figure 6.4 Force F^* , potential ϕ^* , and shifted potential $\phi^*(r^*) - \phi^*(r_c^*)$ for an LJ potential cutoff at $r_c = 2.5\sigma$. Note that there is a discontinuity in both the potential and force at the cutoff. $\phi_{BG}^*(r^*)$ is a potential that smoothly interpolates the potential and derivative to zero at $r_c^* = 2.5$, avoiding the discontinuities [43].

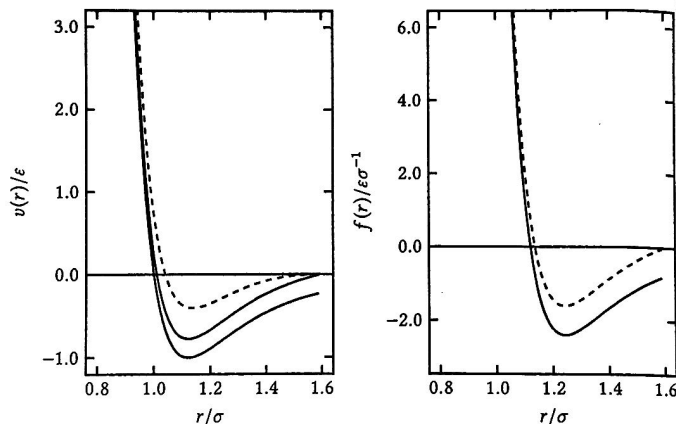


Fig. 5.2 Magnitude of the pair potential $v(r)$ and the force $f(r)$, for the Lennard-Jones and shifted Lennard-Jones potentials (solid lines), and the shifted-force modification (dashed lines). Note that, for illustration, we have chosen a very short cutoff distance, $r_c = 1.6\sigma$.

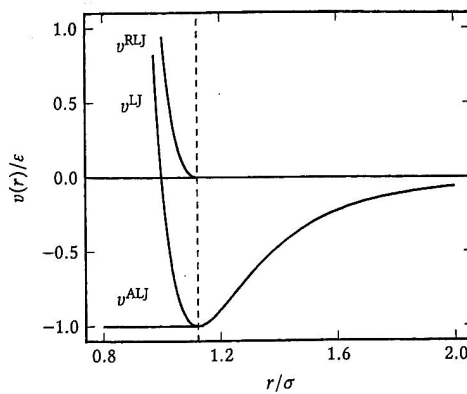
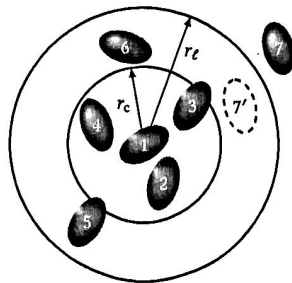
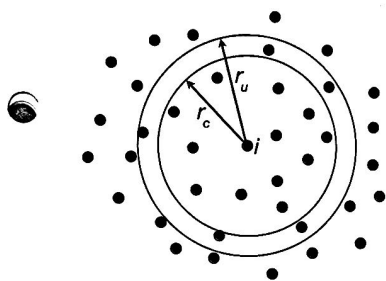


Fig. 1.5 The separation of the Lennard-Jones potential v^LJ into attractive and repulsive components, v^ALJ and v^RLJ , respectively. The vertical dashed line shows the position of r_{min} .



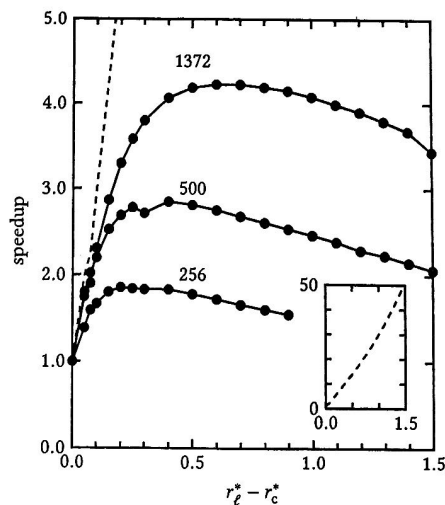
A&T

Fig. 5.3 The cutoff sphere, radius r_c , and its skin, radius r_ℓ , around a molecule 1. Molecules 2, 3, 4, 5, and 6 are on the list of molecule 1; molecule 7 is not. Only molecules 2, 3, and 4 are within the range of the potential at the time the list is constructed.



LESAR

Figure 3.6 Construction of a list of neighbors for atom i . The potential cutoff is r_c , while the upper limit for distances within the list is r_u , as discussed in the text.



A&T

Fig. 5.4 Speedup with Verlet list. Example results are shown for the Lennard-Jones potential, with cutoff $r_c^* = 2.5$, and various values of skin thickness $r_\ell^* - r_c^*$, for the indicated system sizes N . The state point is $\rho^* = 0.78$, $T^* = 0.85$, and the timestep is $\delta t^* = 0.005$. The curves show timesteps per CPU-second, normalized by the speed for zero skin thickness (when the list is updated every step). The dashed line (also shown in the inset) gives the average number of steps between updates, which is almost independent of system size.

A & T, 2nd Edition, P. 197

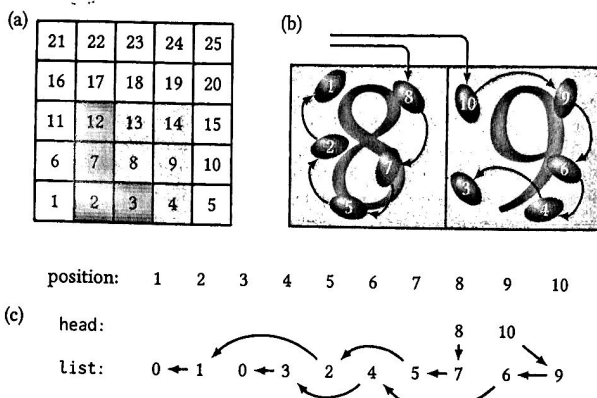
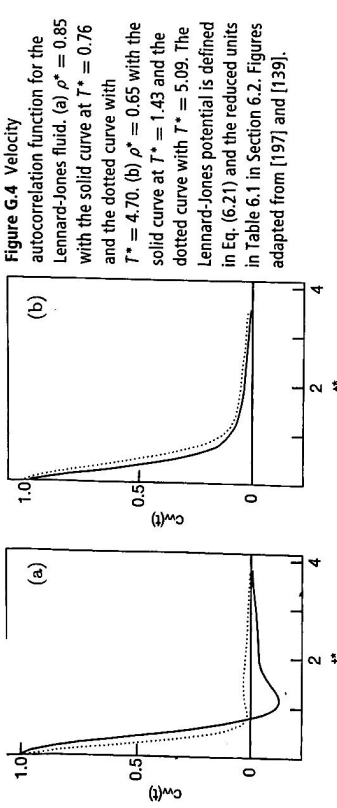


Fig. 5.5 The cell method in two dimensions. (a) The central box is divided into $s_c \times s_c$ cells ($s_c = 5$). A molecule in cell 8 may interact with molecules in any of the shaded cells. In an MD program only the light-shaded neighbours of cell 8 need be examined in the inner loop over cells. (b) A close-up of cells 8 and 9, showing the molecules and the link-list structure. (c) The head and list array elements corresponding to these two cells. Each entry gives the position of the next in the list array.

15.5 Fluctuations and errors



The diffusion constant is related to the velocity autocorrelation function by [223]

$$D = \lim_{t \rightarrow \infty} \frac{k_B T}{m} \int_0^t c_{vv}(t') dt' = \lim_{t \rightarrow \infty} \frac{1}{3} \int_0^t \langle \mathbf{v}_i(t') \cdot \mathbf{v}_i(0) \rangle dt'. \quad (\text{G.42})$$

Equation (G.42) is an example of a *Green-Kubo* relation, relating a macroscopic transport coefficient (e.g., D) to integrals over time correlation functions. Other Green-Kubo relations are available, for example, for the shear viscosity and thermal conductivity. In Chapter 6 we discuss how to use the molecular dynamics methods to evaluate c_{vv} and similar functions. Comparing Eq. (G.42) with the relation for the diffusion constant at long times in Eq. (2.2),

$$D = \frac{1}{6t} \langle \mathbf{r}^2 \rangle, \quad (\text{G.43})$$

where $\langle \mathbf{r}^2 \rangle$ is the mean square displacement. Equating the two equations implies

$$\langle \mathbf{r}^2 \rangle = 2t \int_0^t \langle \mathbf{v}_i(t') \cdot \mathbf{v}_i(0) \rangle dt'. \quad (\text{G.44})$$

It is straightforward to prove Eq. (G.44) starting from $\mathbf{r}(t) = \int_0^t \mathbf{v}(\tau) d\tau$,¹⁷ thus establishing that Eq. (G.43) is equivalent to Eq. (G.42).

¹⁷ $\mathbf{r}(t) = \int_0^t \mathbf{v}(\tau) d\tau$, so

$$\begin{aligned} \langle \mathbf{r}^2 \rangle &= \left\langle \int_0^t \mathbf{v}(\tau_1) d\tau_1 \cdot \int_0^t \mathbf{v}(\tau_2) d\tau_2 \right\rangle \\ &= \int_0^t d\tau_1 \int_0^t d\tau_2 \langle \mathbf{v}(\tau_1) \cdot \mathbf{v}(\tau_2) \rangle \\ &= \int_0^t d\tau_1 \int_0^n d\tau_2 \langle \mathbf{v}(\tau_1) \cdot \mathbf{v}(\tau_2) \rangle + \int_0^t d\tau_1 \int_0^n d\tau_2 \langle \mathbf{v}(\tau_1) \cdot \mathbf{v}(\tau_2) \rangle \\ &= 2 \int_0^t d\tau_1 \int_0^n d\tau_2 \langle \mathbf{v}(\tau_1) \cdot \mathbf{v}(\tau_2) \rangle \end{aligned}$$

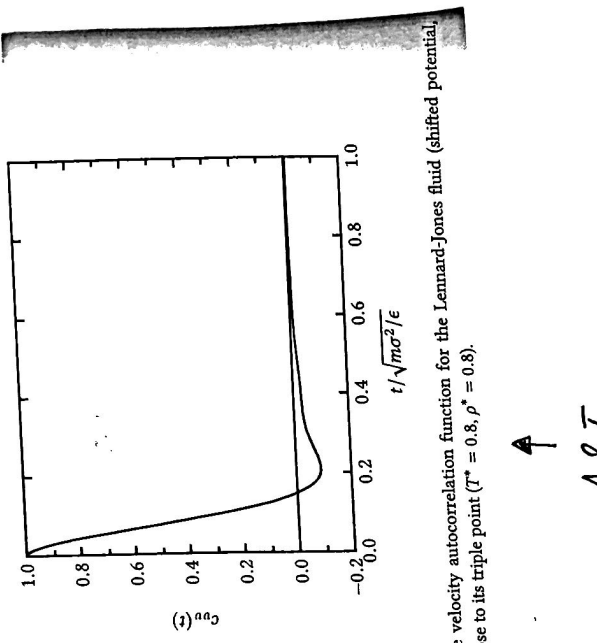
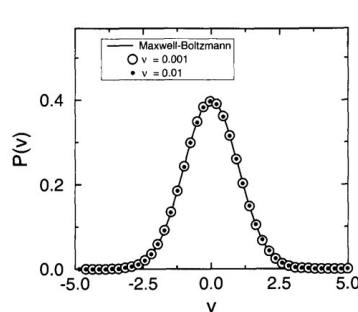


Fig. 2.3 The velocity autocorrelation function for the Lennard-Jones fluid (shifted potential) at its triple point ($T^* = 0.8, \rho^* = 0.8$). $r_c = 2.5a$) close to its triple point ($T^* = 0.8, \rho^* = 0.8$).

A ∇
A ∇T

LESA/N

15.6 Thermostats



Andersen thermostat faithfully reproduced stationary properties.

Figure 6.1: Velocity distribution in a Lennard-Jones fluid ($T = 2.0$, $\rho = 0.8442$, and $N = 108$). The solid line is the Maxwell-Boltzmann distribution (6.1.1), and the symbols are from a simulation using $\nu = 0.01$ and $\nu = 0.001$ as collision rates.

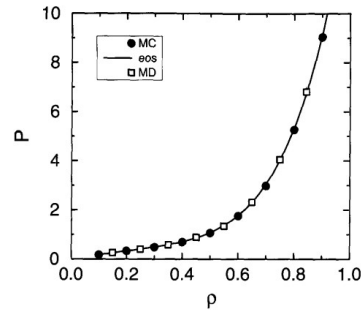


Figure 6.2: Equation of state of the Lennard-Jones fluid ($T = 2.0$ and $N = 108$); comparison of the Molecular Dynamics results using the Andersen thermostat (open symbols) with the results of Monte Carlo simulations (closed symbols) and the equation of state of Johnson *et al.* [62].

Dynamical properties with the Andersen thermostat critically depend on coupling strength

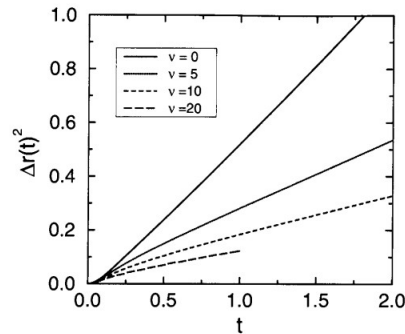


Figure 6.3: Mean-squared displacement as a function of time for various values of the collision frequency ν of the Lennard-Jones fluid ($T = 2.0$ and $N = 108$).

15.7 Structure of liquids; examples for $g(r)$

[19] Groct, Mol. Phys. 62, 867 (1987).

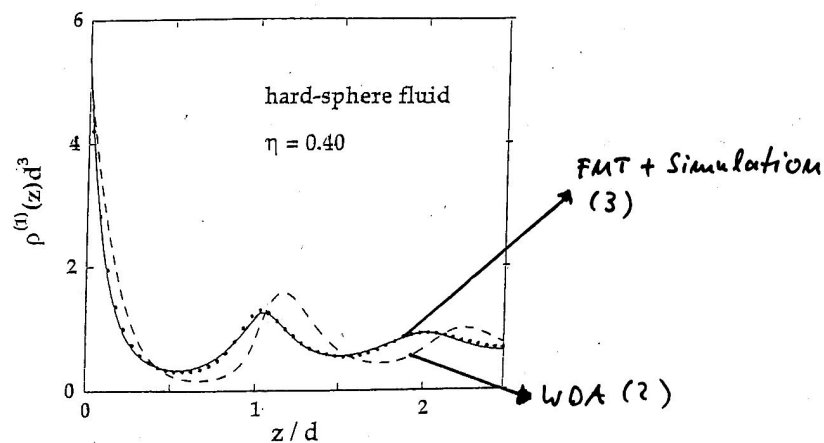


FIG. 6.4. Density profile of a hard-sphere fluid close to a hard wall at a packing fraction $\eta = 0.40$. The full curve is calculated from fundamental-measure theory and the points show the results of Monte Carlo calculations.¹⁹ The dashed curve is calculated from the simpler weighted-density approximation provided by (6.2.22).

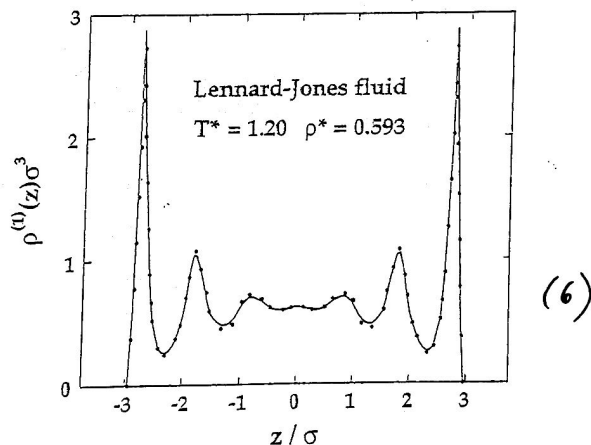


FIG. 6.5. Density profile of a Lennard-Jones fluid in a slit of width $L = 7.5\sigma$. The curve is calculated from fundamental-measure theory and the points show the results of a Monte Carlo simulation.²⁰ After Kierlik and Rosinberg.²¹

Figure 1.2. Typical atomic configurations in a gas (left), liquid (middle) and crystalline solid (right).

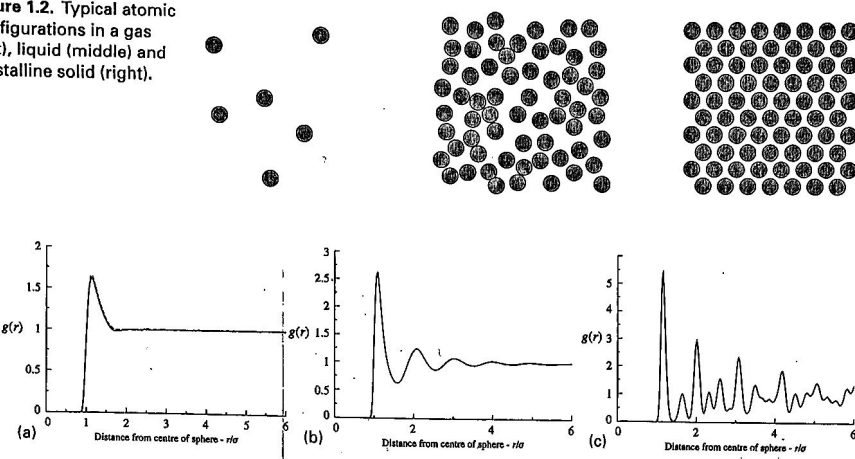


Figure 1.3. Typical pair distribution functions for (a) a gas, (b) a liquid and (c) a solid. These functions have been generated using a molecular dynamics simulation (see section 1.6) of atoms interacting through a Lennard-Jones potential (equation (1.9), figure 1.4). The Boltzmann factor for the Lennard-Jones potential has been superimposed on the gas-phase distribution function (dashed curve). The thermodynamic states are: $T = 2\epsilon/k_B$, $\rho\sigma^3 = 0.05$ (gas), $T = \epsilon/k_B$, $\rho\sigma^3 = 0.8$ (liquid), $T = 0.2\epsilon/k_B$, $\rho\sigma^3 = 0.9$ (solid).

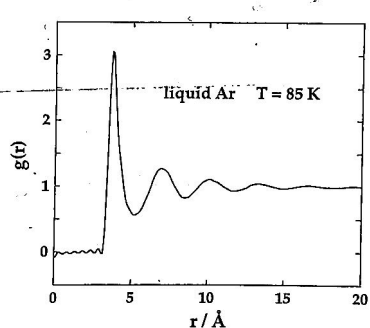
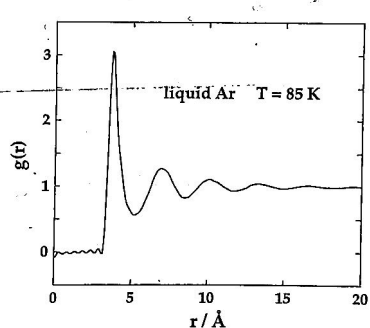
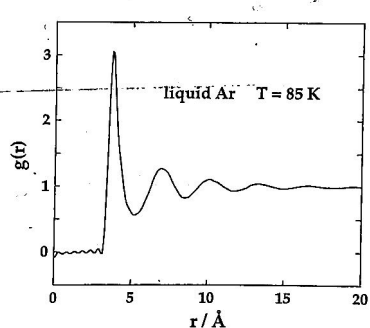


FIG. 2.1. Results of neutron-scattering experiments for the radial distribution function of liquid argon near the triple point. The ripples at small r are artefacts of the data analysis. After Yarnell *et al.*⁷

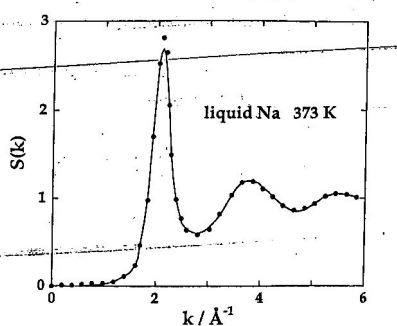
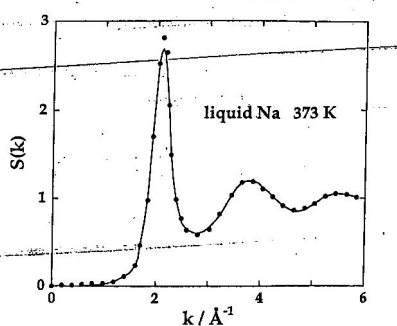
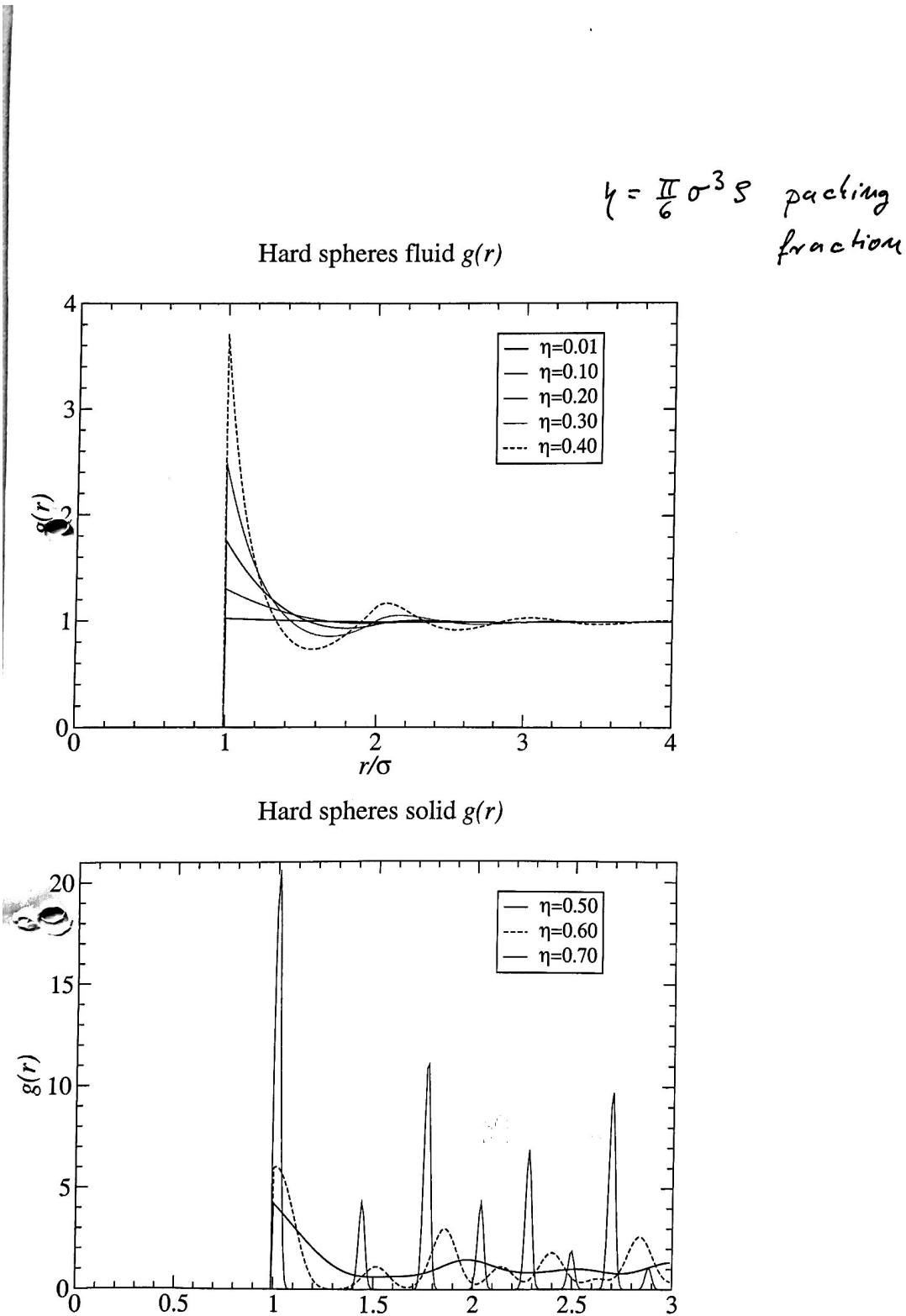


FIG. 3.2. Structure factor of liquid sodium near the normal melting temperature. The points are experimental x-ray scattering results⁸ and the curve is obtained from a Monte Carlo calculation⁹ for the r^{-4} potential under the same thermodynamic conditions.





Explicit-water molecular dynamics (MD) computer simulations
of $\text{Na}^+ \text{Cl}^-$.

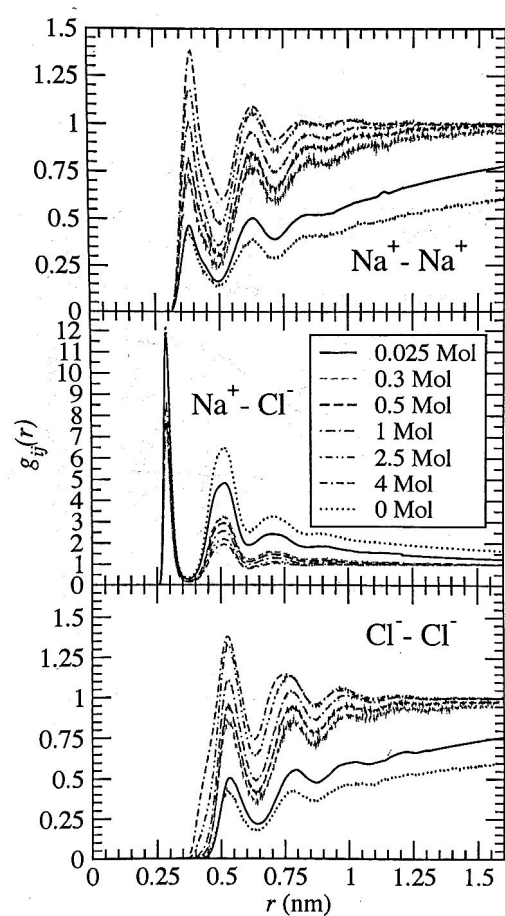


FIG. 3: MD results for the radial distribution functions for NaCl at different salt concentrations.
Note that also the extrapolated curve for zero concentration (0 M) is shown.

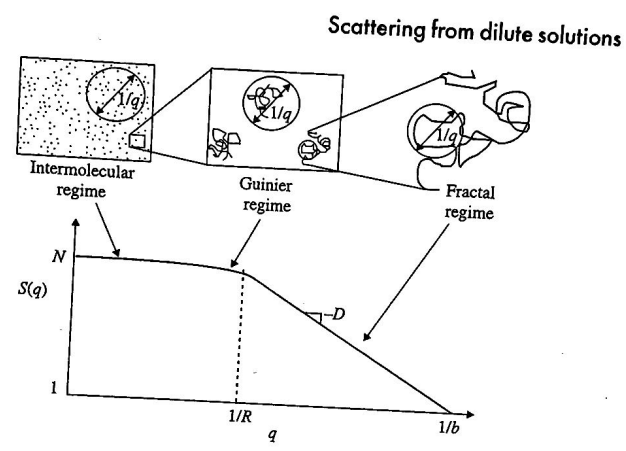


Fig. 3.19
Scattering function for a dilute solution
on logarithmic scales.

15.8 Molecules and polymers

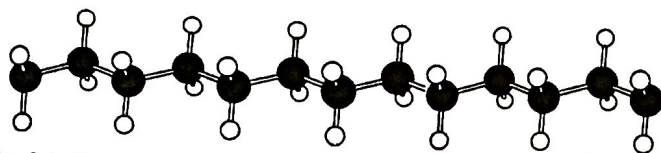


Fig. 2.1. The steric structure of PE. Rotations about the C-C bonds result in a change in the conformation

G. STROBL
POLYMER
PHYSICS

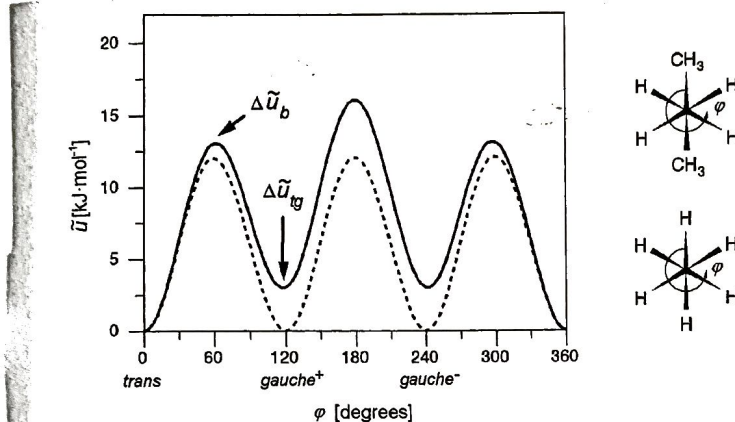


Fig. 2.2. Potential energies associated with the rotation of the central C-C bond for ethane (broken line) and butane (continuous line). The sketches show the two molecules in views along the C-C bond

Table 2.1. Characteristic ratios C_∞ of some selected polymers derived from viscosity measurements under theta conditions at the indicated temperatures (data from Flory [1])

| Polymer | Solvent | T [°C] | C_∞ |
|------------------------------------|----------------------------|----------|------------|
| polyethylene | dodecanol-1 | 138 | 6.7 |
| polystyrene (atactic) | cyclohexane | 35 | 10.2 |
| propylene (atactic) | cyclohexane | 92 | 6.8 |
| polyisobutylene | benzene | 24 | 6.6 |
| poly(vinylacetate) (atactic) | <i>i</i> -pentanone-hexane | 25 | 8.9 |
| poly(methylmethacrylate) (atactic) | various solvents | 4–70 | 6.9 |
| poly(oxyethylene) | aqueous K_2SO_4 | 35 | 4.0 |
| poly(dimethylsiloxane) | butanone | 20 | 6.2 |

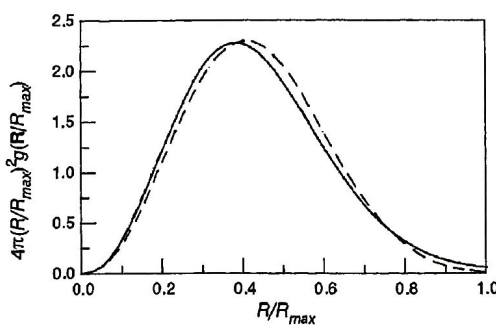


Fig. 2.8. Exact distribution function for the end-to-end distance vector of a chain of five freely jointed segments (broken line) compared to the Gaussian distribution function with the same value of $\langle R^2 \rangle$ (continuous line)

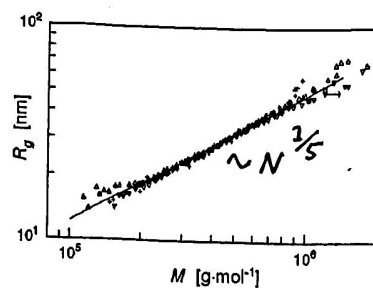


Fig. 2.17. Relation between the radius of gyration R_g and the molar mass M , observed in light scattering experiments on dilute solutions of PS in toluene. The continuous straight line corresponds to the scaling law Eq. (2.83). Data from Winternantel et al. [5]

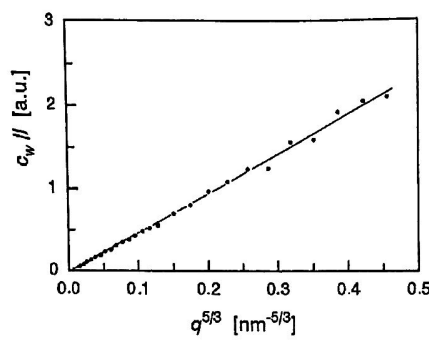


Fig. 2.18. Intensities obtained in a neutron scattering experiment on dilute solutions of (deuterated) PS ($\bar{M}_w = 1.1 \times 10^6$ g mol⁻¹) in CS₂ ($c_w = 10^{-3}$ g cm⁻³). The straight line corresponds to the scattering law characteristic for expanded chains. Data from Farnoux [6]

S. STROBL
POLYMER
PHYSICS

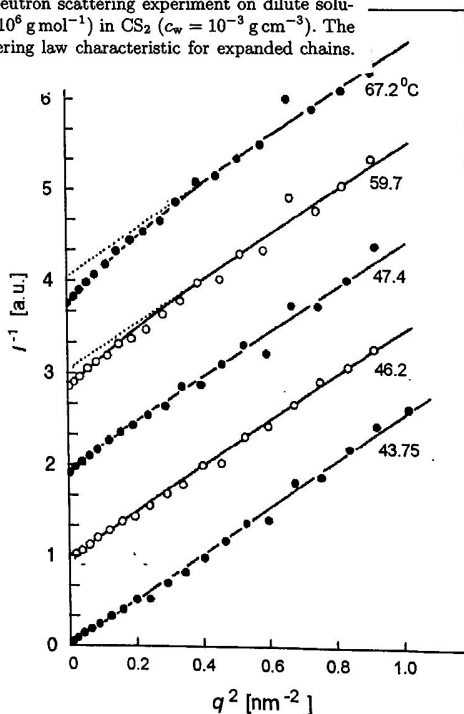


Fig. 2.19. Neutron scattering intensities $I(q)$ measured for dilute solutions of PS in cyclohexane ($\bar{M}_w = 3.8 \times 10^6$ g mol⁻¹; $qR \gg 1$) at the indicated temperatures above the theta point ($T = 35$ °C). The straight lines correspond to the scattering law of ideal chains (subsequent curves are shifted upwards by constant amounts). Data from Farnoux et al. [7]

Rubinstein, Polymer Physics

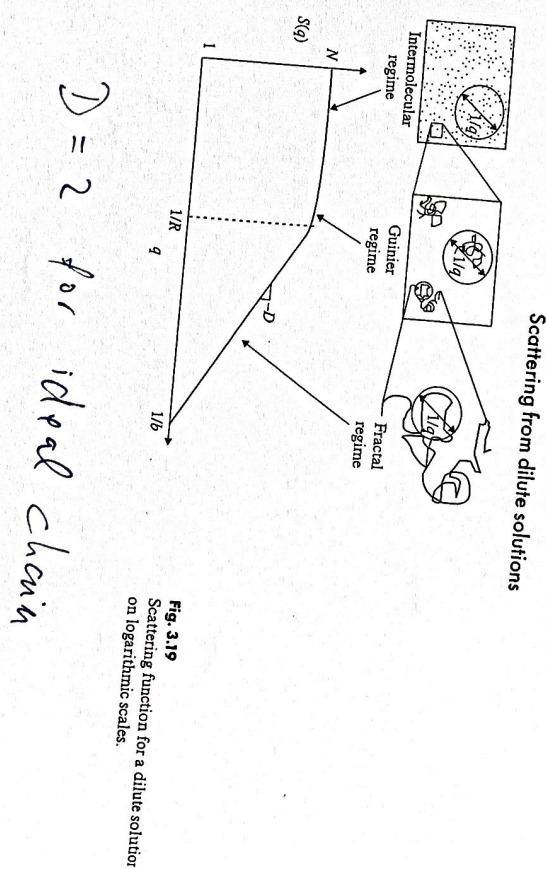


Fig. 3.10
Scattering function for a dilute solution
on logarithmic scales.

$D = 2$ for ideal chain

15.9 Force fields

Constrained dynamics

We can achieve an increase in time scales in molecular dynamics of chemically realistic models by suppressing the fast vibrations. We start by recognizing that the fast internal vibrations are usually decoupled from the overall translational and rotational motion of the molecules. Thus, keeping the bonds and bond angles fixed should not greatly affect the overall properties of the system. We can keep those motions fixed by using an algorithm that introduces constraints into the system, which we will illustrate by a simple example.

Suppose that we have a system of diatomic molecules whose atoms are, for convenience, restricted to the x axis, as shown in Figure 8.8a. The vibrations of the molecule are very fast relative to the translational motion of the molecule, so that the overall properties of the system can be accurately modeled even if the bond lengths are fixed.

Suppose that at time t the atoms have positions $x_1(t)$ and $x_2(t)$, as shown in Figure 8.8a, where the separation between them is d , the known bond length. The forces on the two atoms, F_1 and F_2 , will depend on the neighboring molecules, so there is no reason to think that they

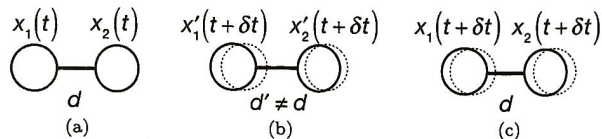


Figure 8.8 Application of a constraint algorithm. (a) Atom positions at time t , with the interatomic separation equal to the bond length, d . (b) Solid circles indicate the positions at $t + \delta t$ after applying the Verlet algorithm without constraints, with the interatomic separation d' not equal to the bond length. (c) Solid circles indicate the positions at $t + \delta t$ after applying the constraints, with the interatomic separation d' now equal to the bond length.

would be the same. We can use the Verlet algorithm from Eq. (6.11) to determine the positions at time $t + \delta t$,

$$\begin{aligned} x'_1(t + \delta t) &= 2x_1(t) - x_1(t - \delta t) + \frac{F_1}{m_1} \delta t^2 \\ x'_2(t + \delta t) &= 2x_2(t) - x_2(t - \delta t) + \frac{F_2}{m_2} \delta t^2, \end{aligned} \quad (8.20)$$

where m is the mass and the prime indicates unconstrained positions. These positions are shown in Figure 8.8b. The problem is that

$$d' = x'_2(t + \delta t) - x'_1(t + \delta t) \quad (8.21)$$

does not necessarily equal the bond length, d . We can force the bond length to be fixed at d by applying a constraining force [109, 280].

Define the energy

$$\sigma = d^2 - (x_2 - x_1)^2, \quad (8.22)$$

which is 0 when the instantaneous bond length, $x_2 - x_1$, equals the equilibrium value, d . We can derive a force from this energy by taking the negative of the gradient,

$$\mathbf{G} = -\frac{\lambda}{2} \nabla \sigma, \quad (8.23)$$

where λ is a parameter that we will determine below. For our one-dimensional problem, the constraining forces are

$$\begin{aligned} G_1 &= -\frac{\lambda}{2} \frac{d\sigma}{dx_1} = -\lambda(x_2 - x_1) = -\lambda d \\ G_2 &= -\frac{\lambda}{2} \frac{d\sigma}{dx_2} = \lambda d. \end{aligned} \quad (8.24)$$

Adding the constraining forces to the equations of motion in Eq. (8.20), we have

$$\begin{aligned} x_1(t + \delta t) &= x'_1(t + \delta t) - \frac{\lambda}{m} d \delta t^2 \\ x_2(t + \delta t) &= x'_2(t + \delta t) + \frac{\lambda}{m} d \delta t^2. \end{aligned} \quad (8.25)$$

CSAR

1/2

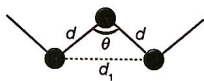


Figure 8.9 Bond angle constraint as a fixed distance [280].

We now apply the constraint

$$(x_2(t + \delta t) - x_1(t + \delta t))^2 = d^2, \quad (8.26)$$

which leads to the equation

$$\left(d' + \frac{2d \delta t^2}{m} \lambda \right)^2 = d^2, \quad (8.27)$$

or

$$\frac{4d^2 \delta t^4}{m} \lambda^2 + \frac{4dd' \delta t^2}{m} \lambda + (d')^2 - d^2 = 0. \quad (8.28)$$

Solving the quadratic equation in Eq. (8.28) determines the value of λ needed to constrain the molecular length. This is inserted in Eq. (8.25), yielding the constrained bond length, as shown schematically in Figure 8.8c. This procedure could be done at each time step for each molecule, keeping the bond length fixed.

Imagine applying this procedure to a polyatomic molecule. Each atom is bonded to two others, so there would be two constraint equations to keep the two bond lengths fixed. Bond angles can also be fixed. For *n*-alkanes, for example, the bond angle can be fixed by a distance criterion, as shown in Figure 8.9, introducing a constraint equation that couples each atom to its second-nearest neighbors along the chain by fixing the next-nearest-neighbor distance to $d_1 = 2d \sin(\theta/2)$, where $\theta = 109^\circ 28'$ for alkane chains. Thus, each atom will have two additional constraints. Solving for the coefficients in the constraint equations thus becomes a far more challenging computational procedure than in our simple example, involving solving a matrix equation at each time step. In the SHAKE algorithm [280], an approximate form of the equations is used and an iterative procedure followed to determine the appropriate coefficients. More details, and a description of the effect of using constrained dynamics on the ensemble averages, are presented in the book by Frenkel and Smit [109].

LESAR

2/2

LESAR

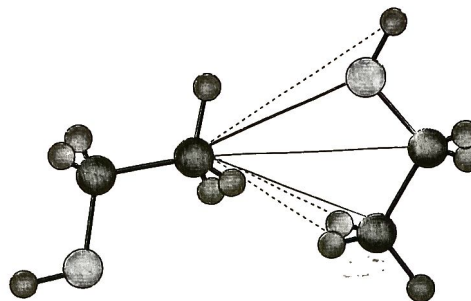


Figure 8.6 Atom-atom interactions between two ethanol (C_2H_5OH) molecules: carbons in dark gray, oxygen atom in light gray, and hydrogen atoms in medium gray. The interactions between C and O are shown as dark solid lines, between C and C as light solid lines, and between C and H as dashed lines. For clarity, only some interactions are shown.

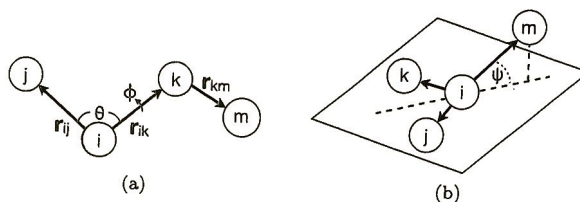


Figure 8.7 Angles and distances used in intramolecular potentials.

$$\begin{aligned} \mathcal{V} = & \sum_{\text{bonds}} \frac{1}{2} k_r (r_{ij} - r_0)^2 + \sum_{\text{angles}} \frac{1}{2} k_\theta (\theta_{ijk} - \theta_0)^2 \\ & + \sum_{\text{torsions}} \sum_n k_{\phi,n} [\cos(n\phi_{ijk\ell} + \delta_n) + 1] + \sum_{\text{non-bonded pairs}} \left[\frac{q_i q_j}{4\pi\epsilon_0 r_{ij}} + \frac{A_{ij}}{r_{ij}^{12}} - \frac{B_{ij}}{r_{ij}^6} \right]. \quad (1.37) \end{aligned}$$

A&T

CLASS I

Table 1.2 Force fields and their domains of application. This list is not complete and simply includes representative examples of some of the force fields commonly used in liquid-state simulations.

| Force field | Class | Domain of Application | Source |
|----------------|-------|--|-------------------------|
| OPLS | I | peptides, small organics | Jorgensen et al. (1996) |
| CHARMM22 | I | proteins with explicit water | Mackerell et al. (1998) |
| CHARMM27 | I | DNA, RNA, and lipids | Mackerell et al. (1998) |
| AMBER ff99 | I | peptides, small organics, RESP charges | Wang et al. (2000) |
| GAFF | I | small organics, drug design | Wang et al. (2004) |
| GROMOS ffG45a3 | I | lipids, micelles | Schuler et al. (2001) |
| COMPASS | II | small molecules, polymers | Sun (1998) |
| clayFF | II | hydrated minerals | Cygan et al. (2004) |
| MM4 | II | small organics, coordination compounds | Allinger et al. (1996) |
| UFF | II | full Periodic Table (including actinides) | Rappe et al. (1992) |
| AMBER ff02 | III | polarizable atoms | Cieplak et al. (2001) |
| AMOEBA | III | polarizable multipoles, distributed multipoles | Ponder et al. (2010) |
| MARTINI | III | coarse-grained, proteins, lipids, polymers | Marrink et al. (2007) |
| ReaxFF | III | chemical reactions | van Duin et al. (2001) |

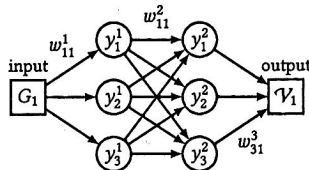
CLASS II: HIGHER ORDER,
BEYOND HARMONIC APPROX.CLASS III: INCLUDES
EXPLICIT POLARIZABILITY

A & T

Example 5.1 Learning the potentials with a neural network

For complicated intermolecular potentials, such as those developed from *ab initio* calculations, it can be cost-effective to teach the computer to estimate the potential energy of a particular atom from a knowledge of its environment in the liquid. This can be done by constructing an artificial neural network (Behler, 2011).

In this approach, the Cartesian coordinates of a particular atom, i , are used to calculate a set of μ symmetry functions, G_i^μ . The first of these functions, $\mu = 1$, might depend on the radial distribution of all the other atoms around i . The second might depend on the distribution of triplets around atom i through the variable $\cos \theta_{ijk}$, and so on (see e.g. Behler and Parrinello, 2007, eqns (4) and (5)). Symmetry functions of different order can be combined with weights $w_{i\mu}^s$ to produce an overall $G_i = \sum_\mu w_{i\mu}^s G_i^\mu$. The G_i are the input to a simple neural network of the kind shown.



There is a separate network for each atom, containing a number of hidden layers (two in this example) each with a number of nodes (three in this example). The value y_m^ℓ held by the network at a particular node, m , in layer, ℓ , is calculated as a function of the weighted sum of the connected nodes in the previous layer, that is, $y_m^\ell = f(\sum_{n=1}^3 w_{nm}^\ell y_n^{\ell-1})$ for $\ell = 2$ in our example. The activation function is often taken to be $f(x) = \tanh(x)$, although different functions can be used for different layers. The output from the network is the potential energy, V_1 . The outputs from all the separate networks can be added to produce the total potential energy, V_{net} . For a number of training configurations the full V_{QM} is also calculated. The weights, w , in the network, and symmetry functions, are adjusted to minimize $|V_{\text{net}} - V_{\text{QM}}|$ for the training set. The same connectivity and inter-layer weights are used in the different networks established for each atom. Once the optimum weights have been established, the network can be used to accurately estimate the potential and forces for an unknown configuration.

Morawietz et al. (2016) have employed neural network potentials in *ab initio* molecular dynamics simulations of water. The efficiency of the approach enabled them to show that the relatively weak, isotropic van der Waals forces are crucial in producing the density maximum and the negative volume of melting of the fluid.

15.10 Coarse graining; Hamaker, DLVO and Depletion potentials

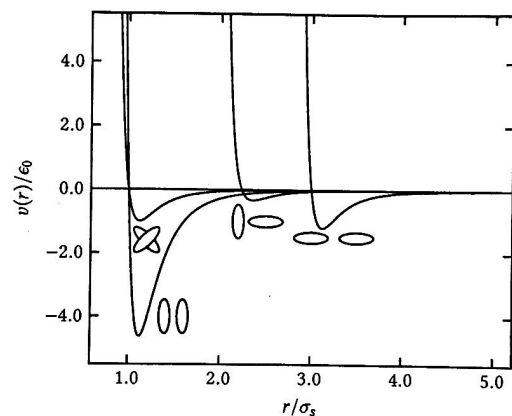
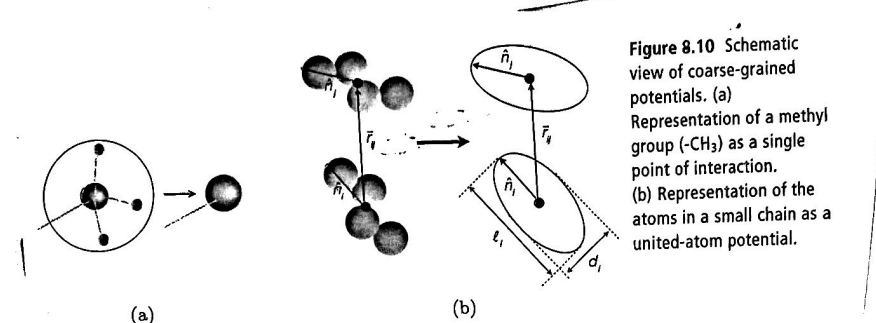
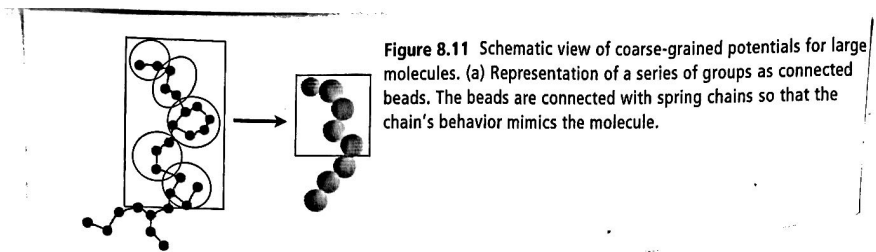


Fig. 1.11 The Gay-Berne potential, with parameters $\mu = 1$, $v = 3$, $\kappa = 3$, $\kappa' = 5$ (Berardi et al., 1993), as a function of centre–centre separation, for various molecular orientations.

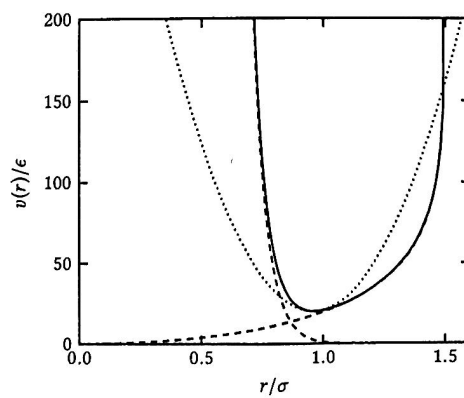


Fig. 1.12 The potential between bonded atoms in a coarse-grained polymer (solid line) together with its component parts (dashed lines): the attractive FENE potential, eqn (1.33) with $R_0 = 1.5\sigma$ and $k = 30\epsilon/\sigma^2$, and the repulsive Lennard-Jones potential, eqn (1.10a). Also shown (dotted line) is a harmonic potential, fitted to the curvature at the minimum. See Kremer and Grest (1990) for details.

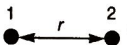
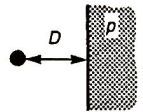
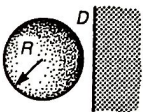
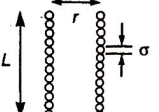
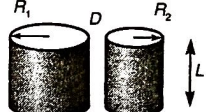
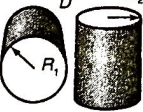
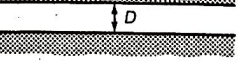
| | |
|---|--|
| Two atoms  $w = -C/r^6$ | Two spheres  $W = \frac{-A}{6D} \frac{R_1 R_2}{(R_1 + R_2)}$ |
| Atom-surface  $w = -\pi C p / 6D^3$ | Sphere-surface  $W = -AR/6D$ |
| Two parallel chain molecules  $W = -3\pi CL/8\sigma^2 r^5$ | Two cylinders  $W = \frac{AL}{12\sqrt{2} D^{3/2}} \left(\frac{R_1 R_2}{R_1 + R_2} \right)^{1/2}$ |
| Two crossed cylinders  $W = -A\sqrt{R_1 R_2}/6D$ | Two surfaces  $W = -A/12\pi D^2 \text{ per unit area}$ |

Fig. 11.1. Non-retarded van der Waals interaction free energies between bodies of different geometries calculated on the basis of pairwise additivity (Hamaker summation method). The Hamaker constant A is defined as $A = \pi^2 C \rho_1 \rho_2$ where ρ_1 and ρ_2 are the number of atoms per unit volume in the two bodies and C is the coefficient in the atom-atom pair potential (top left). A more rigorous method of calculating the Hamaker constant in terms of the macroscopic properties of the media is given in Section 11.3. The forces are obtained by differentiating the energies with respect to distance.

HamakerConstants.png (PNG Image, 1295 × 756 pixels)

<http://soft-matter.seas.harvard.edu/images/4/49/HamakerConstan..>

| Substance | A_{11} (10^{-26} J) | Polyvinyl acetate | 8.91 | Methyl ethyl ketone | 4.53 |
|------------------------------------|----------------------------------|----------------------------|-----------|---------------------|--------------------|
| Graphite | 47.0 | Polyvinyl alcohol | 8.84 | Water | 4.35, 3.7, 4.38 |
| Gold | 45.3, 45.5, 37.6 | Natural rubber | 8.58 | Hexane | 4.32 |
| Silicon carbide | 44 | Polybutadiene | 8.20 | Diethyl ether | 4.30 |
| Rutile (TiO_2) | 43 | Polybutene-1 | 8.03 | Acetone | 4.20, 4.1 |
| Silver | 39.8, 40.0 | Quartz | 7.93 | Ethanol | 4.2 |
| Germanium | 29.9, 30.0 | Polyethylene oxide | 7.51 | Ethyl acetate | 4.17 |
| Chromium | 29.2 | Polyvinyl chloride | 7.5 | Polypropylene oxide | 3.95 |
| Copper | 28.4 | Hydrocarbon (crystal) | 7.1 | Pentane | 3.94, 3.8 |
| Diamond | 28.4 | CaF_2 | 7 | PTFE | 3.8 |
| Zirconia ($\alpha\text{-ZrO}_2$) | 27 | Potassium bromide | 6.7 | Liquid He | 0.057 |
| Silicon | 25.5, 25.6 | Hexadecane | 6.31 | | |
| Metals (Au, Ag, Cu) | 25 – 40 | Fused quartz | 6.3 | | |
| Iron oxide (Fe_3O_4) | 21 | Polymethylmethacryl ate | 6.3 | | |
| Selenium | 16.2, 16.2 | Polydimethylsiloxane | 6.27 | | |
| Aluminum | 15.4, 14, 15.5 | Potassium chloride | 6.2 | | |
| Cadmium sulfide | 15.3 | Chlorobenzene | 5.89 | | |
| Tellurium | 14.0 | Dodecane | 5.84, 5.0 | | |
| Polyvinyl chloride | 10.82 | Decane | 5.45 | | |
| Magnesia | 10.5, 10.6 | Toluene | 5.40 | | |
| Polyisobutylene | 10.10 | 1,4-Dioxane | 5.26 | | |
| Mica | 10, 10.8 | <i>n</i> -Hexadecane | 5.1 | | |
| Polyethylene | 10.0 | Octane | 5.02, 4.5 | | |
| Polystyrene | 9.80, 6.57, 6.5, 6.4, 7.81 | Benzene | 5.0 | | |
| | | <i>n</i> -Tetradecane | 5.0 | | |
| | | Cyclohexane | 4.82, 5.2 | | |
| | | Carbon tetrachloride | 4.78, 5.5 | | |

ISRAELACHVILI

TABLE 11.3 Hamaker constants for two media interacting across another medium

| Interacting media | | | Hamaker constant $A (10^{-20} \text{ J})$ | | |
|-------------------------------------|-------------|-------------------------------------|---|------------------------------|--|
| 1 | 3 | 2 | Eq. (11.13) ^a | Exact solutions ^b | Experiment |
| Air | Water | Air | 3.7 | 3.70 | |
| Pentane | Water | Pentane | 0.28 | 0.34 | |
| Octane | Water | Octane | 0.36 | 0.41 | |
| Dodecane | Water | Dodecane | 0.44 | 0.50 | |
| Hexadecane | Water | Hexadecane | 0.49 | 0.50 | 0.5 ^d 0.3–0.6 ^{d,e} |
| Water | Hydrocarbon | Water | 0.3–0.5 | 0.34–0.54 | 0.3–0.9 ^f |
| Polystyrene | Water | Polystyrene | 1.4 | 0.95–1.3 ^c | |
| Fused quartz | Water | Fused quartz | 0.63 | 0.83 | |
| Fused quartz | Octane | Fused quartz | 0.13 | | |
| PTFE | Water | PTFE | 0.29 | 0.33 | |
| Mica | Water | Mica | 2.0 | 2.0 | 2.2 ^g |
| | | | | | |
| Alumina (Al_2O_3) | Water | Alumina (Al_2O_3) | 4.2 ^j | 5.3 ^b | 6.7 ⁱ |
| Zirconia ($n\text{-ZrO}_2$) | Water | Zirconia ($n\text{-ZrO}_2$) | 13 ^j | | |
| Rutile (TiO_2) | Water | Rutile (TiO_2) | 26 ^j | | |
| Ag, Au, Cu | Water | Ag, Au, Cu | — | 30–40 ^c | 40 (gold) ^h |
| Water | Pentane | Air | 0.08 | 0.11 | |
| Water | Octane | Air | 0.51 | 0.53 | |
| Octane | Water | Air | -0.24 | -0.20 | |
| Fused quartz | Water | Air | -0.87 | -1.0 | |
| Fused quartz | Octane | Air | -0.7 | | |
| Fused quartz | Tetradecane | Air | -0.4 | | -0.5 ^h |
| $\text{CaF}_2, \text{SrF}_2$ | Liquid He | Vapour | -0.59 | -0.59 ⁱ | -0.58 ⁱ |

^a Based on dielectric data of Table 11.2, assuming mean values for v_e .^b Hough and White (1980).^c Parsegian and Weiss (1981).^d Lis *et al.* (1982).^e Ohshima *et al.* (1982).^f Requena *et al.* (1975).^g Israelachvili and Adams (1978).^h Derjaguin *et al.* (1978).ⁱ Sabisky and Anderson (1973).^j Velamakanni (1990, thesis); Horn *et al.* (1988a).

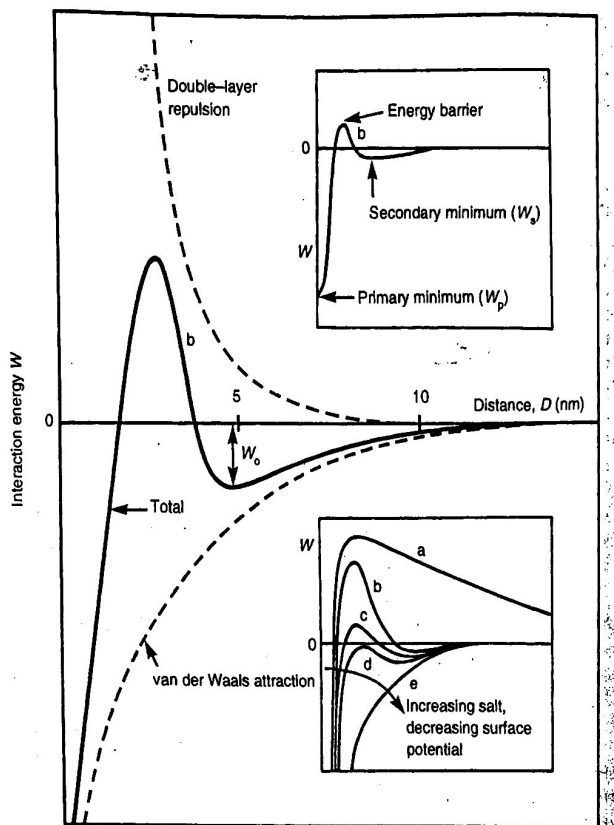


Fig. 12.12. Schematic energy versus distance profiles of DLVO interaction. (a) Surfaces repel strongly; small colloidal particles remain 'stable'. (b) Surfaces come into stable equilibrium at secondary minimum if it is deep enough; colloids remain 'kinetically' stable. (c) Surfaces come into secondary minimum; colloids coagulate slowly. (d) The 'critical coagulation concentration'. Surfaces may remain in secondary minimum or adhere; colloids coagulate rapidly. (e) Surfaces and colloids coalesce rapidly.

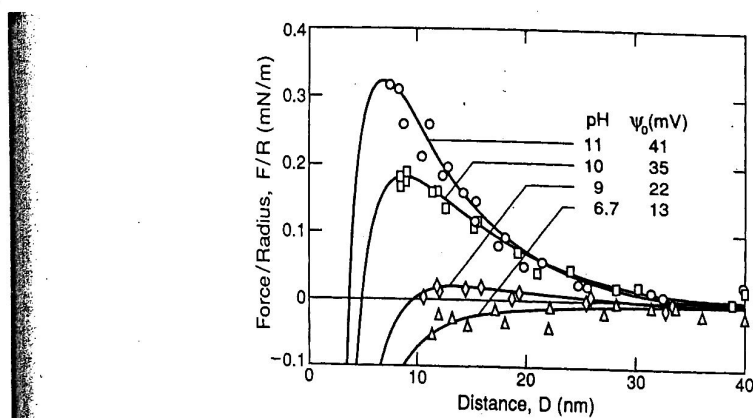
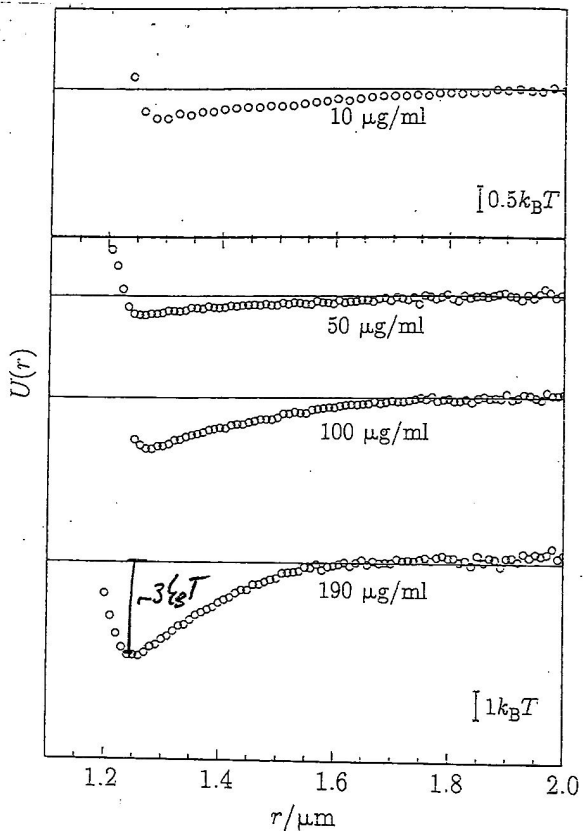


Fig. 12.14. Classic DLVO forces measured between two sapphire surfaces in 10^{-3} M NaCl solutions at different pH. The continuous lines are the theoretical DLVO forces for the potentials shown and a Hamaker constant of $A = 6.7 \times 10^{-20}$ J (from Horn et al., 1988a).

Depletion potentials

Figure 2.6. Measured depletion potential (in units of $k_B T$) between two silica spheres of diameter $\sigma = 1, 2 \mu\text{m}$, induced by solutions of DNA molecules, versus separation r between the spheres, for increasing polymer concentrations (from top to bottom). The energy scales are indicated by the vertical bars in the top panel (corresponding to the dilute regime) and in the lower panel, where the concentrations are in the semi-dilute regime. After R. Verma, J.C. Crocker, T.C. Lubensky and A.G. Yodh, *Phys. Rev. Lett.* **81**, 4004 (1998).



Bibliography

- [1] [Andersen 1980]
GREINER, NEISE, STÖCKER, Thermodynamics and Statistical Mechanics, Springer (1995).
- [2] [Andersen 1980]
HANSEN and McDONALD, Theory of Simple Liquids, 4th Edition, Elsevier (2013).
- [3] [Andersen 1980]
BARRT and HANSEN, Basic Concepts for Simple and Complex Liquids, Cambridge Univ. Press (2010).
- [4] [Israelachvilli 2011]
J. N. Israelachvilli, Intermolecular and Surface Forces. Academic Press, Elsevier. Third Edition, (2011).
- [5] [Andersen 1980]
KALCHER and DZUBIELLA : J. Chem. Phys. 130, 134507 (2009).
- [6] [Andersen 1980]
McQuarrie: Statistical Mechanics, University Science Books (2000).
- [7] [Andersen 1980]
RUBINSTEIN and COLBY: Polymer Physics, Oxford University Press (2003).
- [8] [Allen and Tildesley 2017]
ALLEN; TILDESLEY: Oxford University Press, Second edition (2017)
- [9] [Frenkel and Smit 2002]
DAAN; FRENKEL and BEREND; SMIT: Understanding Molecular Simulation: From Algorithms to Application. Academic Press, Second edition (2002)
- [10] [Lesar 2013]
RICHARD; LESARD: Introduction to Computational Materials Science: Fundamentals to application. Cambridge University Press (2013)
- [11] [Andersen 1980]
ANDERSEN: J. Chem. Phys. 72, 2384 (1980)
- [12] [Berendsen 1984]
BERENDSEN: JCP, 81, 3684 (1984)
- [13] [Fennel 2006]
WOLF et. al.: JCP, 110, 8254 (1999)
- [14] [Fennel 2006]
FENNEL et. al.: JCP, 124, 234104 (2006)

- [15] [Hoover 1985]
HOOVER: Phy. Rev. A, 31(3), 1695 (1985)
- [16] [Martyna 1994]
MARTYNA et al.: JCP, 101, 4177 (1994)
- [17] [Nosé 1984]
NOSE: Molecular Physics, 52(2), 255 (1984)
- [18] [Paranello 1981]
PARANELLO; RAHMAN: J. Appl. Phys. 52, 7182 (1981)
- [19] [Rose 1984]
ROSE et. al.: Phy. Rev. B 29 2963 (1984)
- [20] [Tuckerman 2006]
TUCKERMAN et al.: J. Phys. A Math. Gen 39, 5629 (2006)
- [21] [Tuckerman 2006]
Zwanzig: Nonequilibrium Statistical Mechanics, Oxford University Press (2001).
- [22] [Dill and Bromberg 2010]
DILL and BROMBERG, Molecular Driving Forces: Statistical Thermodynamics in Biology, Chemistry, Physics, and Nanoscience, Garland Science (2010).
- [23] [van Kampen 2007]
van KAMPEN, Stochastic processes in Physics and Chemistry, Elsevier (2007).
- [24] [Anishchenko 2007]
ANISHCHENKO et al., Nonlinear Dynamics of Chaotic and Stochastic Systems, Springer (2007).
- [25] [Strogatz 2018]
STROGATZ, Nonlinear Dynamics and Chaos: With Applications to Physics, Biology, Chemistry, and Engineering, CRC Press, (2018).